Innovative Shear Connections for the Accelerated Construction of Composite Bridges

by

Yu-Ta Chen

A thesis
presented to the University of Waterloo
in fulfillment of the
thesis requirement for the degree of
Master of Applied Science
in
Civil Engineering

Waterloo, Ontario, Canada, 2013

Author’s Declaration

I hereby declare that I am the sole author of this thesis. This is a true copy of the thesis, including any required final revisions, as accepted by my examiners.

I understand that my thesis may be made electronically available to the public.

Abstract

Accelerated bridge construction methods are being progressively used to construct and replace bridges in North America. Unlike traditional bridge construction methods, accelerated bridge construction methods allow bridges to be built in a shortened period of time on the construction site. These methods reduce the road closure time and the traffic disruption that are associated with bridge construction. One of these methods is carried out by prefabricating the bridge elements offsite and then assembling them onsite in a time-efficient way to build the bridge. This construction method can be used to build steel-precast composite bridges, where steel plate girders are connected to full-depth precast concrete deck panels. For the expeditious construction of composite bridges, a proper shear connection detail is needed to develop composite action between the steel plate girders and the precast concrete deck panels.

This research project investigated two types of shear connection that would accelerate the construction of steel-precast composite bridges. First, finite element analysis was used to study the behaviour of composite bridge girders with panel end connections. The girders were analyzed for their load-displacement behaviour, cross-sectional stress and strain profile, and connection force distributions. Secondly, experimental push tests were conducted to study the load-slip behaviour of bolted connections. The effects of steel-concrete interface condition, bolt diameter and bolt tension on the shear capacity of bolted connections were analyzed.

Based on the finite element analysis results, it is concluded that the panel end connected girder exhibited strong composite action at service and ultimate load. The level of composite action decreased slightly when the panel end connection stiffness was reduced by a factor of ten.

Based on the experimental results, it is concluded that the total shear capacity of the bolted connection is the sum of the friction resistance and the bolt dowel action resistance. The friction resistance of the connection depends on the interface condition and the bolt clamping force. An analytical model that can predict the ultimate shear capacity of bolted connections has been developed and recommended. The proposed model is shown to give reliable predictions of the experimental results. It should be noted that bolted connections exhibit good structural redundancy because the bolt fracture failures do not happen simultaneously.

Acknowledgements

I would like to thank my supervisors Dr. Scott Walbridge, P.Eng., and Dr. Jeff West, P.Eng., for providing mentorship and advice on my research work and academic life. I would also like to thank Dr. Lei Xu, P.Eng., and Dr. Bob McKillop, P.Eng., for reviewing my thesis and providing constructive feedback.

Many thanks are due to Matthew Bowser, P.Eng., Bridge Engineer at McCormick Rankin Corp. for his guidance on the finite element analysis portion of the work.

Furthermore, I would like to thank the Civil Engineering Structure Laboratory technicians Richard Morrison, Doug Hirst, and Robert Sluban for their invaluable help on the experimental part of my research program. Thanks are also extended to Winston Chen and Matthew Sjaarda for their assistance during the fabrication and testing of the specimens.

Research funding is appreciatively received and acknowledged from the Steel Structures Education Foundation and the Natural Sciences and Engineering Research Council of Canada. Research material donations made by the following suppliers are also acknowledged: Nelson Stud Welding Inc. for the donation of shear studs, Hogg Ready Mix Ltd. for the donation of ready-mix concrete and Sika Canada Inc. for the donation of Sikadur 330.

Lastly, I would like to thank my family and friends for their encouragement and friendship. My experience at the University of Waterloo was a wonderful journey because of their continued support.

Dedication

To my granduncle, who supported and cared for me deeply during my childhood time

Table of Contents

List of Figures

List of Tables

Chapter 1
Introduction

In North America, transportation officials are currently facing a significant cost in repairing and replacing the nation's bridges. According to the report Bridging the Gap [2008] published by the American Association of State Highway and Transportation Officials, almost half of America's bridges would be over 50 years old within the next 15 years. One in four bridges are currently rated as structural deficient and an estimated cost of $140 billion is needed to repair or strengthen them [American Association of State Highway and Transportation Officials 2008]. In Canada, it is estimated that over 40% of the bridges are over 40 years old and a backlog of $10 billion is needed to maintain, rehabilitate or replace them [Newman and Sennah 2011]. Traditional bridge rehabilitation and replacement methods can be very time consuming and costly. Therefore, new bridge construction and replacement methods need to be developed.

Accelerated bridge construction methods are being progressively used to construct and replace bridges in North America [Newman and Sennah 2011]. Unlike traditional bridge construction methods, accelerated bridge construction methods allow bridges to be built in a shortened period of time. These methods reduce road closure time and traffic disruption. In other words, they reduce the road user delay cost that is associated with bridge construction or replacement. Accelerated bridge construction methods have been recently used to address some of the mounting bridge repair and construction backlog [Newman and Sennah 2011].

One of these methods is carried out by prefabricating the bridge elements offsite and then assembling them onsite in a time-efficient way to build the bridge. When steel plate girders are assembled together with full-depth precast concrete deck panels, a composite modular bridge system is formed. For the expeditious construction of a composite modular bridge, a proper shear connection detail is needed to develop composite action between the steel plate girders and the precast concrete deck panels.

This research project was conducted to investigate two types of shear connections that would enable the accelerated construction of steel-precast composite bridges. First, finite element analysis was used to study the behaviour of composite bridge girders with panel end connections. Secondly, experimental push tests were conducted to study the load-slip behaviour of bolted connections.

The following sections present the objectives of this research project and an outline of this thesis.

1.1 Objectives

The purpose of this research project was to examine shear connections that would accelerate the construction of steel-precast composite bridges. The specific objectives of this research project are listed in the following:

- conduct finite element analysis on modular composite bridge girders with panel end connections; analyze the girders' overall load-displacement behaviour, cross-sectional stress and strain profile, and connection force distributions;
- design a push test program to study the load-slip behaviour of bolted connections between steel girder and precast concrete deck panels; vary the test parameters of bolt diameter, bolt tension and steel-concrete interface condition to study their effects on the shear capacity of bolted connections;
- perform push tests in the laboratory and examine the connection failure mechanisms;
- analyze the experimental results of the push tests; examine the effects of the test parameters on the bolted connection behaviour; and propose analytical models that are capable of predicting the ultimate shear capacity of bolted connections.

1.2 Thesis Outline

This thesis consists of seven chapters. Chapter 2 presents a literature review on the methods of accelerated bridge construction and replacement. Five types of shear connections that would accelerate the construction of steel-precast composite bridges are also discussed in this chapter. These shear connections include grout pocket shear stud connections, panel end connections, bolted connections, friction connections and shear lug connections. Analytical models of shear strength in bolted connections are also presented to further understand the shear transfer mechanism of bolted connections.

Chapter 3 presents the finite element analysis that was conducted on composite girders models with panel end connections. First, the finite element models are described. Secondly, the finite element analysis results are presented and discussed. The analysis results include the girder load-displacement behaviour, stress and strain profiles and connection force distributions.

Chapter 4 presents the experimental study that was conducted on bolted connections. The test program and the push test specimens are described. This chapter also describes the concrete material

properties and the specimen fabrication process. Moreover, it documents the test setup, specimens instrumentation and test procedures.

In Chapter 5, the experimental results obtained by testing 13 push test specimens are presented and discussed. These results are presented in the form of load-slip curves and load-strain curves as well as photos that illustrate the failure mechanisms. Results from the compression testing of concrete cylinders are also presented in this chapter.

In Chapter 6, the experimental results of the 13 push tests are investigated and analyzed. The effects of the varied test parameters are presented and discussed. These parameters include friction enhancing surfaces, bolt diameter and bolt pretension. This chapter also analyzes the factors that affect the slip load and the peak load of the specimens. It concludes by proposing analytical models that are capable of predicting the ultimate shear capacity of the bolted connections.

Chapter 7 presents the conclusions of this thesis and the significant findings of this research project. It also presents the recommendations for future work that would further advance the state-of-knowledge of shear connections for steel-precast composite bridges.

Chapter 2
Literature Review

This chapter provides a literature review on the methods of accelerated bridge construction and replacement. It also includes a discussion on the various types of shear connections that would accelerate the construction of steel-precast composite bridges. Analytical models for shear strength in bolted connections are presented to further understand the mechanics of bolted connections.

2.1 Accelerated Bridge Construction and Replacement Methods

Transportation officials in Canada and in the USA have been progressively using accelerated bridge construction methods [Newman and Sennah 2011]. Compared to conventional bridge construction methods, the accelerated bridge construction methods allow bridges to be built in a shortened period of time. These methods would reduce the road or lane closure time that is needed for the bridge construction or replacement to take place. When road or lane closure time is reduced, traffic disruption and congestion can be minimized. Besides reducing the road user delay time and the vehicle carbon emissions, the accelerated bridge construction methods can also improve construction site safety. Safety is improved for the construction workers because they would have spent less time in the construction zone that is near the traffic flow.

As mentioned above, one of the key reasons to use the accelerated bridge construction methods to build bridges is to reduce the road user delay cost. In many urban areas, the cost associated with the traffic delay from bridge construction can be significant. Hence, any increase in the construction cost due to the use of the accelerated bridge construction methods can be offset by considering the road user cost saving that is associated with these methods.

Two types of accelerated bridge construction methods are available in the North American construction industry. One of the methods is to construct the entire bridge superstructure offsite and then put the superstructure in-place onsite by using heavy-lifting technology. The other method to accelerate bridge construction is done by prefabricating the bridge elements offsite and then assemble the elements onsite in a time-efficient way to build the bridge. Each of these two methods is described in detail in the following two sections.

2.1.1 Construction with Heavy-Lifting Technology

Accelerated bridge construction can be done with heavy-lifting technology such as the self-propelled modular transporters (SPMTs). For the projects involving SPMTs, the new bridge superstructure is typical constructed on temporary supports in a staging area that is away from the construction site. Once the new bridge superstructure has been constructed offsite and the substructure has been built onsite, the SPMTs can lift the superstructure up from underneath and transport it to its permanent location that is on top of the substructure. In the case of bridge replacement projects, additional temporary supports at the staging area are necessary. After the existing superstructure has been separated from the substructure, it can be lifted to the staging area offsite and placed on top of additional temporary supports. The new superstructure can then be lifted in place onsite on top of the substructure as part of the rapid bridge replacement process.

The accelerated bridge construction method involving the use of the SPMTs typically requires road closure overnight or over the weekend. The construction work that has to be completed onsite includes the operation of excavating, lifting, backfilling and paving. These operations are typically short enough, where they can be completed overnight or over the weekend. Therefore, road closure can be minimized using this accelerated bridge construction method.

The Ministry of Transportation of Ontario (MTO) had successfully completed the rapid bridge replacement process at the Island Park Drive Overpass in 2007 and at the Clyde Avenue Overpass in 2008 [Vachon and Islam 2011]. Both bridge replacements were completed by using the SPMTs and they were completed in 17 hours and in 15 hours, respectively. If the conventional bridge replacement approach had been used for these projects, they would have lasted at least two years on the highway of Ottawa, Ontario. Therefore, construction work on the highway was significantly reduced by using the accelerated bridge replacement method. The MTO had estimated that each of these projects had resulted a net construction saving of $2.4 million [Vachon and Islam 2011].

In the USA, the Utah Department of Transportation (DOT) had also successfully use the rapid bridge replacement method to replace the 4500 South Bridge in Salt Lake City in 2007 [Ardani et al., 2012]. By using SPMTs, the replacement was done in one weekend. If the conventional bridge construction method was used, the construction impact on the motorist was expected to last four months. Hence, traffic disruption and congestion was mitigated when the accelerated bridge replacement method was used. The Utah DOT estimated that the construction cost of the bridge increased by $0.81 million due to the use of the accelerated bridge construction method [Ardani et al., 2012]. However, the DOT

economic analysis suggested that the road users saved $3.24 million due to the accelerated bridge construction and the mitigated user delay cost.

The SPMTs are computer controlled multi-axle platform vehicles that can lift and move bridge systems weighting up to several thousand tons [Newman and Sennah 2011]. Their exact weight capacity depends on their wheel configurations. They have been used extensively to lift and move heavy equipment and structures for the petrochemical and offshore industries [Newman and Sennah 2011]. Figure 2-1 shows SPMTs underneath a bridge superstructure.

Figure 2-1: Self-Propelled Modular Transporters underneath a Bridge Superstructure

2.1.2 Construction with Prefabricated Bridge Elements

Accelerated bridge construction can also be done by using prefabricated bridge elements. When this construction method is used, bridge elements are prefabricated in a designated facility, such as a steel fabrication plant or a precast concrete plant. Once the elements are prefabricated, they can be shipped to the construction site for quick assembling to build the bridge. Proper joint details have to be developed in order to efficiently and effectively assemble the bridge elements together to construct the bridge. This construction method can be used to build a brand new bridge as well as replacing an existing bridge. It can also be used to rehabilitate an existing bridge by replacing the deteriorate

bridge components with brand new prefabricated bridge elements. Movements of the bridge elements in the construction site are typically achieved by using cranes.

Short term road closure or lane closure is necessary when replacing or rehabilitating an existing bridge by using this accelerated bridge construction method. The closure of roads or traffic lanes are needed to allow the bridge construction to take place as bridge elements are assembled onsite. Work on the construction site would be effectively reduced when prefabricated bridge elements are used to build the bridge. Onsite construction work such as formwork placement, reinforcing steel placement, concrete casting and formwork removal can all be eliminated when prefabricated bridge elements are used. In other words, the use of the prefabricated bridge elements would reduce the onsite construction time and speed up the construction process. By speeding up the construction onsite, the duration of the road closure or lane closure associated with the accelerated bridge construction method would naturally be shorter than the ones associated with the convention bridge construction methods. The actual duration of road closure or lane closure depends on the size of the bridge replacement and rehabilitation project.

Besides reducing the onsite construction time and accelerating the bridge construction, the use of the prefabricated bridge elements also present several other benefits. When work on the construction site has been reduced by using prefabricated bridge elements, the environmental impacts on the construction site can be reduced. Using prefabricated bridge elements can also increase the quality control of the materials because these elements are made in a controlled facility such as a precast concrete plant.

The prefabricated steel elements of the bridge are typically assembled onsite by using bolts or welds. Examples of these elements include plate girders, arch members and truss members. In contrast, the precast concrete elements of the bridge can be assembled onsite by using grouts, post-tensioning or cast-in-placed concrete closure pours. Examples of precast concrete elements include full-depth deck panels, prestressed concrete girders, piers, abutments, barrier walls and wingwall [Lam and Tharmabala 2011]. When the prefabricated steel elements are assembled together with the precast concrete elements, a composite modular bridge system is formed. The composite modular bridge system typically consists of steel plate girders and full-depth precast concrete deck panels (Figure 2-2). The most common way to connect the plate girders to the deck panels is by using shear studs in grouted pockets.

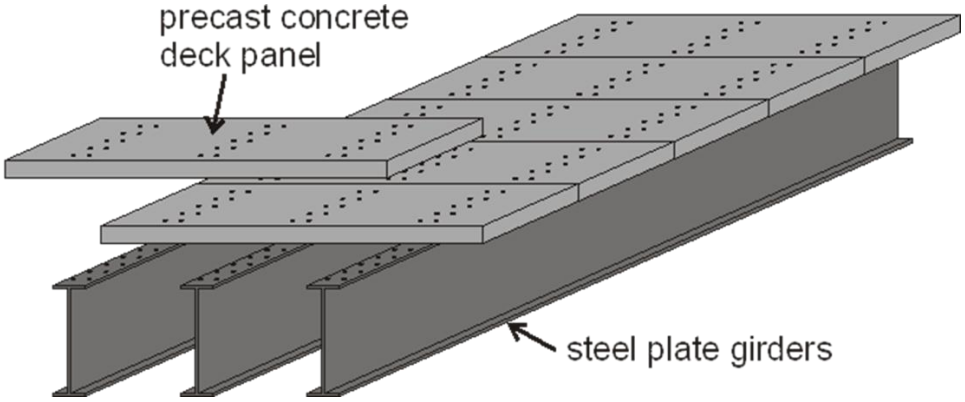

Figure 2-2: Steel-Precast Composite Bridge

As part of an on-going effort to accelerate bridge construction in Ontario, the Ministry of Transportation of Ontario (MTO) had constructed the Little Savanne River Bridge by using prefabricated bridge elements [Lam and Tharmabala 2011]. Steel plate girders and full-depth precast concrete deck panels were used to accelerate the bridge construction. The Little Savanne River Bridge was constructed in 2005 by using 20 precast concrete deck panels that were made composite to the six steel plate girders. The deck panels consisted of precast pockets to allow the placement of groups of shear studs. The shear studs were placed in the pockets and welded on top of the girders' flanges. Composite action was achieved when concrete mixture was used to fill the stud pockets. Based on a proof load test conducted by the MTO in 2006, the structural performance of the Little Savanne River Bridge was excellent and better than the predicted theoretical results [Lam and Tharmabala 2011].

As mentioned in the first paragraph of this section, the accelerated bridge construction method can be used to rehabilitate an existing bridge by replacing the deteriorate bridge components with brand new prefabricated bridge elements. In the USA, this method has been used by several state Departments of Transportation to replace deteriorated bridge decks [U.S. Department of Transportation FHWA 2011]. The deteriorated decks were replaced with full-depth precast concrete deck panels and these new panels were made composite with the girders by using shear studs in grouted pockets. The grouts used in the accelerated bridge construction project were designed to provide high early strength that would reduce the curing time.

2.2 Shear Connection Types

As mentioned in the previous section, accelerated bridge construction can be achieved by using composite modular bridge system. A proper shear connection detail is needed to develop composite

action between the steel plate girders and the full-depth precast concrete deck panels for this system. The following sections present several shear connection details that can be used to connect the steel plate girders to the precast concrete deck panels. A literature review on the shear stud connection, which is commonly used in the conventional bridge construction, is also included in the following section for comparison purposes.

2.2.1 Conventional Shear Stud Connections

Shear stud connection is the most commonly used type of shear connection in conventional composite bridge construction. The studs are welded on top of the girder flange using a weld gun. Stud welding can be done either in the field or in the shop. In conventional bridge construction, the studs are spaced continuously along the span of the bridge rather than in large intervals. This construction method requires an extended period of time to complete because time is required for onsite formwork placement, reinforcing placement, slab casting, slab curing and formwork removal. The shear studs would be embedded in the concrete after the slabs are cast on the construction site. When the concrete are hardened, the studs would bear against the concrete and they would be able to transfer the horizontal shear force at the steel-concrete interface.

The strength of the shear studs needed to transfer the horizontal shear force at the steel-concrete interface has been established from experimental tests [Ollgaard et al. 1971]. Based on the test results, empirical formulas have been developed for calculating the resistance of the welded shear studs. Tests have shown that the height of the stud must be at least four times the diameter of the stud in order to develop the full capacity of the shear connector. Therefore, this condition has become part of the shear connector design requirements written in the Canadian Highway Bridge Design Code [2006]. Clause 10.11.8.3 of the Canadian Highway Bridge Design Code specifies that the factored shear stud resistance is the lesser of the following two equations:

$$q_r = 0.5\, \emptyset_{sc}\, A_{sc}\sqrt{f_c' E_c} \tag{2.1}$$

$$q_r = \emptyset_{sc} F_u A_{sc} \tag{2.2}$$

where q_r is the factored shear resistance of a welded shear stud, ϕ_{sc} is the shear connector resistance factor, A_{sc} is the cross section area of one shear stud connector, f'_c is the specified compressive strength of concrete, E_c is the modulus of elasticity of concrete and F_u is the minimum tensile strength of the stud.

Equation 2.1 is based on test results and it represents the failure mode of concrete crushing [Ollgaard et al. 1971]. When the capacity of the shear stud connection is reached, the concrete adjacent to the studs may failed by crushing. The other failure mode of the shear stud connection is stud fracturing. Stud fracturing may occur after the tensile capacity of the stud has been exceeded. Equation 2.2 forms an expression to calculate the tensile capacity of the stud.

2.2.2 Grout Pocket Shear Stud Connections

The most common way to connect the steel plate girders to the precast concrete deck panels is by using shear studs in grouted pockets. Rather than spacing the shear studs continuously along the span of the bridge, the grouted pocket shear connections have the shear studs welded in groups on top of the girders' flanges. The groups of shear studs are spaced at relatively large distance apart and their locations coincide with the full depth pockets in the precast panels (Figure 2-3). After the concrete deck panels are placed on the girders, the pockets are grouted onsite to form the shear connection. Once the grouts are hardened, composite action is achieved. The groups of shear studs would bear against the hardened grout mixtures to transfer the horizontal shear force at the steel-concrete interface.

Figure 2-3: Precast Concrete Deck Panels with Grout Pockets [Lam and Tharmabala 2011]

Huh et al. [2010] conducted a series of laboratory tests to confirm the effectiveness of the resulting composite action achieved by using the grout pocket shear connections. Four composite girders were constructed and they were subjected to extensive cyclic loading followed by ultimate load tests. The test results demonstrated that the performance of these connections would not be affected by the cyclic loading. The slope of the load-deflection curves remained consistent throughout the entire cyclic load tests. The test results also demonstrated that these connections could achieve the same

level of composite action that was developed in the conventional shear connection systems, as the measured longitudinal strains over the depth of the girders confirmed that full composite action could be achieved.

The grout pocket shear connections require the use of field grouting to connect the steel plate girders to the full depth precast concrete deck panels. The use of field grouting has drawbacks even though it enables the accelerated bridge construction of composite bridges. Firstly, field grouting is expensive and labour intensive on the construction site. Secondly, composite action is not achieved until the grout has cured and attained the adequate compressive strength. In other words, the bridge construction duration is dependent on the grout curing time as well as other factors. Finally, the grouting operation creates a permanent connection between the steel plate girders and the precast concrete decks. The creation of a permanent connection makes deck replacement more difficult in the future.

2.2.3 Panel End Connections

Bowser [2010] developed the concept of panel end connections for the construction of portable steel-precast composite bridges. To fabricate these connections, gusseted bearing plates would be welded on top flange of the steel girder and the precast concrete panels would be fabricated with a steel embed assembly that consisted of shear studs fastened to steel angles (Figure 2-4). The gusseted bearing plates were used to facilitate the connections between the precast concrete deck panels and the steel plate girders. Once the panels were precast, they could be bolted to the bearing plates onsite to construct the steel-precast composite bridge (Figure 2-5). The shear loads from the concrete deck panels would be transferred to the steel bearing plates at each panel end.

To enable composite action between the deck panels and the steel plate girders, the panel ends of these connections should be tightly connected to the gusseted bearing plates. Strict construction tolerance in the longitudinal direction should be used to ensure that the panel ends would be tightly connected to the bearing plates. Slotted holes were proposed at the panel ends of these connections to provide the necessary geometric tolerance in the transverse direction.

The proposed length of the precast concrete deck panels was three metres. In other words, the panel end connections were spaced three metres apart. This spacing would typically be larger than the spacing of other shear connections; therefore, the panel end connectors would need to transfer a large amount of shear force at each of its location.

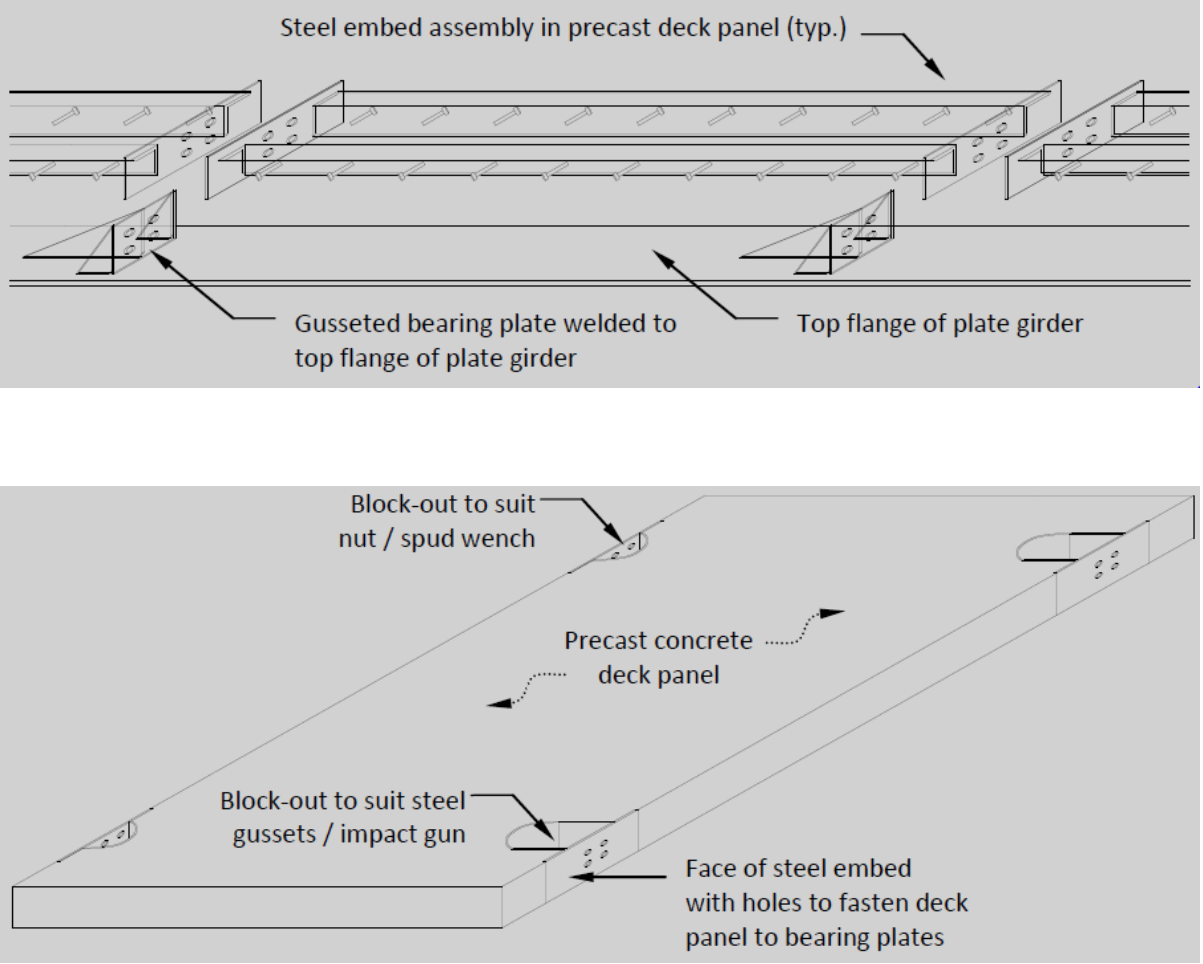

Figure 2-4: Steel Embed Assembly (Top) and Precast Concrete Deck Panel (Bottom) for Panel End Connections [Bowser 2010]

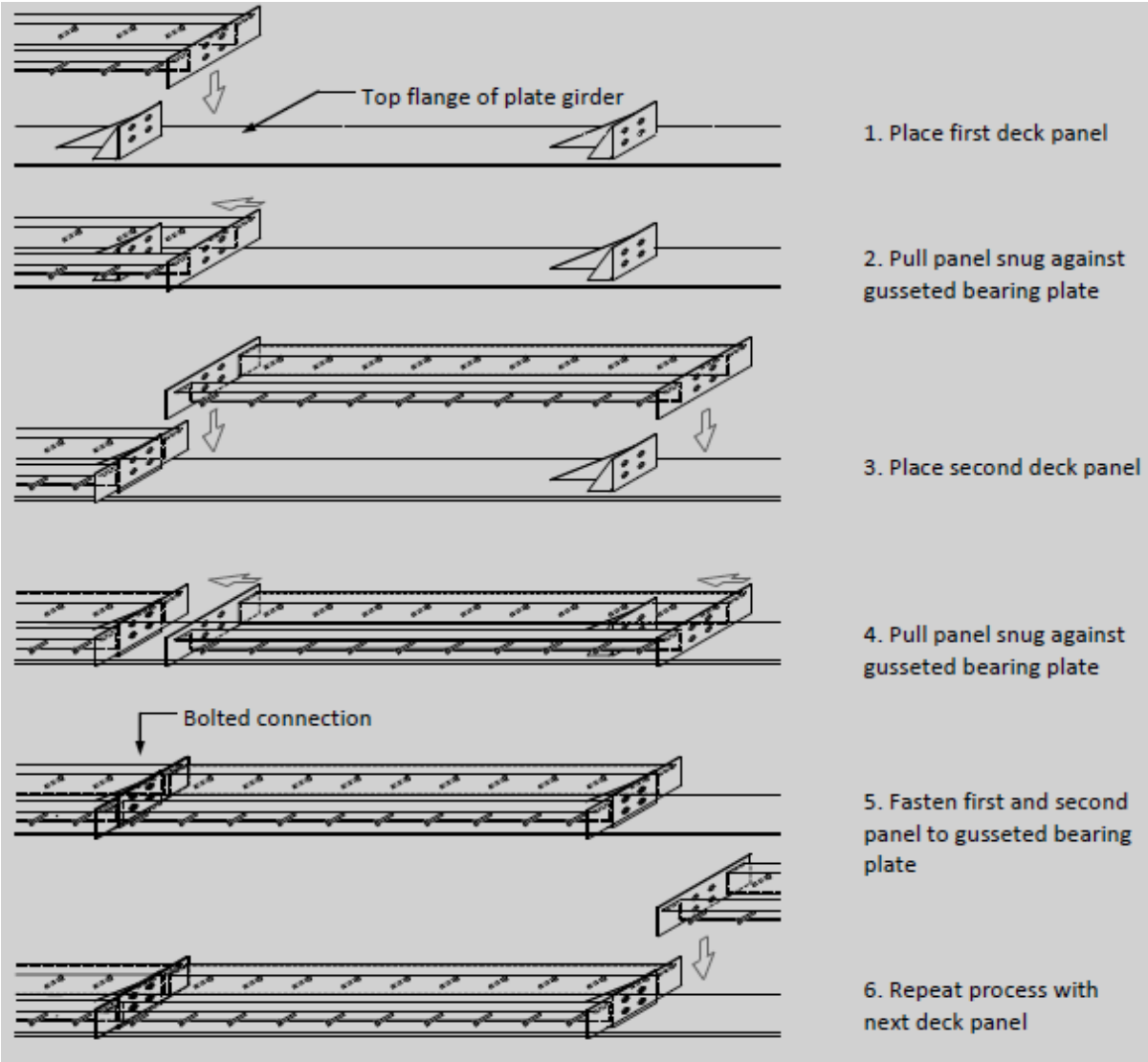

Figure 2-5: Installation Sequence of Panel End Connections [Bowser 2010]

2.2.4 Bolted Connections

Bolt connections can be an innovative alternative to connect the full-depth precast concrete deck panels to the steel plate girders. To prefabricate bolted composite modular bridge systems, bolt holes have to be formed in the precast concrete deck panels and bolt holes have to be drilled on the top flanges of the steel plate girders. Proper construction tolerance should be given so that the holes from the precast concrete decks would align to those on the flanges of the steel plate girders. Once the deck panels are placed on the steel girders onsite, structural bolts can be used to bolt the deck panels to the steel plate girders. Clause 10.4.5 of the Canadian Highway Bridge Design Code [2006] specifies that

only ASTM A325, ASTM A325M, ASTM A490 and ASTM A490M high strength bolts can used for bridge structures. After the bolts are installed as the shear connectors continuously along the span of the bridge, composite action between the concrete panels and the steel girders can be developed.

High strength bolts used in the application of bridge structures are typically pretensioned during the bolt installation process. Pretensioning the bolts would create slip-critical connections, which could work well for structures subjected to repetitive loadings. When the bolts are pretensioned, they are required to be tightened to 70% of the minimum tensile strength of the bolts [Canadian Standards Association 2006]. The most common way to pretension the bolts is by using the turn-of-nut method. When the nuts are turned on against the gripped material and the bolts elongates, pretension is induced in the bolts [Kulak and Grondin 2006].

In 1973, the New York State Thruway Authority (NYSTA) launched a research and development program to evaluate the effectiveness of using bolted connections in steel-precast composite bridges [Issa et al., 1995]. The NYSTA rehabilitated part of the Amsterdam Interchange Bridge by using bolt connections on an experimental basis. Six full-depth precast concrete deck panels were used to replace half of span 2 of the deteriorated bridge decks. The panels were 203 mm x 1.2 m x 6.7 m. Bolt holes were drilled through the sleeves in the panels and they were drilled through the top flange of the girders to allow fastening of the high strength bolts. Full pretensioning of the bolts could not be assured at the time of construction because the NYSTA was concerned that excessive bolt tensioning would result in the breakage of the deck panels. Figure 2-6 showed the bolt connections details for the Amsterdam Interchange Bridge.

The rest of the deteriorated bridge decks were rehabilitated by using conventional cast-in-place concrete decks with shear stud connections [Issa et al., 1995]. The experimental bridge performed very well after the rehabilitation took place. Bridge inspectors had reported that all precast deck panels performed as well as the cast-in-place concrete decks [Issa et al., 1995].

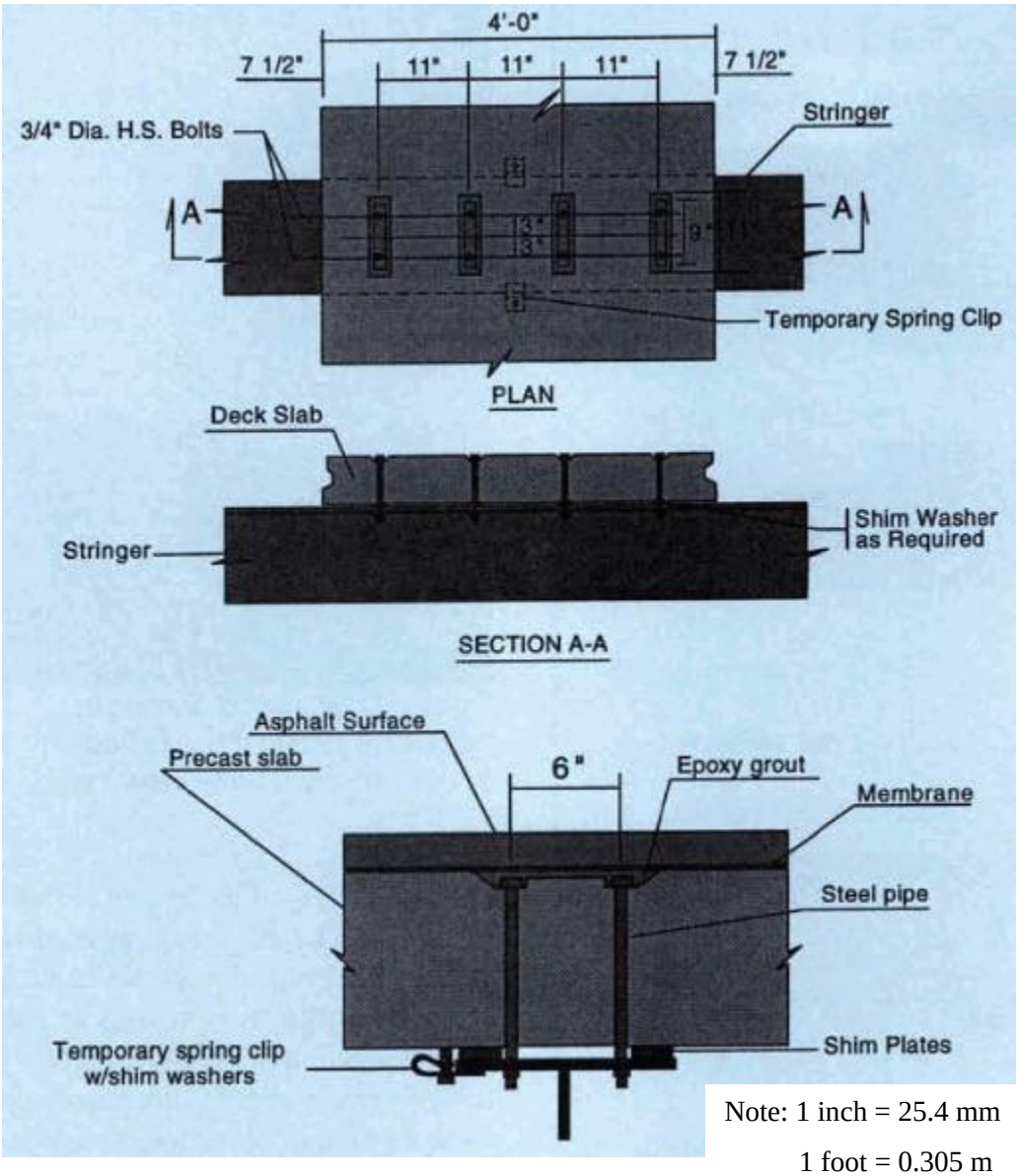

Figure 2-6: Bolt Connections Details for the Amsterdam Interchange Bridge [Issa et al., 1995]

Recently, Au et al. [2010] conducted a laboratory research project to investigate the feasibility of using bolted connections on composite bridge girders. Two identical test specimens were built, where the full-depth precast concrete deck panels were made composite to the steel girders by using bolts. Some hairline cracks were observed in the deck panels after the ASTM A325 bolts were pretensioned. According to the test results, repetitive cyclic loading did not affect the performance of the bolted connection system. The slope of the load-deflection curves remained fairly uniform throughout the entire cyclic load tests. Since the measured deflections were larger than the predicted

values, the bolted connections system appeared to be less stiff than the convention shear stud connection system. The test results also demonstrated that the bolted connections could achieve an effective level of composite action between the panels and the girders. The measured longitudinal strains across the depth of the girders confirmed that composite action could be achieved by using these connections; however, this composite action might not be as strong as the one from the conventional shear stud connections. Au et al. [2010] recommended further testing of the bolted connections system to confirm the above observed composite behaviour. It should be noted that one of the test specimens failed by fatigue fracture unexpectedly. The fatigue failure occurred at the midspan of the steel girder.

Research on using bolted connections had also been done for the application of strengthening existing bridge girders. Kwon et al. [2010] conducted an experimental program to study the effects of using post-installed shear connectors, such as high strength bolts, to develop composite action in existing non-composite slab-on-girder bridges. Two bolted connections specimens were constructed and they were tested under static and fatigue loads. Each specimen consisted of a concrete blocks and a steel plate. The block and the plate were connected by using ASTM A325 high strength bolts after bolt holes were drilled in each of the structural components. The bolted connections were subjected to single shear connector test setup. From the static test results, the load-slip behaviour of the 22 mm diameter bolts was obtained. From the fatigue test results, the high strength bolts exhibited significant higher fatigue strength than the conventional shear stud connectors. Figure 2-7 showed the bolted connections detail studied by Kwon et al. [2010].

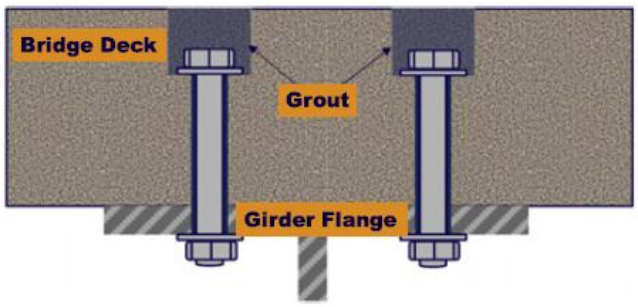

Figure 2-7: Bolted Connections Detail [Kwon et al. 2010]

2.2.5 Friction Connections

The interface friction between the full-depth precast concrete deck panels and the steel plate girders can also be used to resist the horizontal shear force at the steel-concrete interface. The friction

connections can also be used in conjunction with other shear connectors. By increasing the coefficient of friction at the steel-concrete interface, the number of shear connectors required to facilitate the connection would decrease. Therefore, the cost of making the shear connections along the bridge could decrease if the coefficient of friction at the interface was increased.

Papastergiou and Lebet [2010] proposed a new type of friction enhanced surface connection for the construction of steel-precast composite bridge girders. The proposed connection utilized adherence and friction to resist the horizontal shear force at the steel-concrete interface. It consisted of an embossed steel plate welded longitudinally to the top flange of the steel girders (Figure 2-8). The full-depth concrete deck panels were precast with a longitudinal rib that matched the size of the embossed steel plate. During the deck panel fabrication process, retarder, water-jetting and sandblasting were used at the soffit of the panels so that the soffit surface was roughened to increase friction. Once the deck panels were placed on the steel plate girders onsite, high strength grouts were injected to fill any gap between the embossed plate and the deck panels.

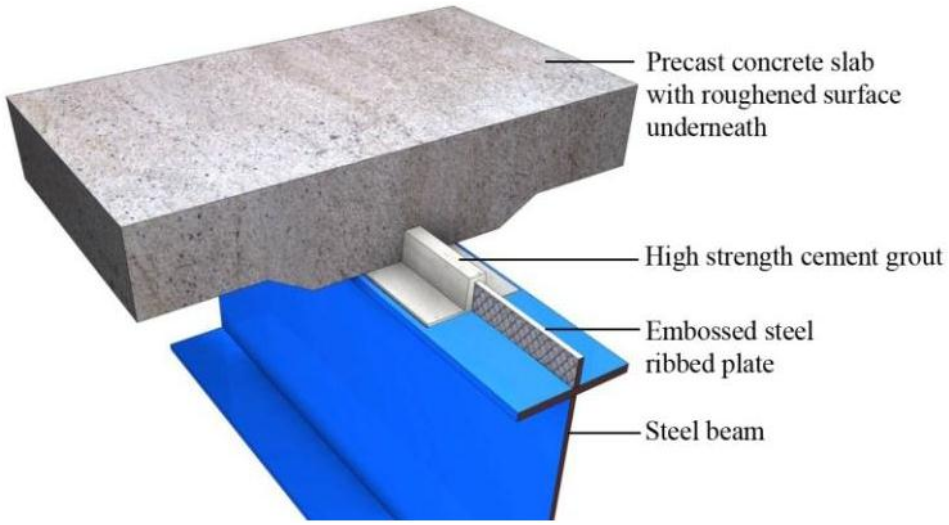

Figure 2-8: Connection by Adherence and Friction [Papastergiou and Lebet 2010]

Direct shear tests were conducted by Papastergiou and Lebet [2010] to study the behaviour of the ribbed steel-grout interface and the roughened concrete-grout interface. Both interfaces were tested under static loads, and they will be tested under fatigue loads in the near future. From the static load test results, the ultimate shear resistance of each interface was plotted as a function of the applied normal stress on the interface. The relationships between the shear stress and the slip value at different normal stress values were also obtained.

Push tests were also conducted by Papastergiou and Lebet [2010] to study the behaviour of the proposed connection where the above two interfaces co-exist. Twelve specimens were constructed and tested under static and fatigue loads. Preliminary results from the static load test showed that the connection had high initial stiffness and low ductility. When the specimen failed ultimately, only a slip value of 1.75 mm was achieved. Preliminary results from the fatigue load test showed that the connection integrity was not affected by the repetitive cyclic loading.

2.2.6 Shear Lug Connections

The concept of shear lug connections is a novel idea that can be used for the construction of composite modular bridges. These connections utilize shear lugs to connect the steel plate girders to the full-depth precast concrete deck panels. To prefabricate the shear lug connections, the lugs have to be welded to the top flanges of the steel plate girders in the steel fabrication shop and match cast holes have to be formed at the soffit of the precast concrete deck panels. The locations of the match cast holes have to coincide precisely with the locations of the shear lugs so that the precast deck panels can be properly placed on the steel plate girders onsite. Furthermore, proper construction tolerance should be detailed so that the shear lugs would be snug against the match cast holes when the precast panels are assembled with the plate girders. Once the panels are placed on the plate girders, composite action is achieved. The shear lugs along the span of the bridge would bear against the match cast holes to transfer the horizontal shear force at the steel-concrete interface.

The shear lug connections are an established type of connections used to connect the steel columns to the concrete foundation [Fisher and Kloiber 2006]. Even though the concept of these connections has never been used for the construction of composite bridges, it has been used to transfer shear forces from the columns to the foundation. When it is used in this application, the steel lugs are welded to the underside of the column base plates and they are placed into the pre-formed voids located at the top of the foundation (Figure 2-9). Interlock between the lugs and the foundation can be created once the lugs are placed into the voided part of the foundation. The shear forces from the columns can be transferred to the foundation because the lugs would bear against the concrete. It should be noted that grouts are typically used between the base plates and the foundation to transfer the compression loads (Figure 2-9). Therefore, the shear lug base plate connections are usually made into a permanent connection.

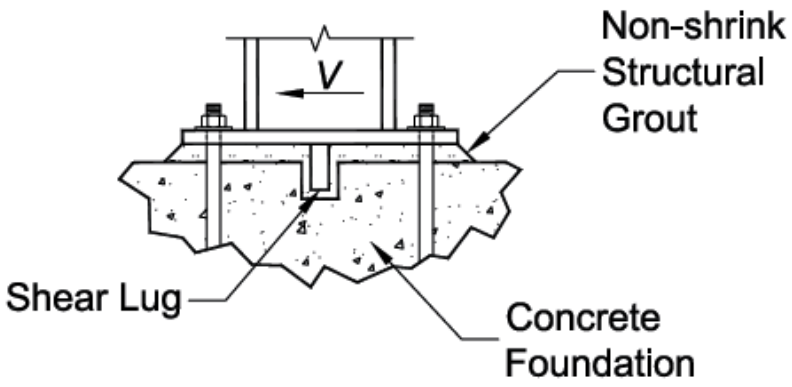

Figure 2-9: Shear Lug Base Plate Connections [Fisher and Kloiber 2006]

2.3 Analytical Models of Shear Strength for Bolted Connections

As mentioned in Section 2.2.4, high strength bolts used in the application of bridge structures are typically pretensioned to create slip-critical connections. Clause 10.18.2.3.1 of the Canadian Highway Bridge Design Code [2006] specifies that all bolted joints required to resist shear shall be designed as slip-critical connections. Slip-critical connections are specified in bridge structures because they perform better than bearing connections when the connections are subjected to repetitive loading. The high strength bolts are pretensioned and the bolt clamping force would create frictional resistance between the jointed parts. Once the frictional resistance of a joint is overcome by external loading, the connected parts would slip until they bear against the bolts and the joint would become a bearing connection.

The following sections present several models that have been used to predict the shear strength of bolted connections. Section 2.3.1 presents slip resistance models for the slip-critical connections. Section 2.3.2 presents ultimate shear capacity models for the bearing connections.

2.3.1 Models of Slip Resistance

Slip-critical connections have low probability of slip at any time during the life of the structure [Kulak et al., 1987]. These connections are used to meet the serviceability requirement where a major connection slip would endanger the serviceability of the structure. Since these connections are used to meet the serviceability limit state requirement, they are designed and evaluated by using service loads and must not slip into bearing under service loads.

Based on first principals, the slip resistance of a bolted joint can be expressed by using the following Equation [Kulak 2005]:

$$V_{slip} = k_s\, m\, n\, T_i \tag{2.3}$$

where k_s is the slip coefficient of the connected materials, m is the number of slip planes, n is the number of bolts in the joint and T_i is the bolt pretension.

Equation 2.3 shows that the slip resistance is dependent on the slip coefficient and the bolt clamping force for any given number of slip planes and bolts. The slip coefficient represents the friction coefficient prior to the initiation of slip and it can only be determined experimentally [Kulak et al., 1987].

The Research Council on Structural Connections published the following design equation (Equation 2.4) to calculate the slip resistance of slip-critical connections [Kulak 2005]. It should be noted that a 5% probability of slip was chosen in order to develop the design equation and this 5% probability of slip corresponded to bolts that were installed by using the turn-of-nut method [Kulak 2005].

$$R_s = \emptyset\, \mu\, D\, T_m\, N_b\, N_s \tag{2.4}$$

where R_s is the slip resistance of the joint, ϕ is the modifier to reflect the bolt hole condition (1.0 for standard holes, 0.85 for oversized and short-slotted holes, 0.70 for long-slotted holes perpendicular to force, 0.60 for long slotted holes in direction of force), μ is the slip coefficient (same as k_s in Equation 2.3), D is the slip probability factor that equals to 0.80, T_m is the specified minimum bolt pretension, N_b is the number of bolts in the joint and N_s is the number of slip planes.

Equation 2.4 is literally the same as Equation 2.3, where the slip resistance of a bolted joint is derived from first principals. The modifier, ϕ, in Equation 2.4 shows that the slip resistance decreases whenever oversized or slotted holes are used. It should be noted that the slip probability factor, D, accounted for the distribution of the actual slip coefficients about their mean value [Kulak 2005].

Clause 10.18.2.3.2 of the Canadian Highway Bridge Design Code [2006] specifies that the slip resistance, V_s, of a bolted joint shall be calculated by using the following equation:

$$V_s = 0.53\, C_1\, k_s m\, n\, A_b\, F_u \tag{2.5}$$

where C_1 is a coefficient that relates the specified initial tension and mean slip to a 5% probability of slip for bolts installed by using the turn-of-nut method, k_s is the mean slip coefficient determined in

the Code or by Approved tests, m is the number of slip planes, n is the number of bolts in the joint, A_b is the nominal cross-section area of a bolt and F_u is the ultimate tensile strength of the bolt.

In Equation 2.5, the term 0.53 A_b F_u represents the bolt clamping force. This term can be written as 0.70 x 0.75 x A_b x F_u [Kulak 2005]. The term 0.70 F_u is 70% of the ultimate tensile strength of the bolt and it is also the required minimum bolt pretension strength according to the Canadian Highway Bridge Design Code [2006]. The term 0.75 A_b converts the nominal cross-section area, A_b, of a bolt to the effective stress area of the bolt through the threads [Kulak 2005]. Therefore, the 0.70 x 0.75 x A_b x F_u term represents the specified minimum bolt pretension force.

According to Equation 2.3, the slip resistance is a product of the slip coefficient, the number of slip planes, the number of bolts in the joint, and the bolt clamping force. Equation 2.5 has all of the above four variables with an additional coefficient of C_1. The coefficient C_1 relates the specified initial tension of 70% F_u and the mean slip coefficient k_s to a probability of slip of 5%. The Canadian Highway Bridge Design Code [2006] provides three sets of values of C_1 and k_s for designers. Each set of values represents a common surface condition between the bolted steel parts.

2.3.2 Models of Ultimate Shear Capacity

As mentioned in Section 2.3, when the slip resistance of a joint is overcome by external loading, the connected parts would slip until they bear against the bolts. In other words, slip-critical connections become bearing connections after the slip resistance of the connections is exceeded. This phenomenon is why slip-critical connections must also be designed as bearing connections subjected to factored loads. The design of bearing connections is conducted at ultimate limit state to prevent the failure of the connections under ultimate loads.

The shear transfer mechanism of bearing connections can be better understood after reviewing the shear transfer models from the American Concrete Institute Building Code. Provision 11.6 of the American Concrete Institute Building Code Requirements [2008] provides guidance on calculating shear transfer across an interface between two materials. This provision can also be used to consider shear transfer across a crack in concrete structures or across an interface between two concretes cast at different times [American Concrete Institute 2008]. Based on Provision 11.6, the shear transfer strength is calculated according to Equation 2.6 when the shear reinforcement is perpendicular to the shear plane. When the shear reinforcement is inclined to the shear plane, the applied shear force at an

interface will produce tension in the reinforcement. In this case, Equation 2.7 can be used to calculate the shear transfer strength.

$$V = \mu\, A_{vf}\, f_y \tag{2.6}$$

$$V = (\mu\, sin\alpha\ + \cos\alpha)\, A_{vf}\, f_y \tag{2.7}$$

where V is the shear transfer strength, μ is the friction coefficient, α is the angle between the shear reinforcement and the shear plane, A_{vf} is the area of shear reinforcement across the shear plane and f_y is the yield strength of the reinforcement.

As shown in Equation 2.6 and 2.7, the shear transfer strength depends on the friction coefficient, the amount of shear reinforcement and the yield strength of the reinforcement. These Equations imply that slip will occur at the shear plane when it is subjected to shear load. They also imply that the slippage movement at the shear plane is sufficiently large enough to yield the reinforcement when ultimate load is applied [American Concrete Institute 2008]. After the reinforcement have yielded, the applied shear force is resisted by the interface friction as well as the dowel action of the reinforcement. It should be noted that Equation 2.6 and 2.7 do not explicitly represent or predict the dowel action contribution of the shear transfer strength.

Clause 10.18.2.3.3 of the Canadian Highway Bridge Design Code [2006] specifies that the factored shear resistance, V_r, of the bolts shall be calculated by using the following equation:

$$V_r = 0.60\, \emptyset_b n\, m\, A_b\, F_u \tag{2.8}$$

where ϕ_b is the bolt resistance factor, n is the number of bolts in the joint, m is the number of shear planes, A_b is the nominal cross-section area of a bolt and F_u is the ultimate tensile strength of the bolt.

Equation 2.8 shows that the shear resistance is dependent on the bolt area and the ultimate tensile strength of the bolt for any given number of shear planes and bolts. This design equation is formulated based on test results, where test results have shown that the shear strength of a high strength bolt is approximately 60% of the tensile strength, F_u, of the bolt [Kulak and Grondin 2006]. It should be noted that the bolt resistance factor, ϕ_b, is taken as 0.80.

Equation 2.8 is to be multiplied by 0.7 if the bolt threads are intercepted by a shear plane [Kulak and Grondin 2006]. When the bolt threads are intercepted by a shear plane, bolt failure may occur through the threads, where the cross-section areas are reduced by 30%. The factored shear resistance of the bolts is reduced when the bolt area available for shear transfer is reduced.

The form of Equation 2.8 is very similar to that of Equation 2.6. The coefficient of 0.6 in Equation 2.8 acts as the effective coefficient of friction. This effective coefficient of friction relates the shear strength of the bolts to the tensile strength of the bolts. Both Equation 2.8 and 2.6 indicate that the shear transfer strength of the bolts is dependent on the cross-section area of the bolts across the shear plane. Equation 2.8 utilizes the ultimate tensile strength of the bolt instead of the yield strength of the bolt to find the bolt shear resistance. Ultimate tensile strength is used because shear deformation of bolts is highly nonlinear and the use of yield strength of bolts would not be appropriate. Equation 2.8 has three more parameters than Equation 2.6. These parameters are the bolt resistance factor, ϕ_b, the number of bolts in the joint, n, and the number of shear planes, m.

As mentioned in Section 2.2.4, Kwon et al. [2010] conducted an experimental program to study the effects of using post-installed shear connectors to develop composite action in existing non-composite slab-on-girder bridges. Prior to the experimental work conducted by Kwon et al. [2010], Hungerford [2004], Schaap [2004], and Kayir [2006] investigated eleven types of post-installed shear connectors for their structural performance and constructability. The post-installed shear connectors were tested under static and fatigue loads by using a single shear test setup. Kayir [2006] compared the static test results of the post-installed shear connectors to the design equations that would predict the ultimate strength of conventional shear studs [Ollgaard et al. 1971]. He also compared these results to the design equations that would predict the ultimate strength of concrete anchors [American Concrete Institute 2005]. None of the design equations conservatively predicted the ultimate strength of all the post-installed shear connectors. Kayir [2006] proposed the following equation (Equation 2.9) to estimate the ultimate strength of the post-installed shear connectors, Q_u, for design purposes:

$$Q_u = 0.5\, A_{sc} F_u \tag{2.9}$$

where A_{sc} is the effective shear area of the connector and F_u is the ultimate tensile strength of the connector.

Equation 2.9 shows that the ultimate shear strength is dependent on the effective shear area of the connector and the ultimate tensile strength of the connector. In this case, the effective shear area of the threaded connector is calculated as 80% of the gross area of the connector [Kayir 2006].

The form of Equation 2.9 is very similar to that of Equation 2.8. The coefficient of 0.5 in Equation 2.9 acts as the effective coefficient of friction. This effective coefficient of friction relates the shear strength of the connectors to the tensile strength of the connectors. Similarly, the coefficient of 0.6 in

Equation 2.8 acts as the effective coefficient of friction and it also relates the shear strength of the connectors to the tensile strength of the connectors. In contrast, Equation 2.9 utilizes the effective shear area of the connector instead of the nominal area of the connector to find the connector shear strength.

Chapter 3
Finite Element Analysis of Composite Girders with Panel End Connections

This chapter describes the finite element analysis that was conducted on composite girders models with panel end connections. First, the finite element models developed are described in Section 3.1. The analysis results in terms of girder load-displacement behaviour, stress and strain profiles, and connection force distributions are then presented and discussed in Section 3.2.

3.1 Finite Element Model Description

After developing the concept of panel end connections, Bowser [2010] conducted a finite element analysis (FEA) to compare the performance of a composite bridge girder with panel end connections to a conventional shear stud bridge girder. Two FEA models were developed by Bowser [2010] using the software ABAQUS. One FEA model was built for the shear stud girder and the other was built for the panel end connected girder. To further study the panel end connections, three additional FEA models were developed in the current study based on the work from Bowser [2010]. They are a panel end connected girder model with reduced connector stiffness, a fully composite girder model and a non-composite girder model. The panel end connected girder model with reduced connector stiffness was built to study the effect of the connector stiffness on the composite behaviour of the girder. To evaluate the degree of composite action in the shear stud and panel end connected girders, the fully composite girder and non-composite girder models were built. All models were identical except for the shear connection details.

The single girder models were developed based on an actual twin girder composite bridge designed for a British Columbia Forest Service L165 truck load [Bowser 2010]. Figure 3-2 shows the section details of the twin girder bridge. The bridge consisted of two stiffened plate girders, a concrete deck slab and shear connectors along the top flanges of the girders. Other bridge components, such as cross bracing, plan bracing and girder splices, were not included as part of the research study because they were expected to have little or no impact on the composite behaviour of the girders. Figure 3-1 shows the overall geometry and boundary conditions of the simply supported 36 m twin girder bridge.

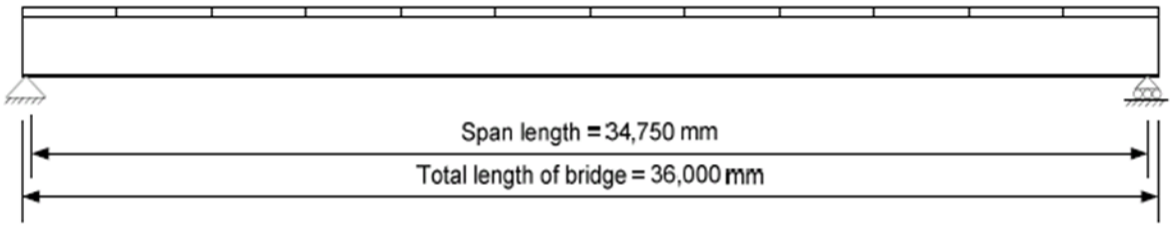

Figure 3-1: Support Conditions of Twin Girder Composite Bridge [Bowser 2010]

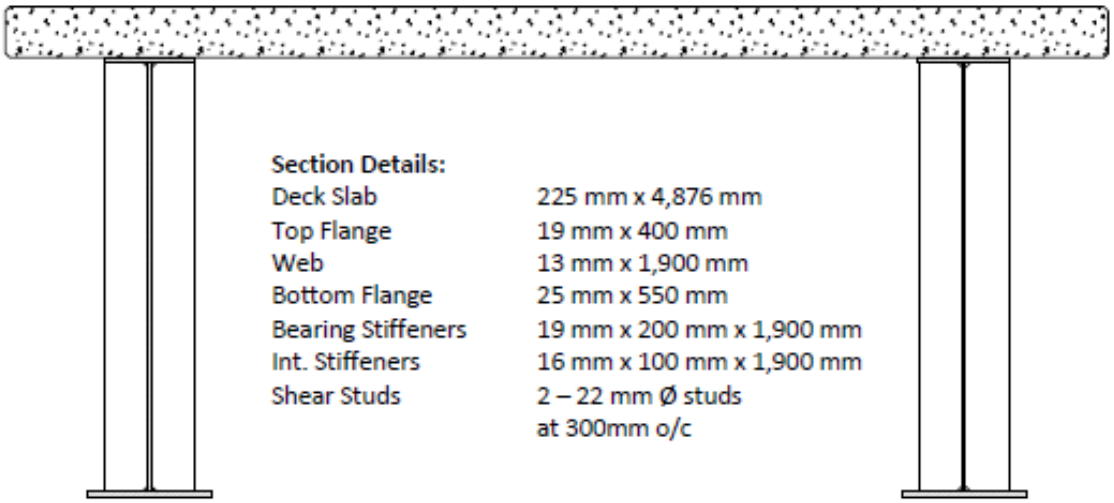

Figure 3-2: Cross-section Details of Twin Girder Composite Bridge [Bowser 2010]

3.1.1 Element Selection

Three dimensional SR4 shell elements were used to model the stiffened plate girder and the concrete deck slab (Figure 3-3). Individual parts of the plate girder including top flange, bottom flange, web and stiffeners were created in ABAQUS and then merged together to form the stiffened plate girder. Four node shell elements were used because they would be able to capture the nonlinear responses, such as steel yielding and local buckling, of the composite plate girder. Brick elements were not used to model the concrete deck slabs because Baskar et al. [2002] found that brick element would restrict the rotation of the deck. Eleven integration points were used for the shell elements that were modelling the concrete deck slabs. The integration points through the thickness of the slab would allow stress and strain values to be computed at various depths. The quantity and location of the steel reinforcing bars were specified in the shell elements used to model the concrete deck slab. In other

words, steel reinforcing bars were automatically incorporated throughout the slab when the slab was modelled using shell elements.

Bowser [2010] introduced initial imperfection in the panel end connected girder model to investigate the effects of flange buckling, lateral torsional buckling and web buckling on the behaviour of composite girder. The objectives of introducing imperfection in the model were to illustrate that finite element analysis was capable of modelling the effects of buckling and to demonstrate that the effects of buckling did not negatively influence the composite response of the panel end connected girder. The initial imperfection in the panel end connected girder model was removed after Bowser [2010] confirmed that the effects of buckling did not negatively influence the response of the girder for the proposed panel end connection spacing. According to Bowser's analysis, flange buckling would not occur in the designed panel end connected girder since the top flange is Class 3 and since it is braced by the concrete deck. Web buckling occurred in the girder when imperfection was introduced in the model. However, the post-buckling shear capacity of the girder predicted by the model exceeded the theoretical shear resistance predicted using the Canadian Highway Bridge Design Code [2006]. As well, it was determined that web buckling failure would not govern the behaviour of the bridge for the truck load position considered in the current study. Since the focus of the study was the effect of the shear connector properties on the stresses and strains through the girder depth, it was decided not to include initial defects in the analysis so that the effects of these defects would not obscure the real focus of the study.

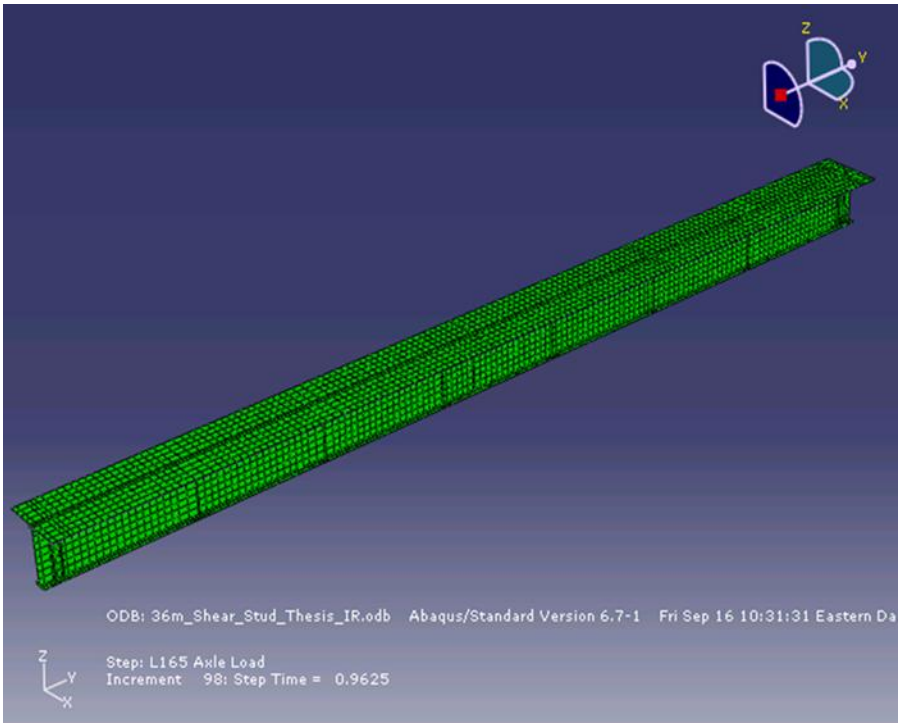

Figure 3-3: Finite Element Model of Composite Bridge Girder

3.1.2 Material Model

Bowser [2010] used a tri-linear stress-strain relationship to model the material property of structural steel of the stiffened plate girder (Figure 3-4). Three assumptions were made to define the tri-linear relationship. Firstly, the modulus of elasticity of the steel material was 200 GPa. Secondly, strain-hardening began only after the strain reached 50% of the ultimate strain. Thirdly, the ultimate strain, which was the strain corresponded to the ultimate stress, was equal to 0.1.

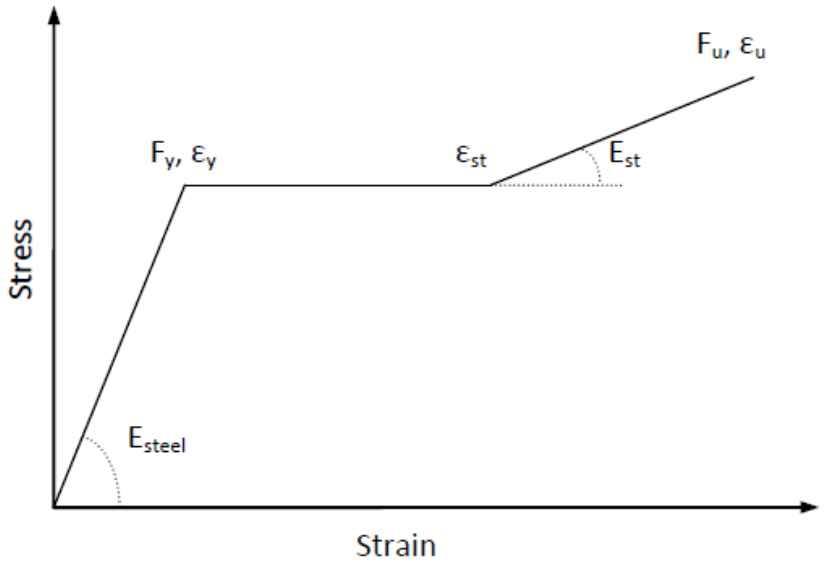

Figure 3-4: Tri-linear Stress-Strain Relationship for Structural Steel [Bowser 2010]

To model the material property of concrete, a stress-strain relationship developed by Carreira and Chu [1985] was used (Figure 3-5). According to this model, the concrete behaviour is linear-elastic up to a stress, σ, of $0.3f'_c$, where f'_c was the concrete compressive strength. When the stress exceeds $0.3f'_c$, a parabolic function is used to model the concrete behaviour,

$$\sigma = \frac{f'_c \cdot \beta \cdot \left(\frac{\varepsilon}{\varepsilon'_c}\right)}{\beta - 1 + \left(\frac{\varepsilon}{\varepsilon'_c}\right)^{\beta}} \tag{3.1}$$

where ε is the concrete strain, ε'_c is the concrete strain corresponded to the maximum concrete stress and β is a value defined by Equation 3.2.

$$\beta = \left(\frac{f'_c}{32.4}\right)^3 + 1.55 \tag{3.2}$$

To input the stress-strain relationship of the concrete into the ABAQUS models, a discrete representation of Figure 3-5 was used. Twelve data points that captured the shape of the stress-strain curve were selected from Figure 3-5 and linear segments between these points were assumed.

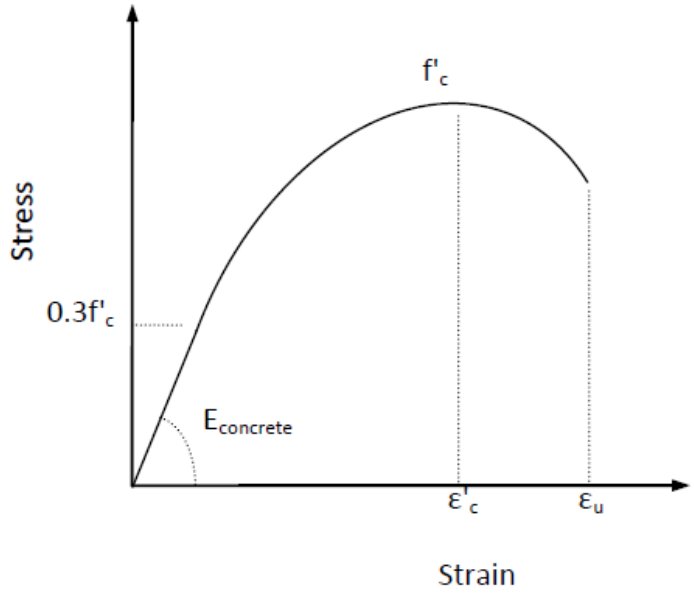

Figure 3-5: Stress-Strain Relationship for Concrete [Bowser 2010]

3.1.3 Composite Interaction Model

Every girder model had two properties that were set to specify the interaction between the concrete deck and the steel plate girder. First, a hard contact restraint was specified between the concrete deck and the steel plate girder. This restraint ensured that the soffit of the concrete deck was in contact with the top of the upper flange of the steel plate girder. It should be noted that a friction coefficient of 1.0 was used to further define surface condition between the concrete deck and the steel plate girder. Secondly, connector elements were specified between the concrete deck and the steel plate girder to enable composite action.

Connector elements were used to model the behaviour of the shear connections so that shear forces could be transferred between the steel plate girder and the concrete deck slab in the models. For the shear stud girder model, the load-slip properties of the shear stud connection were defined in the connector elements. Equation 3.3 describes the load-slip behaviour assumed in the shear stud girder model. This nonlinear relationship was developed by Hanswille et al. [2006].

$$P_i = P_{u,0} \cdot \left(1 - e^{-1.22 \cdot \delta_i^{0.59}}\right) \quad (3.3)$$

where P_i is the load transferred by a shear stud, $P_{u,0}$ is the static strength of a shear stud and δ_i is the slip.

Similar to the definition of nonlinear material behaviour, the load-slip properties of the connector elements in ABAQUS can only be done by using specific data points with straight line segments assumed in between. To develop the shear stud girder model, Bowser [2010] plotted the load-slip behaviour of the shear stud based on Equation 3.3. Eight data points that described the load-slip behaviour were subsequently chosen and the linear segments between these points were assumed. The first of these linear segments describes the initial (elastic) behaviour of the shear stud connection.

The fully composite girder model and the non-composite girder model were developed based on the shear stud girder model. The fully composite girder model was the same as the shear stud girder model except for one important difference: the shear studs were assumed to be infinitely stiff, thus preventing slip between the concrete deck slab and the steel plate girder. Similarly, the non-composite girder model was the same as the shear stud girder model except that its shear studs were assumed to have no stiffness so that slip at the steel and concrete interface could freely occur.

For the panel end connected girder model, the load-slip properties of the panel end connections were defined based on the properties of the gusset plates (recall that three gusset plates were used for each shear connector, as shown in Figure 2-4). Each of the gusset plates was designed and modelled to behave in an elastic – perfect plastic manner. Bowser [2010] estimated the gusset plate stiffness and yield load, given its geometry and the steel shear modulus (77 000 MPa) and strength (350 MPa). The connection elastic stiffness and yield load were found to be 5 501 237 N/mm and 3 333 749 N.

The panel end connected girder model with reduced connector stiffness was built based on the original panel end connected girder model developed by Bowser [2010]. In this model, however, the panel end connection stiffness was reduced to 500 000 N/mm, which was approximately ten times less than the original proposed connection stiffness. The same connector strength was assumed.

3.1.4 Applied Loading

In each of the five FEA models (fully composite, non-composite, shear stud and the two panel end connected models), the British Columbia Forest Service L165 truck load was placed at the location that would result in the maximum girder moment. The loads were applied in two steps. First, the dead

load associated with the plate girder and the concrete slab (increased by 20% to account for the miscellaneous details, such as cross bracing and plan bracing) was introduced. Next, the truck axle loads were applied gradually in load increments of less than 1% of the predicted ultimate load of the shear stud girder. Figure 3-6 shows the British Columbia Forest Service L165 truck load and Figure 3-7 shows the normal stress distribution for the shear stud girder at ultimate load.

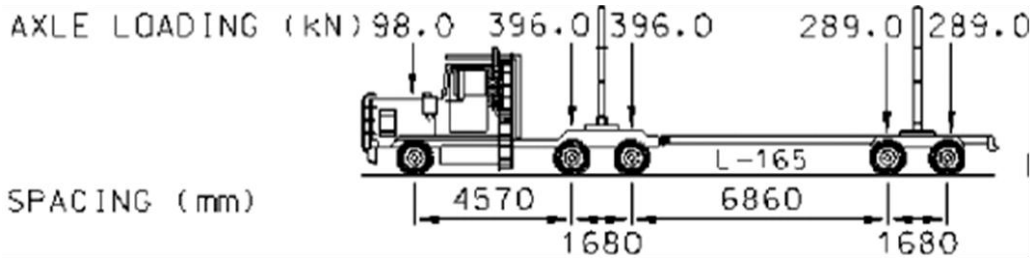

Figure 3-6: British Columbia Forest Service L165 Truck Load [Bowser 2010]

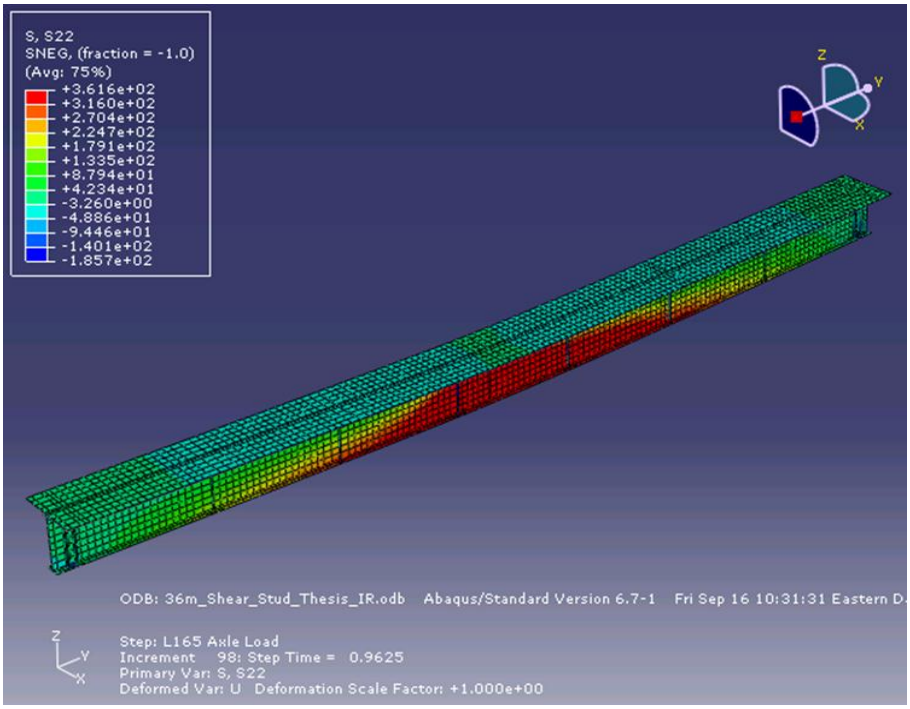

Figure 3-7: Longitudinal Normal Stress Distribution of Shear Stud Girder Model at Ultimate Load

3.2 Finite Element Analysis Results

The finite element analysis (FEA) results were analyzed to better understand the behaviour of the panel end connected girder models. First, the overall girder behaviour in terms of moment-deflection response was compared between the five models. The effect of shear connection type on the cross-sectional behaviour of the girders was examined at both service and ultimate load levels. At each load level, the stress and strain distributions over the girder depth were plotted for cross-sections at the third axle load location, where the moment was maximum. Finally, the connection force distributions along the girder span were plotted from the five model analyses. Both service and ultimate load levels were used to examine the effect of shear connection type on the shear flow at the steel-concrete interface.

3.2.1 Load-Displacement Behaviour

Figure 3-8 compares the overall girder behaviour of the five finite element models. The moment-displacement response of the shear stud girder was essentially the same as that of the pure composite girder. The panel end connected girder with actual (calculated) stiffness had a similar moment-displacement response to the shear stud girder. The main difference between these two girders was that the panel end connected girder had an ultimate moment capacity that was only 1% less than that of the shear stud girder. As the load was applied to these two girders, the panel end connected girder deflected slightly more than the shear stud girder. At the ultimate load, the deflection of the panel end connected girder was 4% larger than that of the shear stud girder. When the stiffness of the panel end connections was reduced to 500 000 N/mm, the overall girder behaviour changed only slightly. The ultimate moment capacity decreased by less than 1% and the deflection value increased by 13% when the panel end connection stiffness was decreased to 500 000 N/mm. As expected, the ultimate capacity of the non-composite girder was much less than the ultimate capacity of the composite girders (Table 3-1).

It should be noted that all models, except the non-composite girder model, failed by concrete crushing at the top fibre of the deck at ultimate load. As mentioned in Section 3.1.4, all models were analyzed by using load control, where the truck axle loads were applied gradually in load increments. The models failed when they could not take any additional load increase. Concrete crushing failure was confirmed when the concrete strain at the top fibre of the deck at maximum moment location exceeded the crushing strain. The non-composite girder model failed by web buckling as a result of a large amount of compressive stress acting over a large portion of the girder web depth.

Table 3-1: Ultimate Moments and Deflections of the FEA Girder Models

	Girder Models				
	Pure Composite	Shear Stud	Panel End Connected (actual *k*)	Panel End Connected (reduced *k*)	Non-Composite
Moment (kN m)	18 829	18 793	18 617	18 533	14 157
Deflection (mm)	473	470	488	554	337

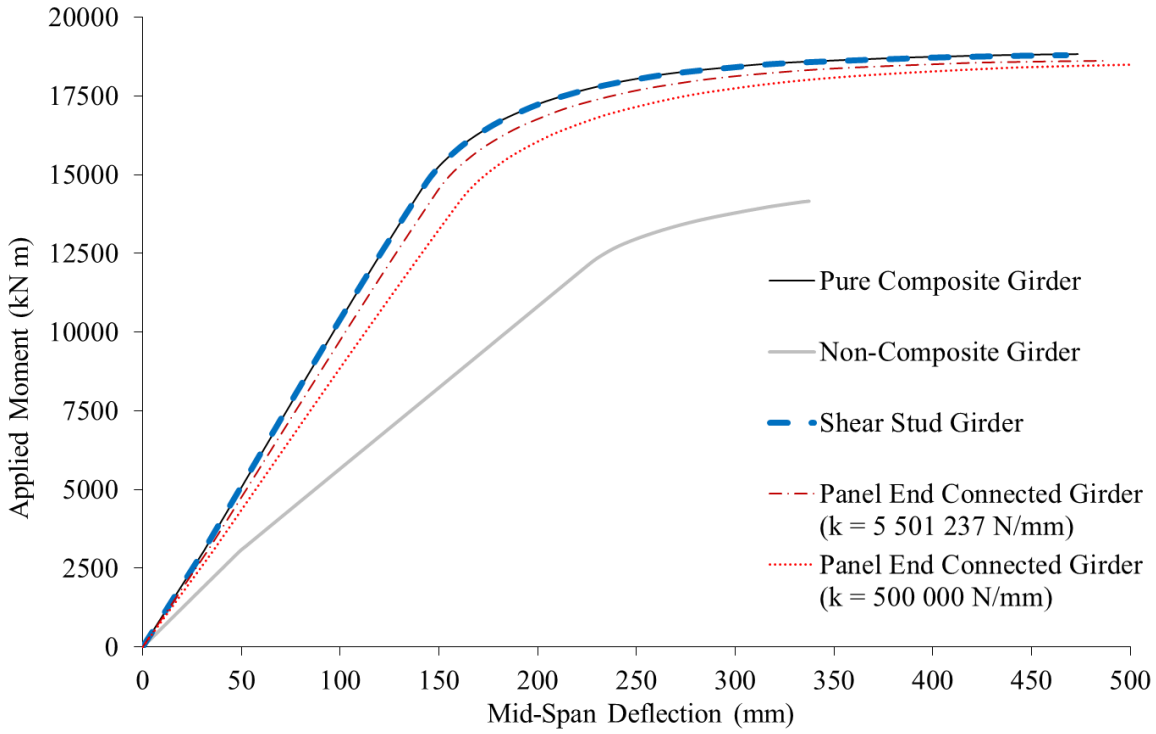

Figure 3-8: Comparison of Moment-Deflection Responses

3.2.2 Stress and Strain Profiles through Composite Girder Depth

Figure 3-9 and 3-10 present the girder cross-sectional behaviour at the third axle load (i.e. maximum moment) location under the service moment (i.e. under the unfactored dead and live load). It should

be noted that the difference in the applied moment at the midspan and under axle 3 was always less than 1% because the horizontal distance between the two locations is only 455 mm.

Figure 3-9 presents the normal stress distributions under service load. The stress distribution for the shear stud girder was essentially identical to that of the pure composite girder. The panel end connected girder with actual connector stiffness had a similar stress distribution to the shear stud girder. The only difference between these two distributions was that the panel end connected girder had slightly more compression stress in the plate girder. When the stiffness of the panel end connections was decreased to 500 000 N/mm, the amount of compression stress in the plate girder was increased. As expected for the non-composite girder, half of the steel cross section was in compression and the other half was in tension. Thus, the stress distribution for this model is significantly different from those seen in the other models.

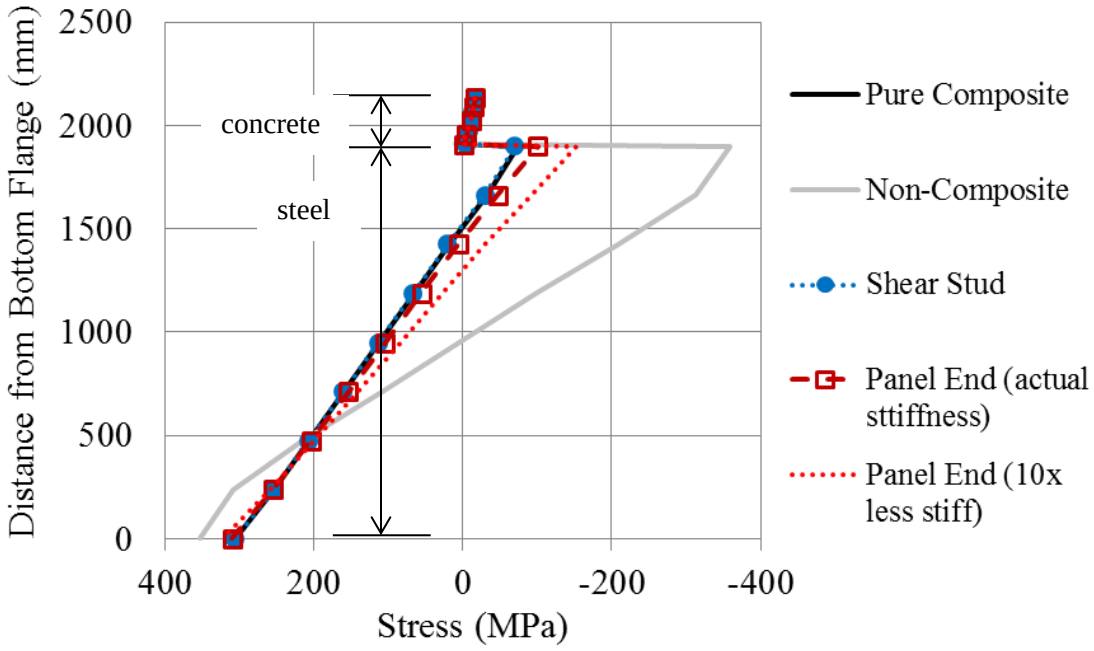

Figure 3-9: Stress Distributions under Service Load at Maximum Moment Location

Figure 3-10 presents the strain distributions for the girders under service load at the maximum moment location. The strain distribution of the pure composite girder was perfectly linear because slip at the steel and concrete interface was prevented. In contrast, a small strain discontinuity exists in the case of the shear stud girder. A larger strain discontinuity exists at the steel-concrete interface for the panel end connected girder with original stiffness. This discontinuity existed because there was not a panel end connector at the maximum moment location. The panel end connectors were placed

every 3 m along the span of the girder and the maximum moment location did not coincide with this connector layout. When the panel end connections stiffness was decreased to 500 000 N/mm, the strain discontinuity slightly increased (Figure 3-10 Bottom). This behaviour was expected because the panel end connections deformed more when their stiffness was decreased. The non-composite girder had the largest strain discontinuity at the steel-concrete interface because the concrete deck was able to freely slip on the steel girder. As shown on Figure 3-10, strong composite action was achieved at service load at the maximum moment location for the shear stud and panel end connected girders. The level of composite action decreased when the shear stud connections were replaced with panel end connections. It decreased even further when the panel end connections stiffness was decreased.

All of the models were loaded to failure in the FEA program. Furthermore, all of the models failed by concrete crushing at the maximum moment location except for the non-composite model, which failed prematurely by web buckling. Table 3-1 presents the moment at the maximum moment location when each model aborted. The moment capacities of the pure composite, shear stud and panel end connected girders, regardless of panel end connections stiffness, were all within 1.6% of each other.

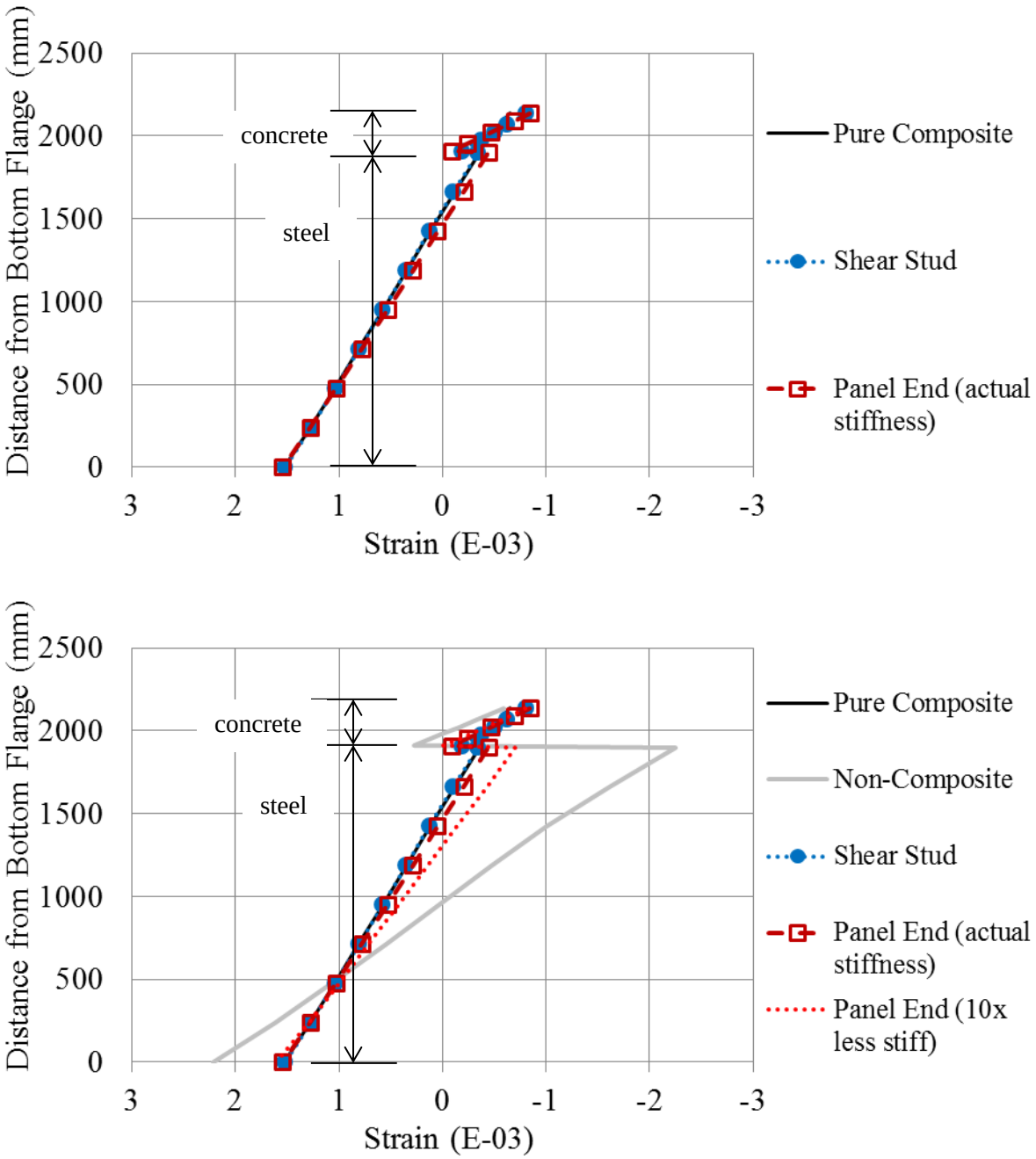

Figure 3-10: Strain Distributions under Service Load at Maximum Moment Location – Three Models Only (Top) and All Five Models (Bottom)

Figure 3-11 presents the stress distributions of the girders under ultimate load at the maximum moment location. Composite action was observed from the pure composite, shear stud and panel end connected girders. All of these girders exhibited composite action wherein their plastic neutral axes

were near the top flange of the steel girders (Figure 3-11). These FEA results were in good agreement with the theoretical hand calculation results. Using the Canadian Highway Bridge Design Code [2006], the plastic neutral axis of the composite girder was found to be 4.7 mm below the top flange of the steel plate girder.

As expected, the stress distributions of the shear stud and panel end connected girders were bounded by the results for the pure composite and non-composite girders. The stress distribution for the shear stud girder was similar to that of the pure composite girder. The only difference between these two distributions was that the compression stress at the top flange of the shear stud girder was slightly higher than that of the pure composite girder. The panel end connected girder with actual stiffness had a similar stress distribution when comparing to the shear stud girder. The top flange area under compression stress increased and the stress level increased when the shear stud connections were replaced with panel end connections. When the panel end connections stiffness was decreased to 500 000 N/mm, the compression stress level at the top flange of the plate girder was further increased. In summary, the portion of the steel cross section in compression increased when the level of composite action decreased (e.g., from pure composite model to shear stud model to panel end connected model to non-composite model).

A nonlinear stress distribution of the concrete deck was observed for every girder except for the non-composite one, where it failed by web buckling. Tensile stress was shown at the bottom layer of the concrete deck for the four other girders because each deck was modelled with steel reinforcing bars. It should be noted that the shear stud girder, the panel end connected girder and the panel end connected girder with reduced connector stiffness exhibited partially non-composite behaviour. All of these girders exhibited partially non-composite behaviour because their bottom part of the concrete deck was in tension and their top flange of the plate girder was in compression. At the ultimate load, every girder had yielded in tension at the bottom at a stress of 350 MPa.

The stress distribution of the concrete deck was linear for the non-composite girder. Compressive stress was shown at the top part of the reinforced concrete deck and tensile stress was shown at the bottom part of the reinforced concrete deck. At ultimate load, the non-composite girder had yielded in both compression and tension at a stress of 350 MPa.

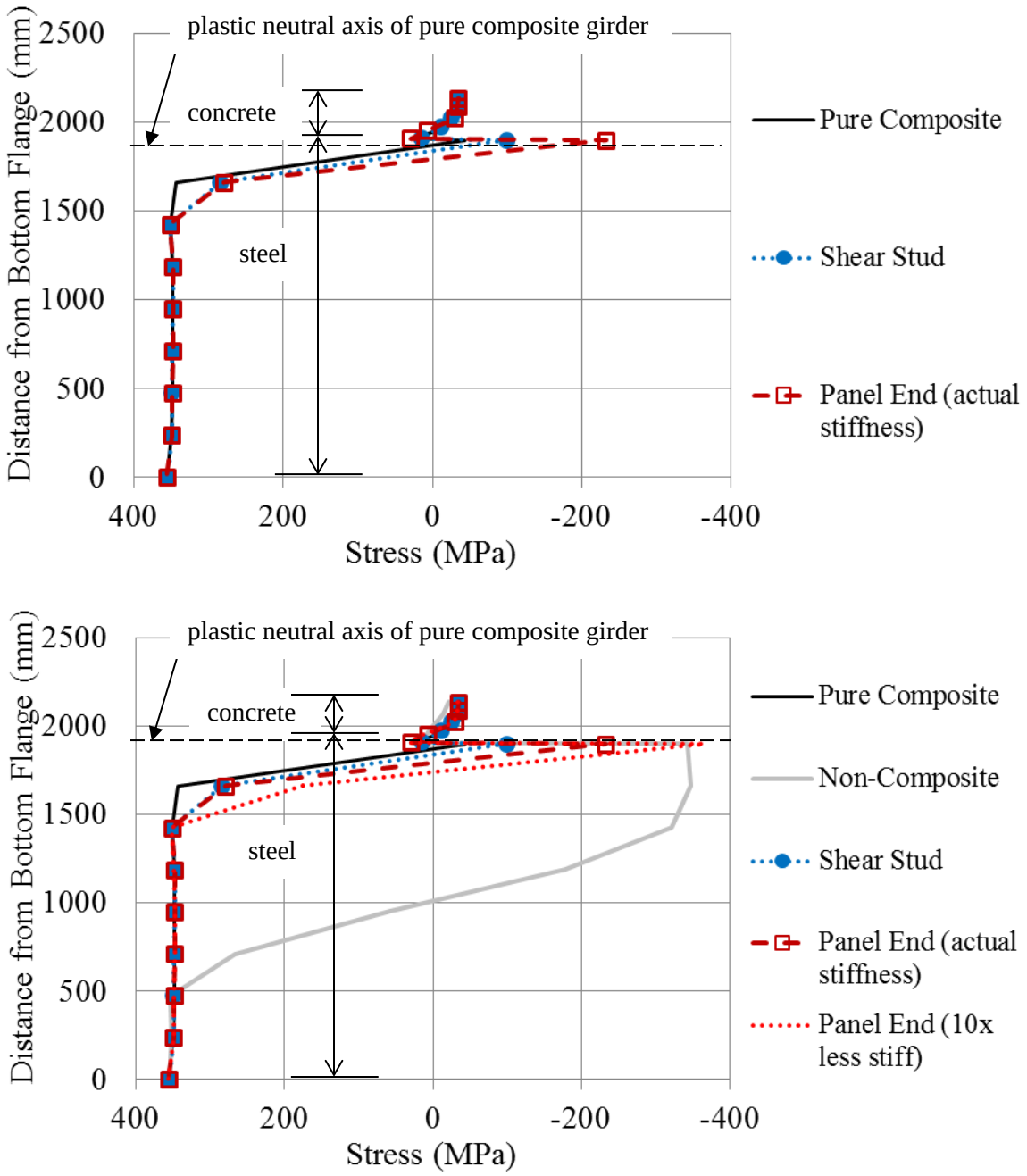

Figure 3-11: Stress Distributions under Ultimate Load at Maximum Moment Location – Three Models Only (Top) and All Five Models (Bottom)

Figure 3-12 presents the strain distributions of the girders under ultimate load at the maximum moment location. For the pure composite girder, no strain discontinuity occurred at the steel-concrete interface because slip at the interface was prevented in the model. For the shear stud and panel end

connected girders, a strain discontinuity exists at the steel-concrete interface. Strong composite action was observed for the shear stud and panel end connected girders. This was true even for the panel end connected girder with reduced connection stiffness. As the strain discontinuity at the interface increased, the level of composite action achieved decreased (i.e., from pure composite model to shear stud model to panel end connected model to non-composite model).

Rather than having a linear shape, the strain distributions of Figure 3-12 form a slightly nonlinear shape for the pure composite, shear stud and panel end connected girders. The nonlinear distributions were due to the combined bending and shear effects, where the ultimate moment caused bending deformations and the third axle load at ultimate caused shear deformations. The strains in the steel for the non-composite girder remained very low because the girder failed prematurely by web buckling. Web buckling of the non-composite girder was observed when the deformed shape of the girder at ultimate load was plotted in ABAQUS.

The shear stud girder strain distribution was bounded by those of the pure composite and the non-composite girder. In contrast, the panel end connected girders strain distributions lay outside of those boundaries. The two strain distributions from the panel end connected girders generally had greater strain values than those of a pure composite girder because the panel end connected girders were more flexible in terms of girder deflections and deformations. By using panel end connectors, the girder would be less stiff than the shear stud girder because it would have significantly larger discrete connector spacing than those from the shear studs. Such reduction in the overall girder stiffness had increased the girder vertical deflection by 4%. The deflection of the girder further increased by 13% when the panel end connectors stiffness was reduced from its original proposed value to 500 000 N/mm. As the vertical deflection increased, the longitudinal deformations, such as strains, of the girder would increase.

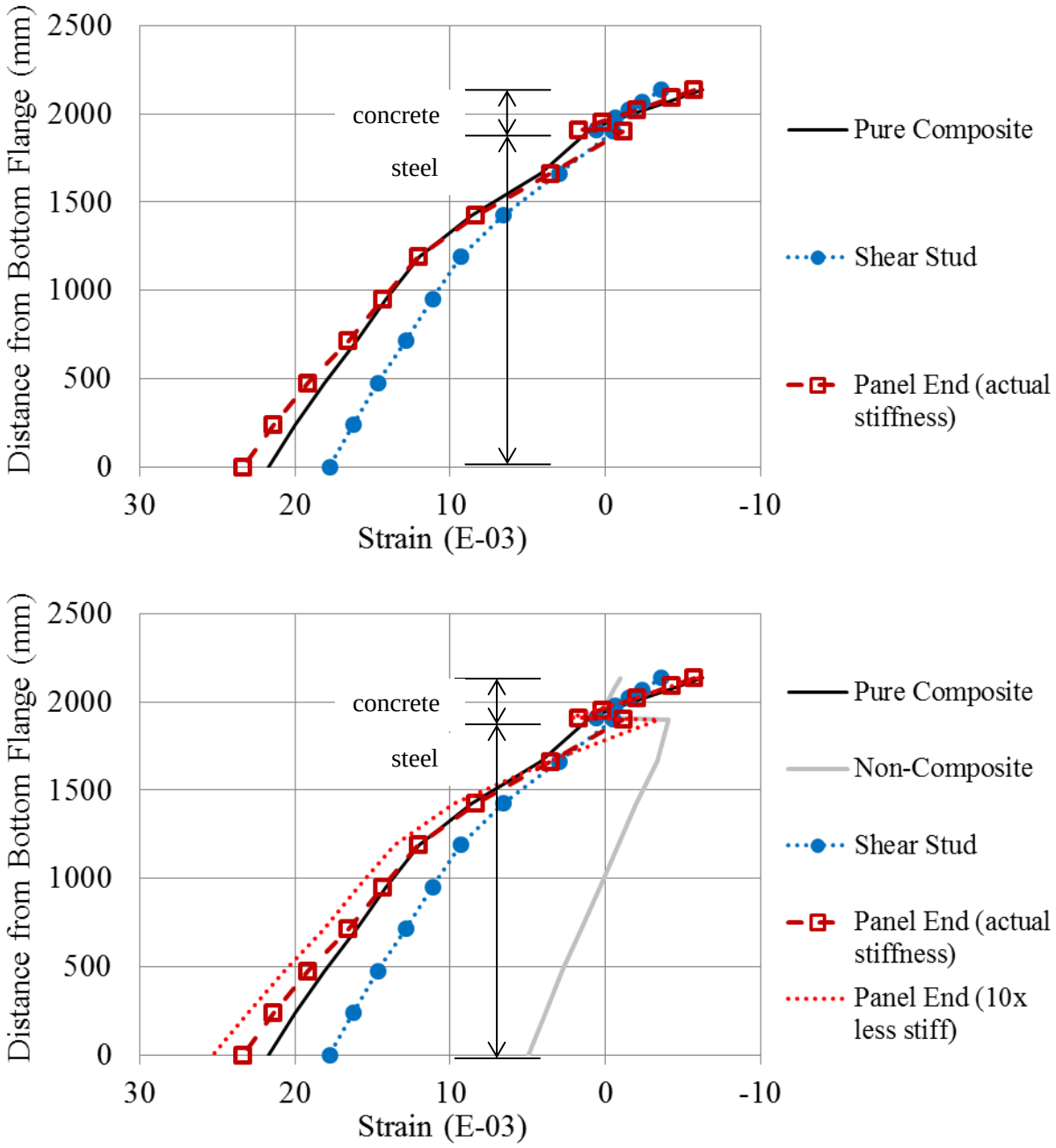

Figure 3-12: Strain Distributions under Ultimate Load at Maximum Moment Location – Three Models Only (Top) and All Five Models (Bottom)

3.2.3 Connection Force Distributions along the Girder Span

The connection force distributions along the girder span were computed from each FEA model to examine the effect of shear connection type on the shear flow at the steel-concrete interface. The

connection force distributions along the 36 m girder span were computed at service load and at ultimate load. Figure 3-13 and 3-14 present these distributions. It should be noted that the connection force distributions for the non-composite model were not plotted on these figures because the shear flow at the steel-concrete interface for the non-composite model was simply zero. For the non-composite model, the concrete deck slab was able to freely slip along the steel plate girder with negligible friction; therefore, no shear force was transferred at the steel-concrete interface for this model.

The theoretical shear flow along the girder span was calculated by using Equation 3.4 and the theoretical elastic shear flow diagrams were plotted on Figure 3-13 and 3-14. As shown in Equation 3.4, the shear flow,q_x, is a function of the shear force, V_x, at point x along the bridge [Salmon and Johnson 1990].

$$q_x = \frac{V_x Q}{I} \tag{3.4}$$

where Q is the first moment of area and I is the elastic transformed section of moment of inertia.

Figure 3-13 presents the connection force distributions under service load. The shear flow distribution for the shear stud girder was identical to that of the pure composite girder. Both distributions had peak shear flow values that were slightly greater than the calculated theoretical values. This implied that the pure composite girder and the shear stud girder were able to transfer more interface shear force than theoretically predicted at service load. When the shear stud connections were replaced with panel end connections, the shear flow at the steel-concrete interface decreased slightly. In other words, the amount of shear force transferred at the interface was decreased when the shear stud connections were replaced with panel end connections. When the stiffness of the panel end connections was decreased to 500 000 N/mm, the shear flow at the steel-concrete interface was further decreased. The two shear flow distributions from the panel end connected girders closely matched the theoretical shear flow distribution calculated by using Equation 3.4. It should be noted that all connection forces under service load were in the elastic range. The shape of the shear flow plot from each model resembled the shape of the theoretical shear flow diagram everywhere except near the girder ends. The shear flow from each model decreased near the girder ends because the girder supports were 625 mm away from the end of the girder. When the supports were place at a distance from the girder ends, the local maximum shear force tended to be concentrated at the supports and not at the ends of the girder.

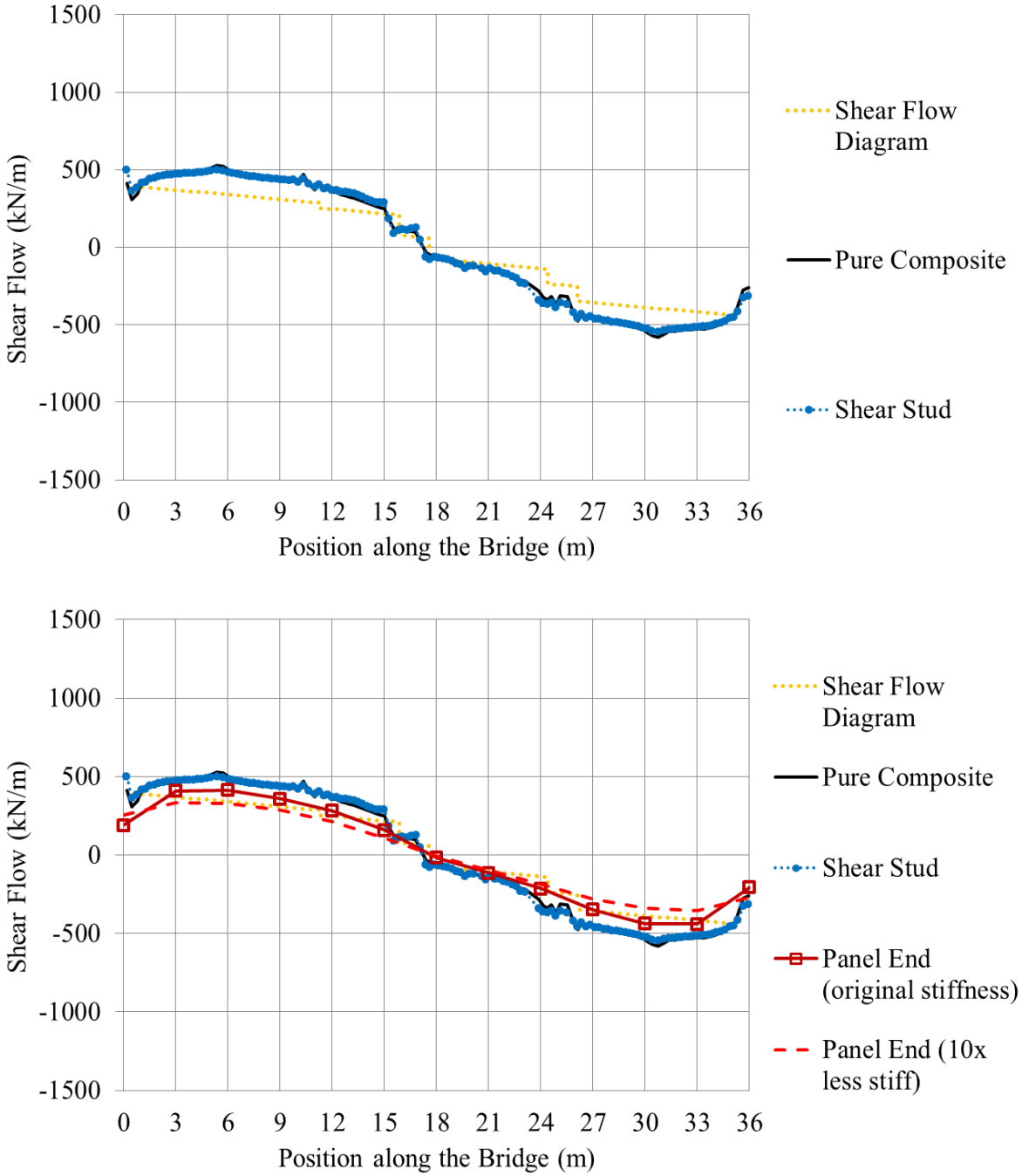

Figure 3-13: Connection Force Distributions under Service Load – Two Models (Top) and Four Models (Bottom)

Figure 3-14 presents the connection force distributions at ultimate load. The shear flow distribution for the shear stud girder was similar to that of the pure composite girder. These two distributions

could be differentiated by the jumps in shear flow that happened near mid-span. The distribution from the pure composite girder had high shear flow jumps near mid-span because a plastic hinge had formed at the maximum moment location for this model. The plastic hinge that formed 455 mm to the left of mid-span caused large shear forces near the mid-span at ultimate load. In contrast to the pure composite girder, the shear stud girder had lower shear flow jumps near mid-span. A shear stress concentration at the steel-concrete interface was prevented for the shear stud girder because the ductile shear studs would slip and yield as the applied horizontal shear force increased. The applied horizontal shear force would be distributed along the length of the girder due to the ductile properties of the shear stud. Therefore, a high interface shear force jump near mid-span was prevented for the shear stud girder.

The shear flow distribution for the panel end connected girder had two distinct differences compared to that of the shear stud girder. First, the panel end connected girder did not have shear flow value jumps near the mid-span. The applied horizontal shear forces were evenly distributed along the length of the girder due to the elastic perfect-plastic properties of the panel end connectors. Secondly, the shear flow for the panel end connected girder was less than that of the shear stud girder. In other words, the amount of shear force transferred at the interface was decreased when the shear stud connections were replaced with panel end connections. When the stiffness of the panel end connections was decreased to 500 000 N/mm, the shear flow at the steel-concrete interface was further decreased.

The shear flow distributions of the pure composite girder and the shear stud girder matched the theoretical shear flow diagram everywhere except where the jumps in shear flow occurred (i.e. near the mid-span). The shear flow distributions for the panel end connected girders matched closely with the theoretical shear flow diagram. The shear flow decreased near the ends of the girders because the supports were placed 625 mm from the ends of the girders. The local maximum shear force occurred at the supports and the shear forces on the cantilever segments of the girders were lower.

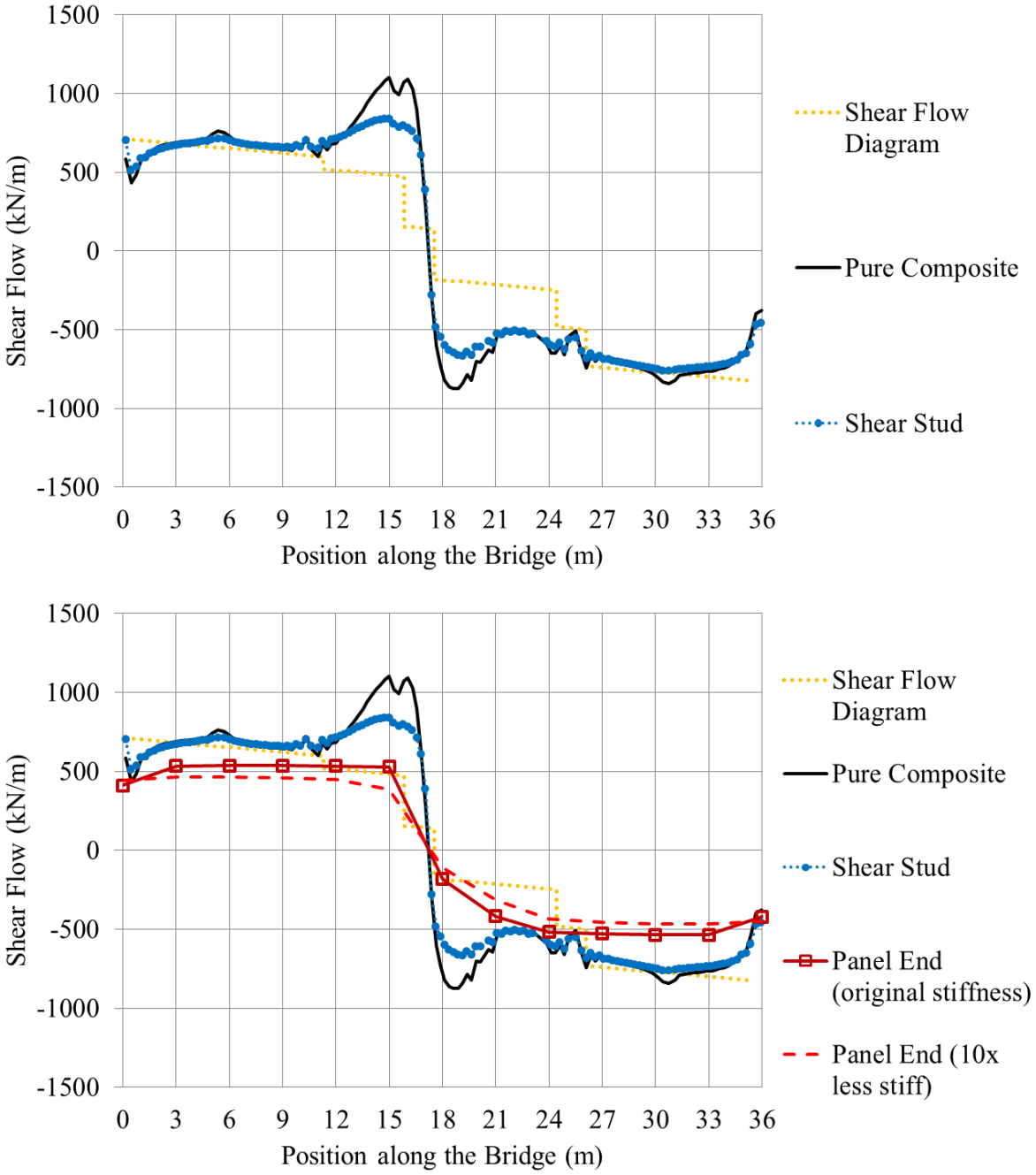

Figure 3-14: Connection Force Distributions at Ultimate Load – Two Models (Top) and Four Models (Bottom)

3.2.4 Summary of Finite Element Analysis Results

At service and ultimate load, a high level of composite action was observed for the panel end connected girders. The level of composite action achieved decreased slightly when the panel end connection stiffness was decreased. The level of composite action of the girders was determined by examining the strain profiles through the composite girder depth. As the strain discontinuity at the steel-concrete interface increased, the level of composite action achieved was assumed to decrease.

Although the panel end connected girders exhibited partial composite behaviour, their overall moment-displacement response was similar to that of the pure composite girder. The panel end connected girder with actual (calculated) stiffness had an ultimate moment capacity that was only 1.5% less than that of the pure composite girder. At ultimate load, the deflection of the panel end connected girder was 3% larger than that of the pure composite girder.

Chapter 4
Experimental Study of Bolted Connections

In this chapter, the main experimental study conducted for the current thesis project is described. First, small scale friction test setup is described in Section 4.1. Secondly, the push test program and specimens are described in Sections 4.2 and 4.3. The material properties of the concrete and specimen fabrication are then discussed in Sections 4.4 and 4.5. Finally, in Section 4.6, the specimen instrumentation and testing procedures are discussed.

4.1 Friction Tests

Small-scale friction tests were conducted to analyze the friction behaviour between the steel surface and the concrete surface (Figure 4-1). Three types of steel surfaces were tested during the experiment: a plain steel surface, a steel surface coated with adhered regular concrete sand and a steel surface coated with adhered concrete sand that passed through a 1.18 mm (#16 US Standard Mesh) sieve. Both sand coatings were applied using the same processes described in Section 4.5. Three types of concrete surface were tested during the experiment: a regular formed surface, a needle peened surface and a sandblasted surface. For each test, a steel plate was placed on top of a concrete prism and the amount of weight required in a bucket to pull the plate off the prism was recorded (Figure 4-1). All steel plates used in the tests were 127 mm in width and 254 mm in length. Furthermore, all concrete prisms used in the tests were 100 mm in width, 100 mm in height and 350 mm in length. Sand and blocks of weight were added to the bucket until the bucket pulled the steel plate off the concrete prism. Each interface between the steel plate and concrete prism was tested three times and the average weight required to pull the plate off the prism was recorded. The friction coefficient between the steel and concrete surface was then calculated using the following equation:

$$F_g = \mu F_N \tag{4.1}$$

where F_g is the weight of the bucket and its contents, F_N is the weight of the steel plate (excluding the weight of the block placed on top of the plate as shown on Figure 4-1) and μ is the friction coefficient.

Initially, a block was placed on top of the steel plate in an attempt to study the effects of increasing the applied normal force, F_N, on the interface (Figure 4-1). This attempt was aimed to study how the friction coefficient would change if the applied normal force was increased by 10 times. Multiple test trials were conducted. However, the weight of the bucket and its contents failed to pull the steel plate

and block off the concrete prism. This test setup failed because the block was very heavy and not enough weight could be generated in the bucket from the existing apparatus. During the multiple trials that were conducted, damage was observed on the pulley string and the bucket handler. The damage was obtained due to the substantial weight that was placed in the bucket. Subsequently, friction tests were conducted without the block on top of the steel plate. All friction test results that were recorded in this thesis were results without the weight of the block.

The contact area between the steel plate and the concrete prism was 100 mm by 229 mm. This area was kept constant throughout the friction tests. It should be noted that the friction coefficient is a coefficient relating the shear stress applied on a surface to the normal stress applied on the same surface. Since the contact area subjected to shear stress and normal stress was the same, it did not needed to be included in the left-hand-side and right-hand-side of Equation 4.1.

It should be noted that the needle peened concrete surface was created by using a peening gun. A peening gun is a piece of equipment used to extend the fatigue life of welded metallic structures [Forgues, 2007]. It has a needle head installed at the tip of the gun. During the peening and post-weld treatment process, the gun was aimed at the welds and the needles of the head vibrate to relieve the residual stresses of the welds [Forgues, 2007]. The peening gun was used to create a needle peened concrete surface. The vibration of the needles made the concrete surface rough to increase surface friction.

Figure 4-1: Friction Test Setup

4.2 Push Test Overview

The experimental program included the fabrication and testing of 13 push test specimens. One of these specimens – the shear stud specimen – served as the control specimen, because composite action is conventionally achieved using shear studs with a cast-in-place concrete deck. The other 12 specimens utilized ASTM A325 bolts to facilitate the composite action between the precast concrete decks and the steel beam.

Various surface conditions were created between the precast concrete decks and the steel beam to study their effects on the overall behaviour of the shear connection. The effects of bolt diameter, bolt tension, and surface conditions between the concrete decks and steel beam were key parameters that were studied in the experimental program. These parameters were thought to directly affect the shear capacity of bolted connections.

The push test specimen consisted of two identical reinforced concrete slabs attached on either side of a steel I-beam section (Figure 4-2). Each slab is attached to a steel flange of the I-beam by some form of connectors. To determine the shear capacity of the connectors, the push test specimen was

vertically loaded such that the interfaces between the reinforced concrete slabs and the steel beam section were subjected to shear.

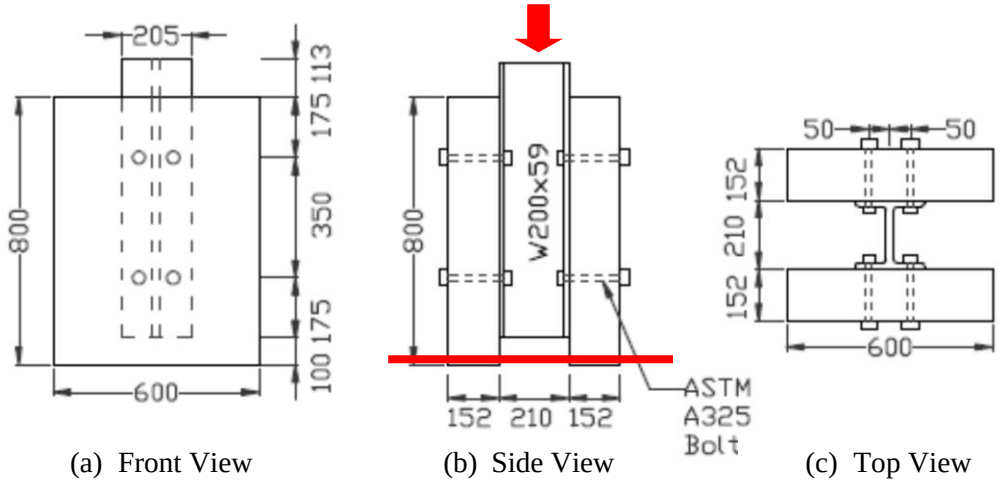

(a) Front View (b) Side View (c) Top View

Figure 4-2: Push Test Specimen Geometry (dimensions in mm)

4.3 Push Test Specimen Description

All of the slabs of the 13 test specimens were 800 mm high, 600 mm wide and 152 mm thick. An I-beam section of W200x59 was chosen for this study. The I-beam was made from 350W steel. As illustrated in Figure 4-2, the bottom ends of the slabs and the I-beam had difference in elevation of 100 mm to accommodate slip between the slabs and the I-beam during testing.

Each slab had top and bottom mat reinforcement (Figure 4-3). The longitudinal reinforcement for each mat consisted of four 10M bars placed at 140 mm centre-to-centre. For the transverse reinforcement, each mat consisted of four 10M bars that were placed at 200 mm center-to-center. All 10M bars were made from 400W weldable low-alloy steel. Furthermore, all reinforcement had a minimum cover of 25 mm. The amount of reinforcement placed in each direction of each mat was designed based Clause 8.18.4.2 of the Canadian Highway Bridge Design Code [2006]. According to this Clause, the deck slabs must had a minimum reinforcement ratio of 0.003 in each reinforcing direction of each mat when they were designed by using the empirical design method.

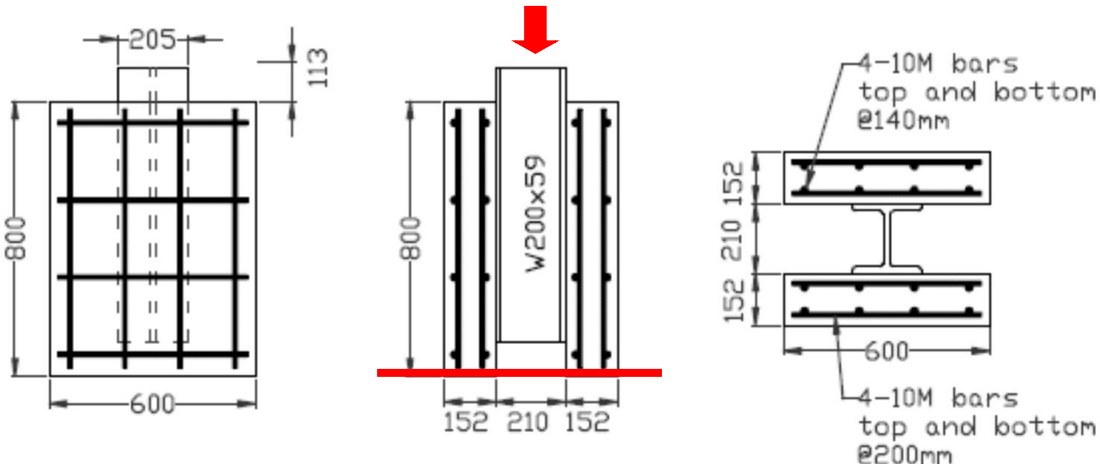

(a) Front View (b) Side View (c) Top View

Figure 4-3: Reinforcement Details of the Push Test Specimen

A total of 13 push test specimens were constructed and tested. Table 4-1 summarized the test matrix of the experimental program. As shown in the table, the 12 bolted specimens were to be differentiated by varying the bolt size, bolt tension and steel-concrete interface condition. Three bolt diameters were used in the experiment: 12.70 mm (designated as S for smallest bolt size), 15.88 mm (designate as M for medium bolt size) and 19.05 mm (designated as L for largest bolt size). The bolts either had no pretension force or they were pretensioned to 70% of the bolt's specified minimum tensile strength. For the three bolt sizes ranging from smallest to largest, the equivalent pretension force of 70% of the bolt's specified minimum tensile strength were 53 kN, 85 kN, and 125 kN, respectively, calculated according to Clause 10.24.6.3 of the Canadian Highway Bridge Design Code [2006]. The steel-concrete interface conditions that were examined in the experiment included: plain surfaces, surfaces with shear lugs, and surfaces "friction enhanced" by sandblasting and adhering aggregate (concrete sand) to the steel.

Table 4-1: Test Matrix of the Experimental Program

		Nelson Studs	ASTM A325 Bolts						
Stud/Bolt Diameter (mm)		19.05	12.70	15.88	12.70	15.88	19.05	15.88	19.05
Bolt Tension (kN)		-	0	0	53	85	125	53	53
Nelson Stud Specimen		NS-0							
Bolted Specimens with Designated Surface	Plain					P M-85			
	Shear Lug		SL S-0	SL M-0	SL S-53				
	Friction Enhanced Type I				FE1 S-53	FE1 M-85	FE1 L-125	FE1 M-53	FE1 L-53
	Friction Enhanced Type II				FE2 S-53	FE2 M-85	FE2 L-125		

4.3.1 Shear Stud Connection

One shear stud "control" specimen was constructed and tested as part of the experimental program. Three pairs of Nelson shear studs were welded on the outside of each flange of the steel beam. Figure 4-4 illustrates the position of the studs. The studs (19 mm in diameter and 75 mm in height) had a minimum ultimate tensile strength of 414 MPa (60 000 psi).

To predict the ultimate capacity of the specimen, the design formulas from the Canadian Highway Bridge Design Code [2006] were used. These two formulas were outlined in Section 2.2.1, where one formula checked for concrete crushing failure while the other checked for stud fracturing failure. The specimen was predicted to fail by stud fracturing at an ultimate load of 1188 kN. This failure mode was predicted when a concrete strength of 35 MPa was assumed. The predicted ultimate load of 1188 kN was the factored resistance of the specimen because a shear stud resistance factor of 0.85 was used in the calculation.

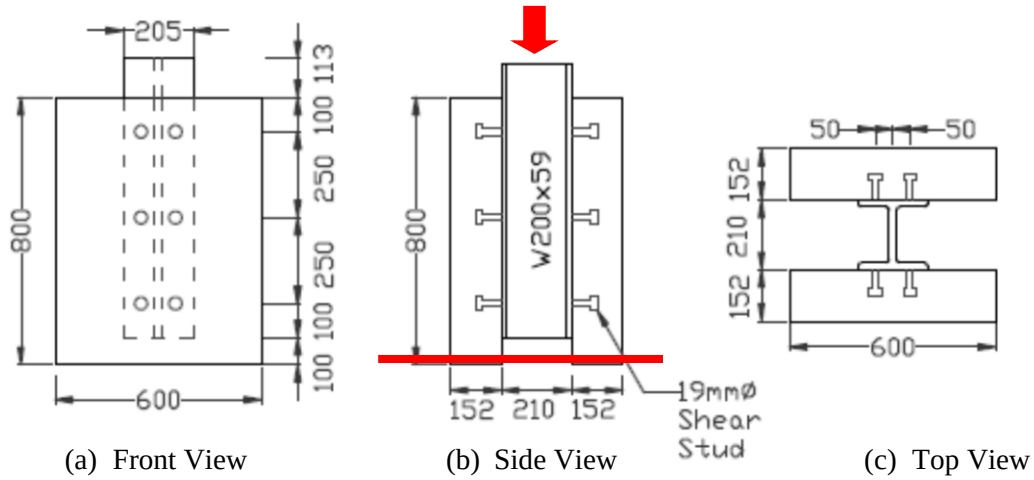

(a) Front View (b) Side View (c) Top View

Figure 4-4: Shear Stud Specimen Geometry

4.3.2 Bolted Connection

Twelve specimens with bolted connections were built and tested in the laboratory. These specimens were designed to study the effects of bolt diameter, bolt tension and steel-concrete interface condition on the connection. Each connection utilized four ASTM A325 bolts to connect the precast concrete deck panel and the steel I-beam. Three different bolt diameters were used: 12.70 mm, 15.88 mm and 19.05 mm. All of the bolts were 8 inches (203 mm) in length and had a specified minimum tensile strength of 825 MPa. As shown in Figure 4-2, the bolts were placed at quarter points, such that they each had an equal tributary length (i.e. 700 mm / 2 = 350 mm) along the steel flange-concrete deck panel contact surface.

One of the 12 bolted specimens had a plain steel-concrete interface condition. This specimen utilized the medium size bolts, which were pretensioned to 70% of the specified minimum tensile strength. The plain steel-concrete interface consisted of the contact surface between the untreated steel flange and the untreated precast concrete deck panel.

4.3.3 Bolted Connection with Shear Lug

Three of the 12 bolted specimens had a shear lug welded onto the top (outside) flange of each steel beam to enhance shear transfer. The use of shear lugs requires the concrete panels to be match cast on the steel beam to provide close tolerances between the shear lug and concrete panel. The shear lugs were fabricated with a trapezoidal shape (Figure 4-5), so that the taper would allow the concrete deck panels to be easily dissembled from the steel section after casting and reassembled during

construction of the composite bridge. The top width, bottom width, height and length of the shear lugs were 1 inch (25 mm), 1.5 inches (38 mm), 1.5 inches (38 mm) and 7.5 inches (191 mm), respectively. The height and length of the shear lugs were designed such that each shear lug would provide an additional shear capacity of 200 kN to the specimens. Fisher and Kloiber [2006] outlined the shear lug design procedure in the Base Plate and Anchor Rod Design Guide. The top width, bottom width and height of the shear lugs were designed such that the taper angles of the shear lugs would be 9 degrees. This taper angle value was consistent to that of a typical concrete-to-concrete shear key connection according to the Precast Prestressed Concrete Bridge Design Manual [2003]. Each shear lug was placed between the two pairs of bolts and at a centre-to-centre distance of 175 mm relative to each pair of bolts. All lugs were made of hot rolled 1010 carbon steel bars.

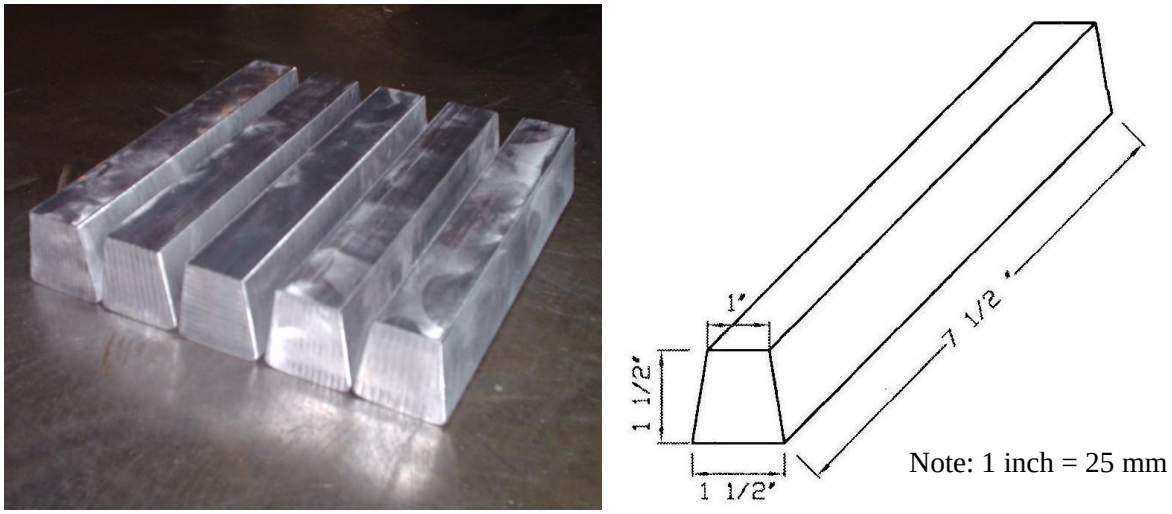

Figure 4-5: Shear Lugs Shape (Left) and Dimensions (Right)

Two of the shear lug specimens utilized the smallest size bolts; one of these had its bolts pretensioned while the other had its bolts finger snug tight (i.e. with no pretension force applied). The third shear lug specimen utilized the medium size bolts with no pretension force applied. The tests on the three shear lug specimens were designed to determine the effects of the shear lugs, the pretension force, and the increase in bolt size on the behaviour of the shear connection.

4.3.4 Bolted Connection with Friction Enhanced Type I Surface

Five of the bolted specimens had their steel I-beam flanges "friction enhanced" by adhering concrete sand to their surfaces. It was hoped that the slip load of the connection would increase when friction at the interface between the steel flange and the concrete slab surface was increased. To do this,

concrete sand was adhered on to each steel flange outer surface to make the outside flange surface rougher. This steel-concrete interface condition was denoted to be a “friction enhanced type I surface”.

Sikadur 330 was used to adhere the concrete sand to the outer steel flange surfaces. It was a two-component structural epoxy resin manufactured by Sika Group [Sika Canada 2012]. Sikadur 330 was chosen because it had excellent adhesion to metals and it was moisture tolerant. It had a tensile strength of 30 MPa and a modulus of elasticity strength of 3.8 GPa. Its high modulus of elasticity strength allowed it to act as a good adhesive to the steel surfaces. The setting time of Sikadur 330 was 30 minutes, which meant that the process of mixing and applying Sikadur 330 should be completed in 30 minutes or less.

Three of the five friction enhanced type I specimens had their bolts pretensioned to 70% of the bolt specified minimum tensile strength. These three specimens utilized small, medium and large size bolts, respectively. The objective of this part of the test matrix was to study the effects of the bolt diameter as the level of bolt pretensioning is held constant. The other two friction enhanced type I specimens had their bolts pretensioned to 70% of the small bolt specified minimum tensile strength (53 kN) even though the two specimens utilized medium and large bolt sizes, respectively.

4.3.5 Bolted Connection with Friction Enhanced Type II Surface

Three of the bolted specimens had both their steel I-beam flange surfaces and their concrete slab surfaces friction enhanced. The steel flanges were friction enhanced in the same manner as described in Section 4.2.4 (i.e. using adhered concrete sand). In addition, for the friction enhanced type II surfaces, the concrete slab surfaces were sandblasted to increase their roughness.

All three friction enhanced type II specimens had their bolts pretensioned to 70% of the bolt specified minimum tensile strength. These three specimens utilized small, medium and large size bolts, respectively. It was hoped that the test results for these specimens would show the effects of varying bolt diameter and increased prestress force in connection behaviour.

4.4 Concrete Material Properties

The specified concrete strength for the deck panels was 35 MPa. Air content Category 1 was specified for the concrete mixture because concrete for bridge decks would typically experience freezing and thawing [Kosmatka et al., 2003]. Air content Category 1 consisted of 5% to 8% of air in the concrete

mixture. A maximum slump of 75 mm was also specified for the concrete mixture. This slump value was consistent with the recommended value from Kosmatka et al. [2003]. A nominal maximum coarse aggregate size of 19 mm was chosen based on the Material Specification for Aggregates – Concrete [2011]. The Material Specification for Aggregates – Concrete [2011] stated that the nominal maximum aggregate size should be 19 mm for concrete structures, unless otherwise specified in the Contract Documents.

4.5 Fabrication of Specimens

813 mm long W200 x 59 I-beams were first cut to length for each specimen (Figure 4-2). The shear studs used in the control (NS-0) specimen were donated by Nelson Stud Welding Inc. and professionally welded onto the I-beam by the company's technian (Figure 4-6). All the bolt holes on the steel I-beams were drilled in the University of Waterloo Engineering Machine Shop to fabricate the bolted specimens. The shear lugs were also fabricated in the UW Engineering Machine Shop and then transversly welded onto the I-beams by one of the shop's certified welders (Figure 4-7). GMAW (gas metal arc welding) was used for the welding process. Six millimeter diameter fillet welds were used along each length of the shear lugs. The weld design was verfied to ensure that weld fracture would not occur in the shear lug specimens. For the friction enhanced type I and type II specimens, concrete sand was adhered on to each steel flange surface with Sikadur 330 adhesive. The steel flange surfaces were first sandblasted to obtain a clean surface condition. Secondly, the Sikadur 330 components were mixed and then placed onto the outside flange surfaces in accordance with the manufacture's specifications [Sika Canada 2012]. Finally, the concrete sand was placed at a rate of one lb/ft^2 (4.89×10^{-3} g/mm^2) on top of the Sikadur adhesive to create the friction enhanced surface (Figure 4-8).

Figure 4-6: Shear Stud Specimen – Before Concrete Casting

Figure 4-7: Shear Lug Specimen – Before Concrete Casting

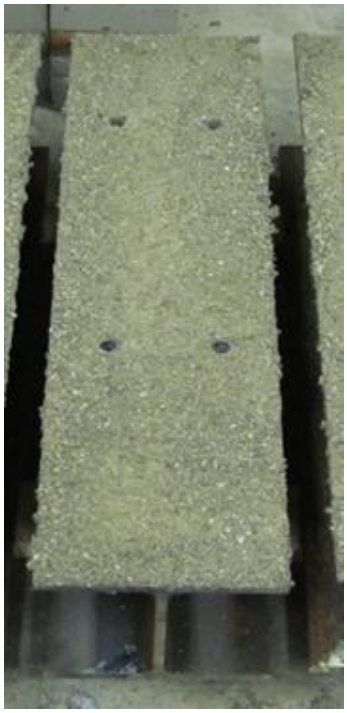

Figure 4-8: Friction Enhanced I-Beam

Vertical slab forms were built for the shear stud specimen and the three bolted shear lug specimens (Figure 4-9). The slabs of these four specimens had to be cast vertically and upside down with respect to the specimen testing configuration so that any potential concrete settlement around the connectors would not significantly affect the test results. Vertical slab casting had to be done for the shear stud specimen because both of the specimen's slabs had to be cast at the same time. Vertical slab casting was also used for the bolted shear lug specimens so that match cast voids would be formed within the slabs when the concrete mixture was poured around the shear lugs. The vertical slab forms were braced using dimensional lumber as illustrated in Figure 4-9 to ensure that the forms would be able to withstand the hydraulic pressure from concrete casting.

Horizontal deck slab forms were built for the remaining nine specimens (Figure 4-10) that did not need to be match cast.

Figure 4-9: Forms for Vertical Casting of Concrete Slabs

Figure 4-10: Forms for Horizontal Casting of Concrete Slabs

All forms were built using ¾ inch (19 mm) thick plywood. The plywood was screwed together at a spacing of six inches (152 mm). All of the 10M reinforcment mats were tied using six-inch loop ties.

For the horizontal slabs forms, the top and bottom reinforcement mats were supported by 4 inch (100 mm) and 1 inch (25 mm) reinforcement chairs, respectively (Figure 4-10). For the vertical slabs forms, the reinforcement was secured in place using wooden planks on the sides (Figure 4-11). All reinforcment was placed in a manner to achieve a concrete cover of 25 mm. Two concrete anchors were placed in each slab. Once the concrete were cast and cured, these anchors would facilitate the movement of the slabs using the fork lift or cranes in the laboratory. All bolt holes were formed using 1 inch (25 mm) inside diameter PVC pipes. The pipes were cut into 6 inch (152 mm) lengths to match the thickness of the concrete slabs. They were secured in place using 7/8 inch (22 mm) diameter wooden dowels. Duct tape was used to seal the top ends of the pipes during concrete casting.

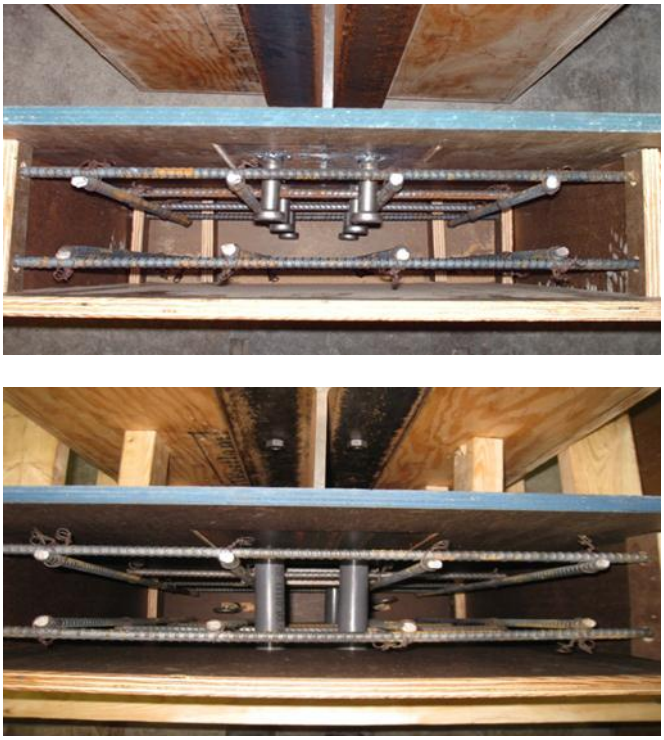

Figure 4-11: Reinforcement Details of Shear Stud (Top) and Shear Lug (Bottom) Specimens

All the slabs were cast using the same batch of concrete supplied by a local ready-mixed concrete producer to minimize the variability of the concrete strength in the slabs (Figure 4-12 and 4-13). Cast-in-place construction was simulated for the shear stud specimen as the Nelson shear studs were cast into the concrete mixture. On the other hand, precast construction was simulated for the bolted specimens. For the shear lug specimens, the steel flanges and shear lugs were oiled to prevent them from bonding to the concrete. During the slab casting period, a total of 36 concrete cylinders were

made from the same batch of concrete. Each cylinder had a diameter and height of 100 mm and 200 mm, respectively. The cylinders were used to monitor the actual concrete strength prior to and up to the date of testing since the actual concrete strength will generally differ from the specified concrete strength.

Figure 4-12: Vertical Casting of Concrete Slabs for Control and Shear Lug Specimens

Figure 4-13: Horizontal Casting of Concrete Slabs for Remaining Specimens

The concrete was consolidated using vibrators and then the slab surfaces were properly finished. Figure 4-13 showed the concrete slabs after casting. After finishing the slab surfaces, the slabs were moist cured for seven days using burlap and water in accordance with the Construction Specification for Concrete Structures [2010].

Figure 4-14: Concrete Slabs after Casting (Top and Bottom)

For the friction enhanced type II specimens, the cured concrete slab panels were sandblasted on one side to create the friction enhanced surface. The sandblasted surface areas of the slab panels consisted

of the areas that would be in contact with the outside steel flanges of the I-beams (Figure 4-16). Sandblasting was completed by professional sandblasting contractor as shown in Figure 4-15.

Figure 4-15: Sandblasting of Concrete Slabs

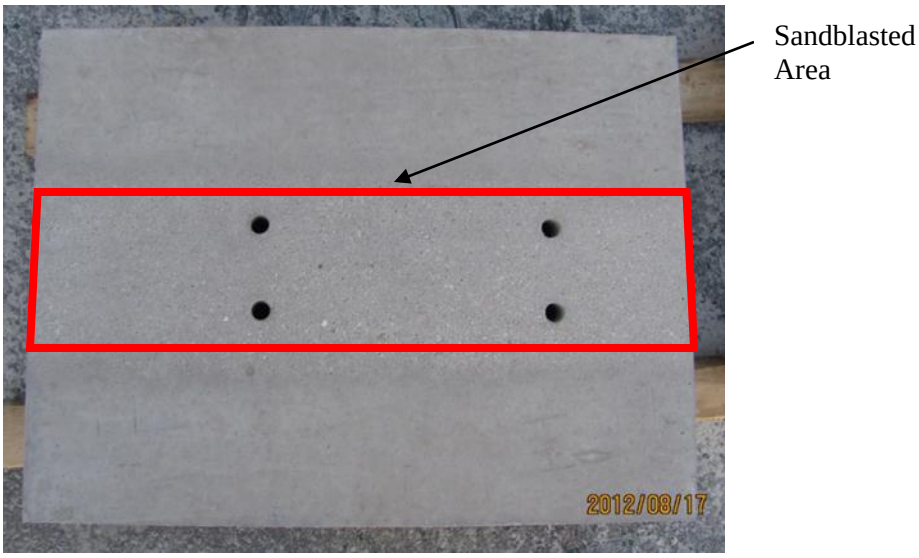

Figure 4-16: Sandblasted Concrete Slab Panel for Friction Enhanced Type II Specimens

4.6 Testing of Specimens

The 13 fabricated specimens were tested under static loading in the MTS 311 1500 kN capacity test frame in the University of Waterloo Structures Laboratory. A test platform was designed and built for the purpose of testing these push test specimens. The platform consisted of three steel plates and three W200x52 I-beams (Figure 4-17). The three steel plates were welded together to form the base of the

platform. Each plate was 50 mm thick. The bottom plate had an existing 75 mm diameter hole, which allowed the welded plates assembly to be threaded onto the MTS 311 test frame. Twelve 25 mm diameter holes were tapped in the top plate to allow the three I-beams to be bolted on top of the welded plates assembly. Web stiffeners were welded to the 584 mm long I-beams to improve the shear capacity of the beams. The beams were bolted to the welded plates assembly by using Grade 8 bolts that were 25 mm in diameter and 50 mm in length. Once the welded plates assembly was threaded onto the MTS 311 test frame and the I-beams were bolted onto the plates assembly, the individual test specimen could be placed on top of the three I-beams for testing.

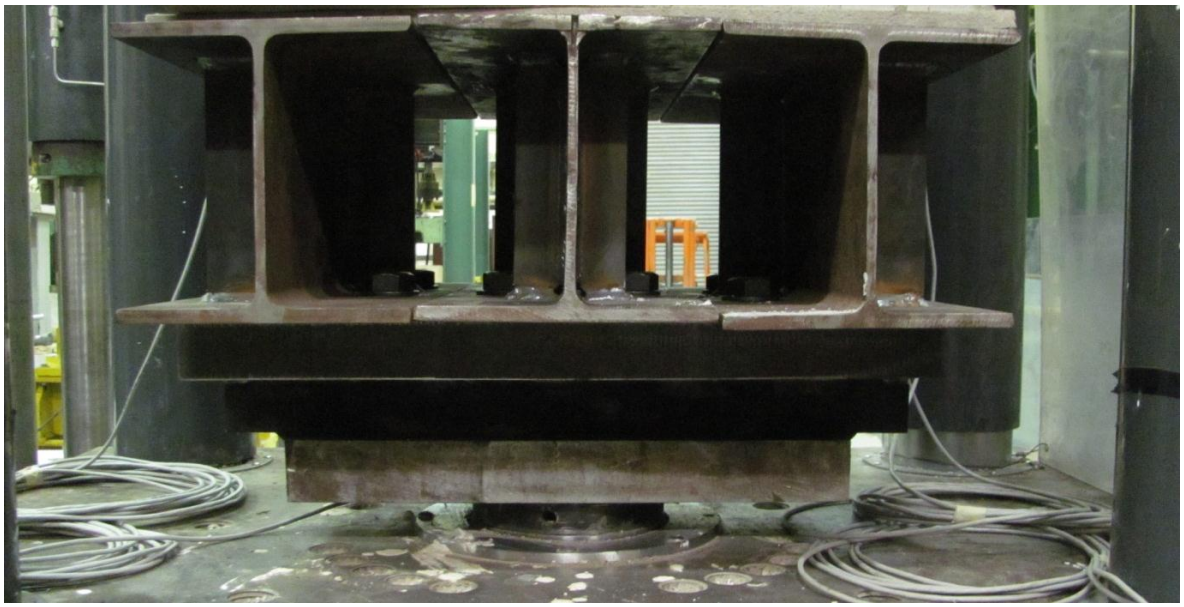

Figure 4-17: MTS 311 Test Platform

4.6.1 Test Setup and Instrumentation

The precast concrete slab panels and the steel I-beams were bolted together according to the specimen geometry (Figure 4-2) to assemble the 12 bolted specimens. Ten of the 12 bolted specimens had strain gauges installed on their bolts to measure the axial strain of the bolts. The specimens that were not strain gauged were specimens FE1 S-53 and FE1 L-125. Each of the strain gauged specimens utilized four strain gauges, where two strain gauges were place on each side of the specimen (Figure 4-18) and each strain gauge was placed at the middle length of a bolt (Figure 4-19). To record the axial bolts strains, the strain gauges were placed at the side of the bolt surface in their final position relative to the specimen.

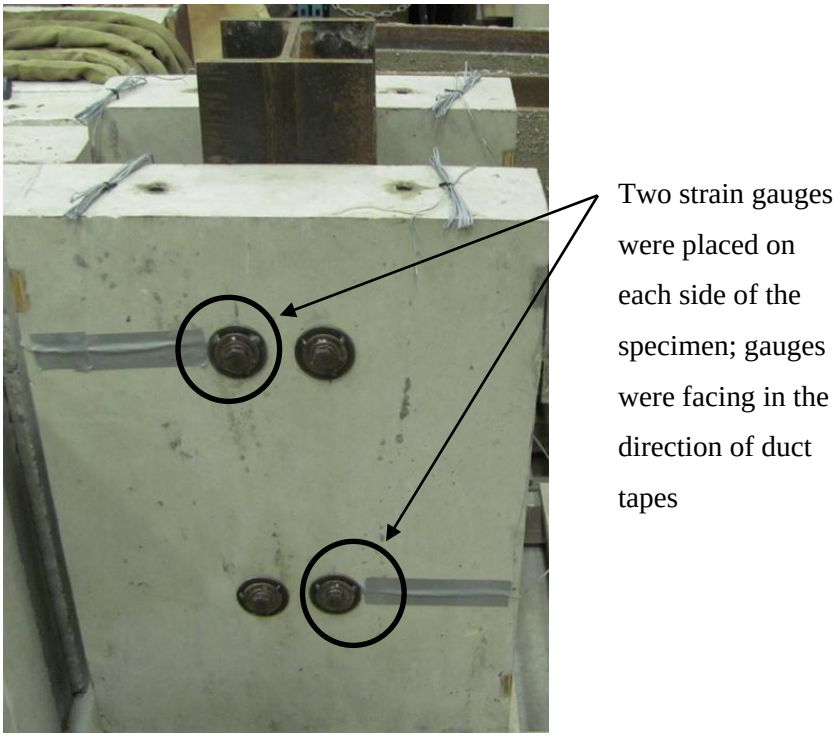

Figure 4-18: Strain Gauges Locations – Top and Bottom Bolts Alternating

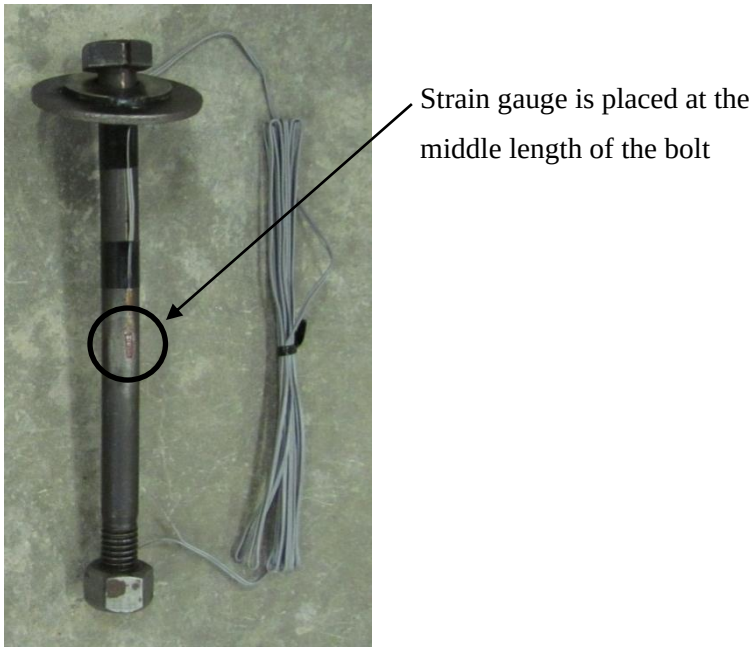

Figure 4-19: Placement of a Strain Gauge on a Bolt

Typical ASTM A325 bolt assemblies utilize ASTM F436 washers to distribute the bolt tension from the bolt heads to the bolted materials. These washers were well-suited for bolting steel plates together because the high yield strength of the steel means that there is little risk of a bearing failure of the steel material under the washer. However, these washers were not suited for bolting steel and concrete elements together because the bearing areas for these washers are not sufficient to distribute the bolt forces without cracking the concrete. To prevent concrete cracking under the bolts, multiple washers were stacked and tack welded together to increase the bolt bearing area against the concrete slab surface (Figure 4-20). Table 4-2 shows the washer assembly that was used for each size of bolts in order to increase bolt bearing area against the concrete slab surfaces. The United States Standard (USS) flat washers were used since they were ready available and they were developed to satisfy most industrial applications. Plate washers were also used because they were suited to increase the bolt bearing area. These washers have an outer diameter of a USS flat washer with a tight inner diameter. It should be noted that all USS flat washers used in the experiment were high strength hardened washers.

Table 4-2: Washer Assemblies Used to Increase the Bolt Bearing Areas

	ASTM A325 Bolts		
	½" (13 mm) diameter	5/8" (16 mm) diameter	¾" (19 mm) diameter
Washer Assembly	1/2 " (13mm) USS flat washer 3/4 " (19mm) USS flat washer 1 1/8" (29mm) plate washer	5/8 "(16mm) USS flat washer 1 1/8" (29mm) plate washer	3/4 " (19mm) USS flat washer 1 1/8" (29mm) plate washer

Figure 4-20: Washer Assembly Used to Increase the 19mm Diameter Bolts' Bearing Area

Specimens P M-85, SL S-53, FE1 S-53, FE1 M-85 and FE1 L-125 had their bolts pretensioned by using the turn-of-nut method. This bolt pretensioning method is widely used and recognized by the Canadian Highway Bridge Design Code [2006]. Due to the fact that the turn-of-nut method could not confirm the precise bolt tension force, and due to concerns raised after the first tests were completed

regarding the accuracy of this method, all other specimen bolts were pretenioned using a torque wrench. The bolt pretension strain readings were used to check the bolt tension achieved using the turn-of-nut method. The bolt strain values read from the data monitor indicated that the turn-of-nut method tended to over pretension the bolts and exceed the specified minimum bolt pretension. The bolt pretension strain readings were also used to check the bolt tension achieved using the torque wrench. The bolt strain values read from the data monitor were close to the expected pretension strain values when the bolts were tightened using the torque wrench. Table 4-3 showed the minimum torque values used to pretension the bolts [Portland Bolt and Manufacturing Company 2012].

Table 4-3: Minimum Torque Values Used to Pretension the ASTM Bolts

Bolt Diameter	Min Bolt Tension	Min Plain Torqueing Value
½" (13mm)	53 kN	100 lb ft (136 N m)
5/8" (16mm)	85 kN	198 lb ft (268 N m)
¾" (19mm)	125 kN	350 lb ft (475 N m)

The test specimens were fork lifted onto the test platform. They were placed such that their slabs were aligned with the platform's stiffeners. Figure 4-21 showed the typical test setup of the experiment. One piece of ½" (13mm) thick homasote was placed between the concrete slabs and the test platform. The semi-low density press board, homasote, ensured that the applied loads would be uniformly distributed over the concrete slab ends and there would be minimal stress concentration as a result. To ensure that the applied loads were uniformly distributed at the top of the specimen, a 25mm thick aluminum plate was placed on top of the I-beam of the specimen.

Four DCDT displacement transducers were used to measure slip between the concrete slabs and the steel I-beam. Two displacement transducers were placed on each side of the specimen and at a position of top and bottom alternating along the steel flange (Figure 4-22). For the shear stud specimen, they were placed 25 mm below the top and bottom pairs of studs. For the bolted specimens, they were placed 25 mm below the bolts. All transducers were secured in the brackets and then the brackets were glued onto the inner side of the steel flanges using glue gun (Figure 4-23). Four aluminum L-angle sections were also glued onto the concrete slab surfaces so that the stems of the transducers could be set against the angle sections.

Figure 4-21: Typical Push Test Setup

Figure 4-22: Placement of Four Displacement Transducers

Figure 4-23: Top (Left) and Bottom (Right) Configuration of the Displacement Transducers

Two key safety measures were put in place before the specimens were tested. Firstly, two C-channels were anchored to the top of the concrete slabs respectively (Figure 4-21). Chains were used to tie the channels to the top of the test frame so that the concrete slabs were prevented from falling out of the test frame in the event of an unexpected specimen failure. Secondly, four wooden boards were placed on the test frame columns (Figure 4-21). The boards were used to prevent the bolts from turning into projectiles in the event of a sudden bolt rupture.

4.6.2 Test Procedure

The shear stud specimen had a peak displacement target of 10 mm. This target value was obtained from Bowser [2010]. The same peak displacement target of 10 mm was assumed for the shear lug specimens. This low peak slip value was assumed because the lugs would bear directly against the concrete during testing. The rest of the bolted specimens had a peak displacement target of 40 mm. This target value was obtained from Kwon et al. [2010].

All of the specimens were tested under static load to failure. The tests were conducted using displacement control to ensure safety during the test and to allow the load-displacement behaviour beyond the peak load to be captured. With displacement control, the controller varies the hydraulic pressure in the jack to achieve a certain actuator displacement. Failure typically occurred when some of the bolts of a specimen were ruptured. In an extreme failure condition, one side of the shear connectors was completed sheared-off and one of the slab panels was separated from the rest of the specimen.

Chapter 5
Experimental Results

In this chapter, the experimental results for the friction and push tests described in Chapter 4 will be presented and discussed. In Section 5.1, the results of the friction tests are presented. In Section 5.2 to 5.6, the push test results are presented for the shear stud connection and bolted connection with no friction enhancement, with shear lugs, and with type I and type II friction enhanced surfaces, respectively. Finally, results from the compression testing of concrete cylinders are presented in Section 5.7. These tests determine the actual concrete strength for each push test specimen.

5.1 Friction Test Results

The results of the friction tests are presented in Table 5-1. The weights of the plain steel plate, concrete sand coated steel plate and finer sand coated steel plate were measured to be 21.65 N, 22.40 N and 22.18 N, respectively. These weights excluded the weight of the steel block that was shown in Figure 4-1. By using the data presented in Table 5-1 and the measured weights of the steel plates, the friction coefficient for each steel-concrete interface was calculated according to Equation 4.1. Table 5-2 shows the calculated friction coefficient at each steel-concrete interface. The regular steel-concrete interface had a friction coefficient of 0.83. The friction coefficient increased when the steel surface was sand coated. Coupling the sand coated steel surface with treatments on the concrete surface such as peening or sandblasting also increased the friction coefficient. The highest friction coefficients were obtained for the following interface conditions: a finer sand coated steel surface with a peened concrete surface (μ = 1.29) and a concrete sand coated steel surface with sandblasted concrete surface (μ = 1.28).

To enhance the interface friction on the push test specimens, concrete sand coating was used on the friction enhanced type I and type II specimens. Concrete sand coating was chosen over the finer sand coating because concrete sand would be readily available in the construction industry. To further enhance the interface friction on the push test specimens, the sandblasting surface was used on the friction enhanced type II specimens. Sandblasting was chosen over peening because sandblasting a large concrete surface can be done quickly and efficiently by professional contractors. Based on the small-scale friction test results, the friction coefficients for the friction enhanced type I and type II specimens are 1.11 and 1.28, respectively.

Table 5-1: Average Bucket Weight Required to Pull Off the Steel Plate

	Steel Plate Surface		
	Plain	Concrete Sand Coating	Finer Sand Coating
Regular Concrete Surface	18 N	25 N	24 N
Peened Concrete Surface	-	27 N	29 N
Sandblasted Concrete Surface	-	29 N	27 N

Table 5-2: Friction Coefficient for the Steel-Concrete Interface

	Steel Plate Surface		
	Plain	Concrete Sand Coating	Finer Sand Coating
Regular Concrete Surface	0.83	1.11	1.09
Peened Concrete Surface	-	1.20	1.29
Sandblasted Concrete Surface	-	1.28	1.21

5.2 Shear Stud Connection Test Results

The shear stud specimen eventually failed by fracturing of the shear studs at a peak load of 1575 kN (Figure 5-1 and Figure 5-2). The concrete slab on the right side of the specimen was seen to completely shear off when the shear studs fractured. As shown in Figure 5-1, the fractured shear studs remained buried within the concrete slab and local concrete crushing underneath the fractured shear studs was observed. The slab that was sheared off had some minor cracks on the top left corner of the slab surface (Figure 5-1). On the other hand, the slab that remained attached to the steel I-beam did not have these cracks but did have significant concrete spalling at the base. As shown on Figure 5-1, this spalling occurred just below the bottom end of the steel I-beam because the tip of the steel flange was bearing down on the slab. The steel flange was bearing against the slab due to a construction defect. Figure 5-2 showed the fractured shear studs after testing. Plastic deformation of the studs was observed on the figure. Stud fracture happened near the base of the studs, just above the stud welds. Shearing of the stud welds did not occur as shown on Figure 5-3.

Figure 5-1: Shear Studs Fracture Failure (Left); Fractured Studs in Concrete Slab (Right)

Figure 5-2: Fractured Shear Studs After Testing

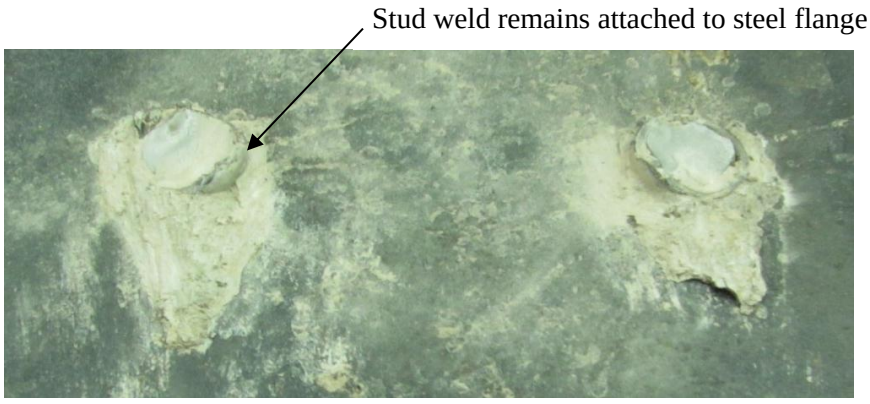

Figure 5-3: Shear Studs Fracture Surface

Figure 5-4 presents the load-slip curves for the shear stud specimen (i.e. specimen NS-0). The four load-slip curves were plotted using data collected from the four displacement transducers. They show reasonably good agreement with each other, indicating symmetric loading and specimen behaviour. These curves show that the behaviour of the shear stud connection was initially linear (elastic). Nonlinear load-slip behaviour was initiated at a load of approximately 1300 kN. The connection eventually exhibited significant nonlinear (plastic) deformation until it reached a maximum load of 1575 kN. The average maximum slip of the connection at stud fracture was 8.4 mm. Based on the load-slip model developed by Hanswille et al. [2006], the slip of the shear stud connection at stud fracture was 8.8 mm. In other words, the test results and the model developed by Hanswille et al. [2006] showed good agreement with each other.

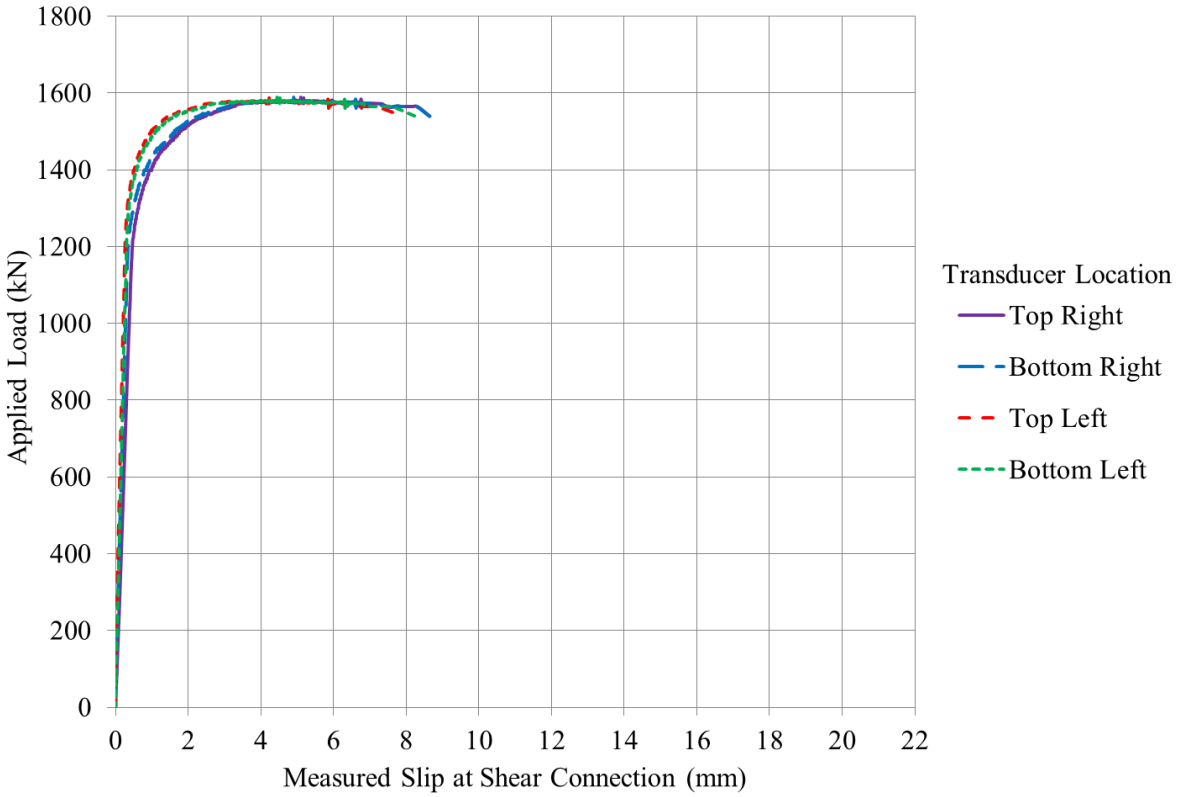

Figure 5-4: Load-Slip Curves for Specimen NS-0

The load-slip curves of the shear stud specimen exhibited good ductility before failure in the sense that the deflection at failure is considerably larger than the deflection at the onset of nonlinear behaviour. However, it should be noted that stud fracture was very suddenly and resulted in complete loss of the connection between the steel I-beam and the concrete slab.

5.3 Bolted Connection Test Results

The bolted plain specimen (i.e. specimen P M-85) failed by fracturing of the bolts (Figure 5-5). It should be noted that bolt fracturing did not happen simultaneously in all bolts. When the specimen reached its ultimate load capacity, two of the bolts fractured and then the applied loads from the test frame decreased. More bolts subsequently fractured as the specimen was reloaded. Since the concrete slab panels were still partially bolted to the steel I-beam after the specimen reached its ultimate capacity, the bolted connection exhibited good structural redundancy. After testing, the concrete slab panels were dissembled from the steel I-beam. No damage was observed on the panels except local concrete crushing underneath the bolts. As shown on Figure 5-5 and Figure 5-6, bolt fractures occurred at the end of the threaded part of the bolts. The fractured surface of the bolts showed that the bolts failed by shear. Shear and bending deformation of the bolts were observed from the figures.

Figure 5-5: Fractured Bolts After Testing – Specimen P M-85

Figure 5-6: Close Up Shot of the Fractured Bolt Surface – Specimen P M-85

Figure 5-7 presents the load-slip curves for specimen P M-85. These curves show that the behaviour of the bolted connection was linear-elastic up to a load of 150 kN. In other words, the connection began to slip and behave nonlinearly above this load. As shown on the figure, two sets of similar nonlinear load-slip curves can be identified since a high level of slip was observed beyond the slip load on the left side. The specimen had an ultimate load of 890 kN. The average maximum slip of the specimen at failure was 9 mm.

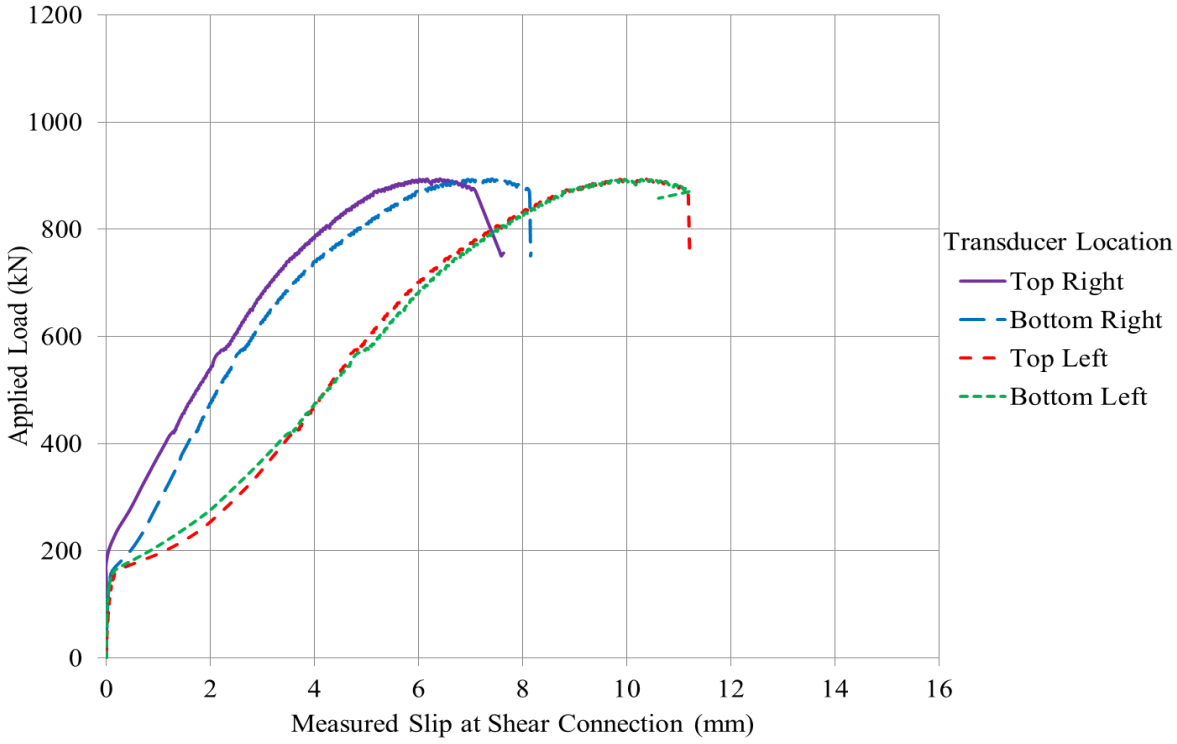

Figure 5-7: Load-Slip Curves for Specimen P M-85

5.4 Bolted Shear Lug Connection Test Results

All shear lug specimens failed by fracturing of the bolts (Figure 5-8). When each specimen reached its ultimate load capacity, several bolts fractured and then the applied loads from the test frame decreased to a lower specimen load level. As expected, shearing of the shear lug welds did not occur in any of the specimens.

Prior to the bolt fracture failure, all shear lug specimens experienced shearing of the concrete wedges underneath the shear lugs. When each specimen was loaded in shear, the steel I-beam displaced downward relatively to the concrete deck panels and the shear lugs were pushing against the bottom side of the concrete match cast holes. Each shear lug deformed the concrete match cast hole to the extent that it enlarged the hole in the deck longitudinal direction (Figure5-9). The deformation of the holes at the end of the test for specimen SL S-0, SL M-0 and SL S-53 were 15 mm, 20 mm and 16 mm, respectively. As shown in Figure 5-9, a concrete wedge was formed beneath each hole as each shear lug was pushed into the concrete. For specimen SL S-0 and SL M-0, the wedges were completely sheared off when the specimens reached failure. The sheared surfaces of the wedges had white dust on the surfaces, which indicated that concrete crushing had occurred along the shear planes of the wedge. Figure 5-10 (a) and 5-11 (a) showed the concrete panels with the wedge sheared off. For specimen SL S-53, the wedges remained attached to the concrete panels after testing. The pretension force in the bolts likely prevented the complete shearing of the concrete wedges in this specimen.

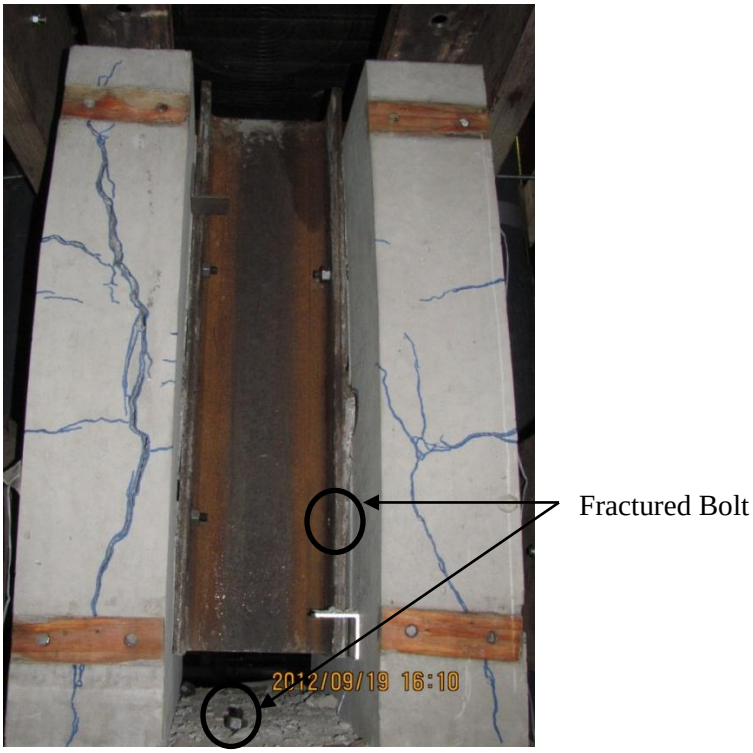

Figure 5-8: Bolt Fracture Failure – Specimen SL S-0

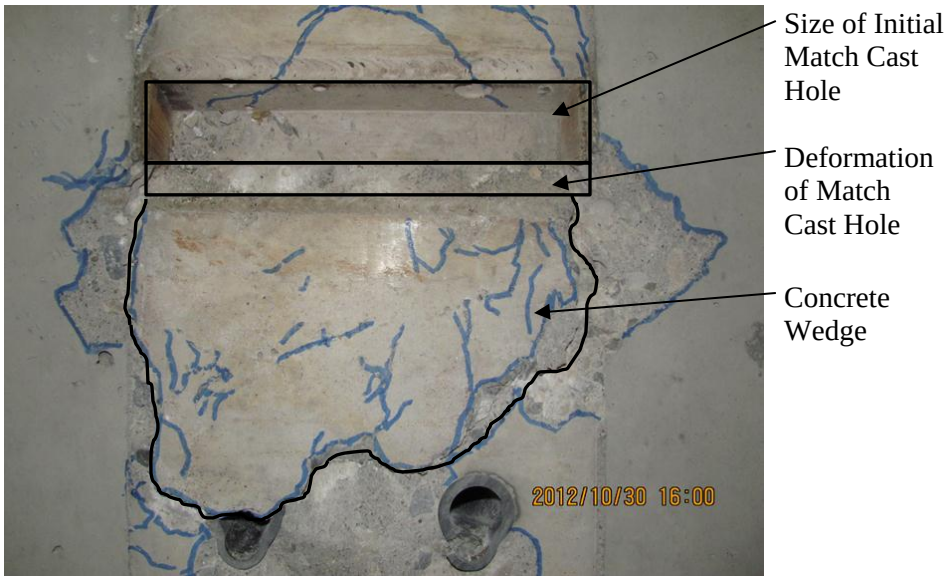

Figure 5-9: Deformed Concrete Match Cast Hole and Its Associated Concrete Wedge

Prior to bolt fracture, all shear lug specimens developed significant cracks on their exterior surfaces. The crack development prior to bolt fracture meant that the shear lug connection would exhibit warning before the failure would occur. Specimen SL S-0 had the most cracks when compared with the other two shear lug specimens. This can be explained by the fact that this specimen utilized small size bolts without any pretensioning. When there were no pretension forces in the bolts, the concrete panels were not tightly clamped together with the steel I-beam and cracks could form more easily as the I-beam slipped in relation to the panels. As mentioned earlier, specimen SL M-0 and SL S-70 had relatively fewer cracks than specimen SL S-0. This observation was most obvious when looking at the panel deck surfaces. The cracks on specimen SL M-0 and SL S-70 also appeared to be less wide and deep than the ones on specimen SL S-0.

To verify the crack depth, both panels of specimen SL S-0 were sawcut longitudinally along the middle of the panel width. Figure 5-10 and 5-11 show the crack patterns observed on the panels after they were sawcut. Figure 5-10 (a) and 5-11 (a) show that cracks extend from the sheared off wedges to the bottoms of the panels. Figure 5-10 (b) and 5-11 (b) show the crack patterns that were developed on the deck surfaces of the specimen. As shown on these figures, the cracks were all over the deck surfaces and they extend from one edge to the other. Figure 5-10 (c), 5-10 (d), 5-11(c) and 5-11(d) show the crack patterns inside the concrete panels. Both of the panels had cracks extending from the match cast holes to the deck surfaces; furthermore, the cracks went through the entire panel depth at a 45° angle. On one of the panels, a crack on the outside deck surface was also observed extending from the sheared off wedge to the bottom of the panel (Figure 5-11(c) and 5-11(d)).

Both panels of specimen SL M-0 were also sawcut. The sawcut surfaces of these panels also displayed 45° angle cracks from the match cast holes to the deck surfaces. In other words, the full depth crack patterns inside these panels were similar to those from specimen SL S-0. It should be noted that concrete deck surface cracks were also observed on specimen SL M-0.

When the shear lug specimens were loaded to failure, concrete spalling occurred in addition to the concrete cracking that was mentioned earlier. Spalling occurred beside the concrete wedges that were sheared off (Figure 5-10 (a) and 5-11(a)). As the specimens were loaded, the shear lugs deformed the concrete underneath the lugs, causing pieces of concrete beside the wedges to spall off. Spalling was also observed underneath the bolt holes as shown in Figure 5-10 (a) and 5-11 (a). Concrete spalling on this part of the specimens was due to the fact that the bolts were bending during the test and the concrete underneath the bolts was crushed due to the bearing forces introduced by the bolts.

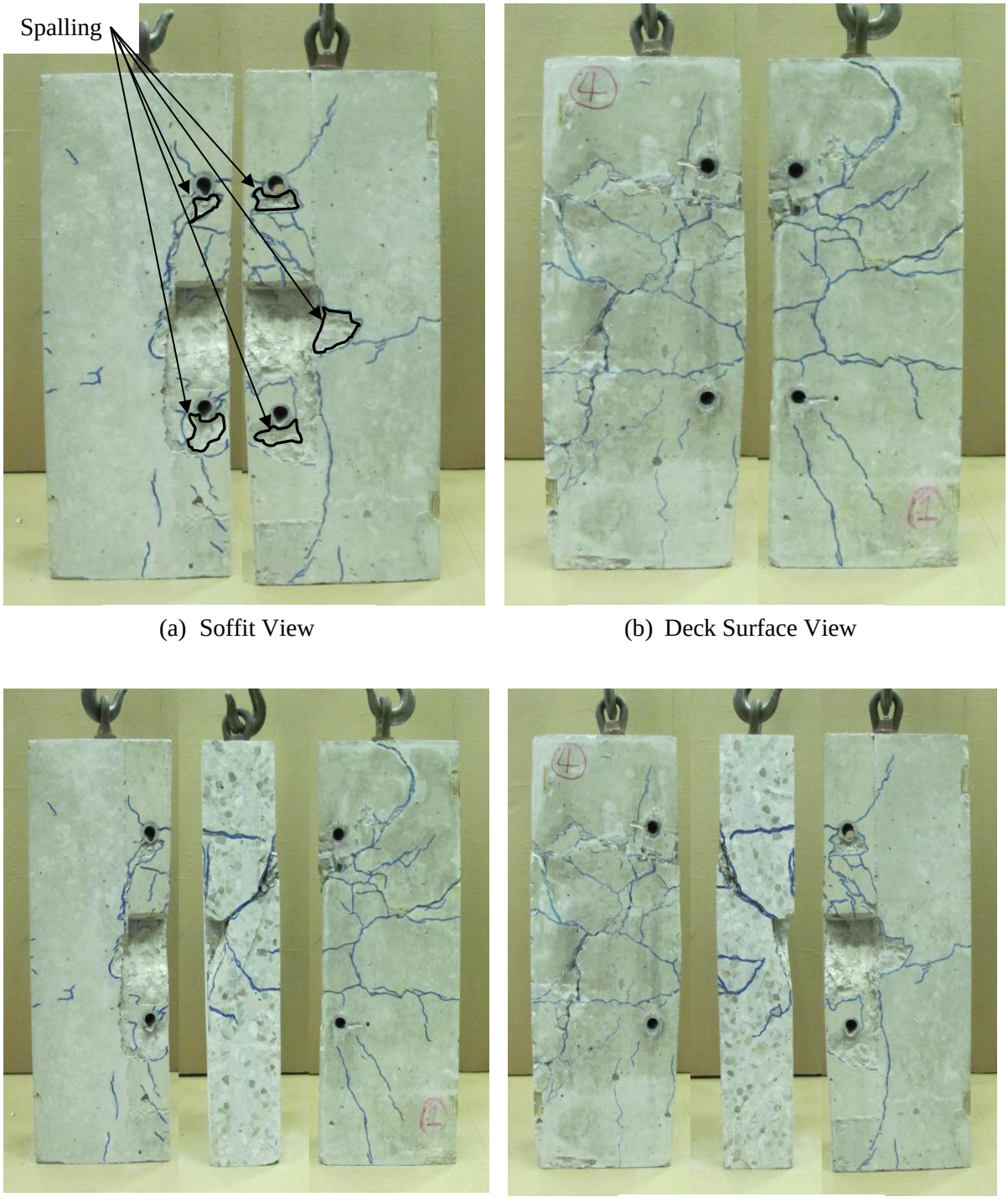

(a) Soffit View

(b) Deck Surface View

(c) Sawcut View

(d) Sawcut View

Figure 5-10: Concrete Crack Pattern for Panel 1 of Specimen SL S-0

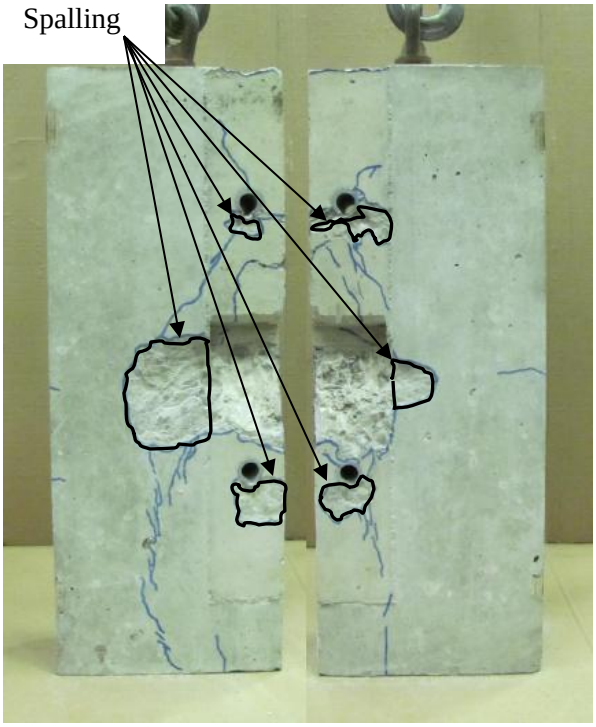

(a) Soffit View

(b) Deck Surface View

(c) Sawcut View

(d) Sawcut View

Figure 5-11: Concrete Crack Pattern for Panel 2 of Specimen SL S-0

Figure 5-12 presents the load-slip curves for specimen SL S-0. The shear lug connection on the right side of the specimen exhibited a higher initial stiffness than the connection on the left. In other words, the connection on the right side had less slip than the connection on the left when the specimen was loaded in the linear-elastic range. The specimen started to behave nonlinearly when the applied load reached 990 kN. As the specimen was loaded in the nonlinear range, the four load-slip curves exhibited similar behaviour, meaning that the increase in load caused an identical increase in slip on both sides. The four load-slip curves exhibited good ductility before failure. The specimen failed at an ultimate load of 1435 kN and the average maximum slip of the specimen before failure was 19.4 mm.

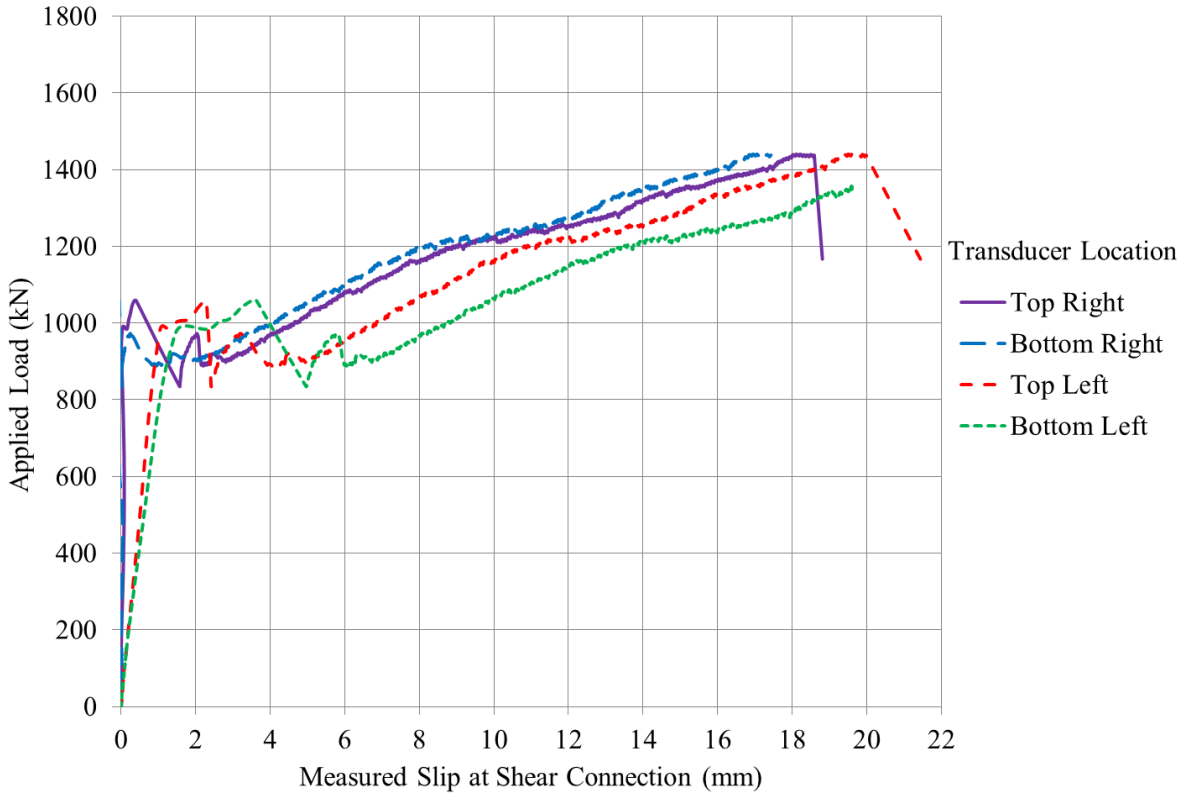

Figure 5-12: Load-Slip Curves for Specimen SL S-0

Figure 5-13 shows the load-strain curves for specimen SL S-0. No strains in the bolts were measured initially because the bolts were not pretensioned. As the specimen was loaded in the linear-elastic range, the strains in the bolts increased gradually and linearly as the applied load increased. As the load-displacement behaviour of the specimen became nonlinear, two distinct sets of load-strain curves could be identified. One set of curves was obtained from the strain gauges on right side of the

specimen and the other set of curves was obtained from the strain gauges on the left side. The gauges on the left side recorded higher strains than the gauges on the right side in this range. As expected, the rate of strain increase in the nonlinear range was greater than the rate of strain increase in the linear-elastic range.

The nominal yield strain of the ASTM A325 ½ inch (12.70 mm) diameter bolts was 3170 microstrain. This strain was calculated by assuming that the bolts had a nominal yield strength of 634 MPa and an elastic modulus of 200 GPa. According to the load-strain curves, the bolts on the left side of the specimen yielded before specimen failure occurred while the bolts on the right side did not.

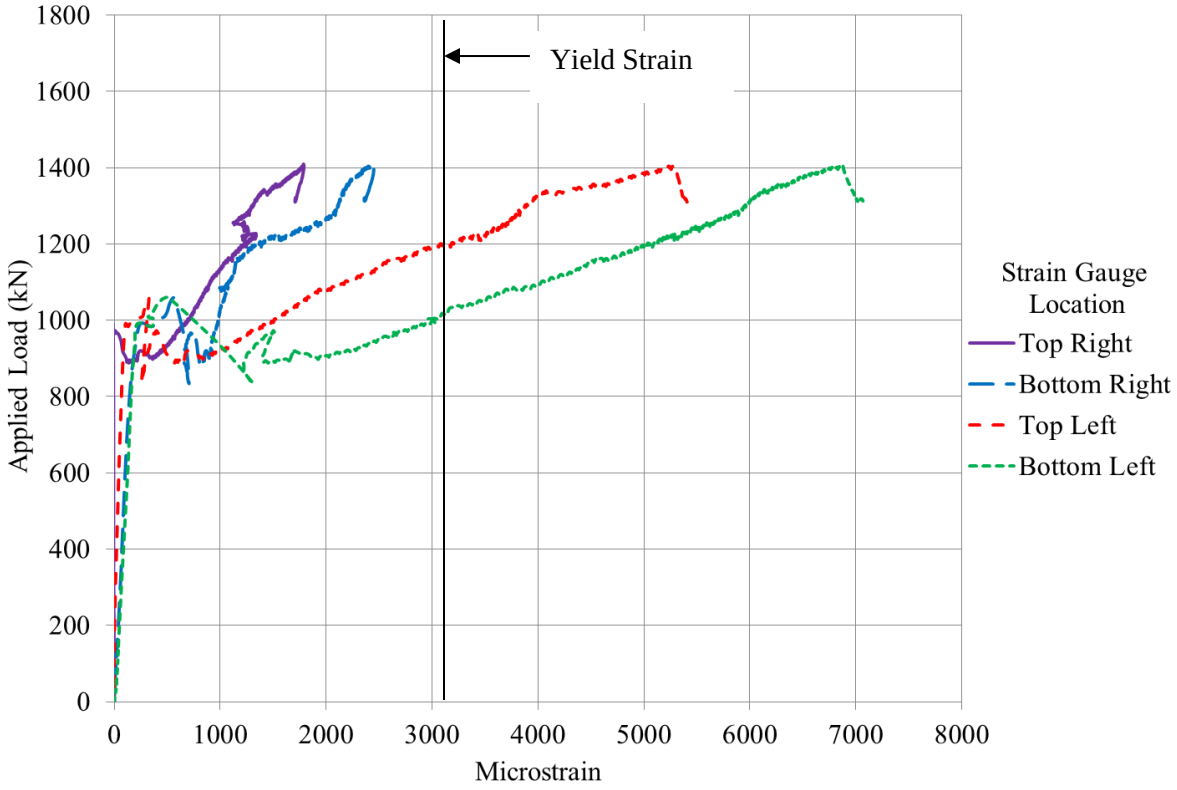

Figure 5-13: Load-Strain Curves for Specimen SL S-0

Figure 5-14 presents the load-slip curves for specimen SL M-0. Two sets of similar load-slip curves were obtained for each side of the specimen. The shear lug connection on the right side of the specimen had greater initial stiffness than the connection on the left. In other words, the connection on the right side had less slip than the connection on the left when the specimen was loaded in the linear-elastic range. The specimen started to behave nonlinearly when the applied load reached 1030 kN. It began to slip nonlinearly as the load stayed roughly constant at a value of 1030 kN. In the

nonlinear range, the load eventually started to increase again as the slip values increased. The four load-slip curves exhibited identical stiffness in the nonlinear range. It should be noted that the connection on the left side of the specimen exhibited more ductility than the connection of the right. The specimen failed at an ultimate load of 1560 kN and the average maximum slip of the specimen before failure was 13.7 mm.

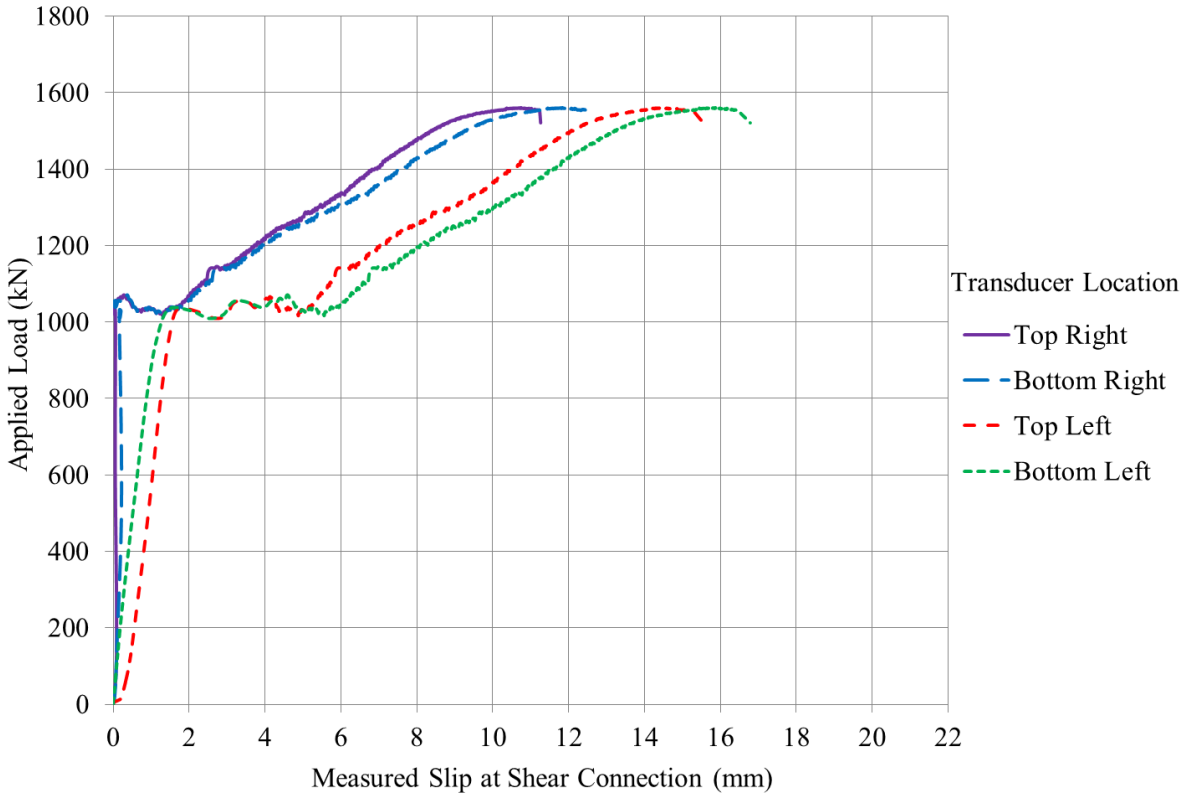

Figure 5-14: Load-Slip Curves for Specimen SL M-0

Figure 5-15 showed the load-strain curves for specimen SL M-0. The shapes of the curves from this Figure greatly resemble those from Figure 5-14. No strains were recorded in the bolts prior to loading since the bolts were not pretensioned. As the specimen slipped in the linear-elastic range, the strains in the bolts increased gradually and linearly as the applied load increased. Since the right side of the specimen barely slipped in the linearly-elastic range, the strain increase in the bolts on the right was very small. As the specimen slipped in the nonlinear range, two distinct sets of load-strain curves could be identified: one represented the strain in the bolts on right side of the specimen and the other represented the strain in the bolts on the left side of the specimen. The strain in the bolts on the left was greater than the strain in the bolts on the right because the left side of the specimen slipped more,

especially in the nonlinear range. As expected, the rate of the strain increase in the nonlinear range was much greater than the rate of the strain increase in the linear-elastic range.

According to the load-strain curves, all of the bolts with strain gauges had yielded before specimen failure occurred. As mentioned earlier, the yield strain calculated for the ASTM A325 bolts was 3170 microstrain.

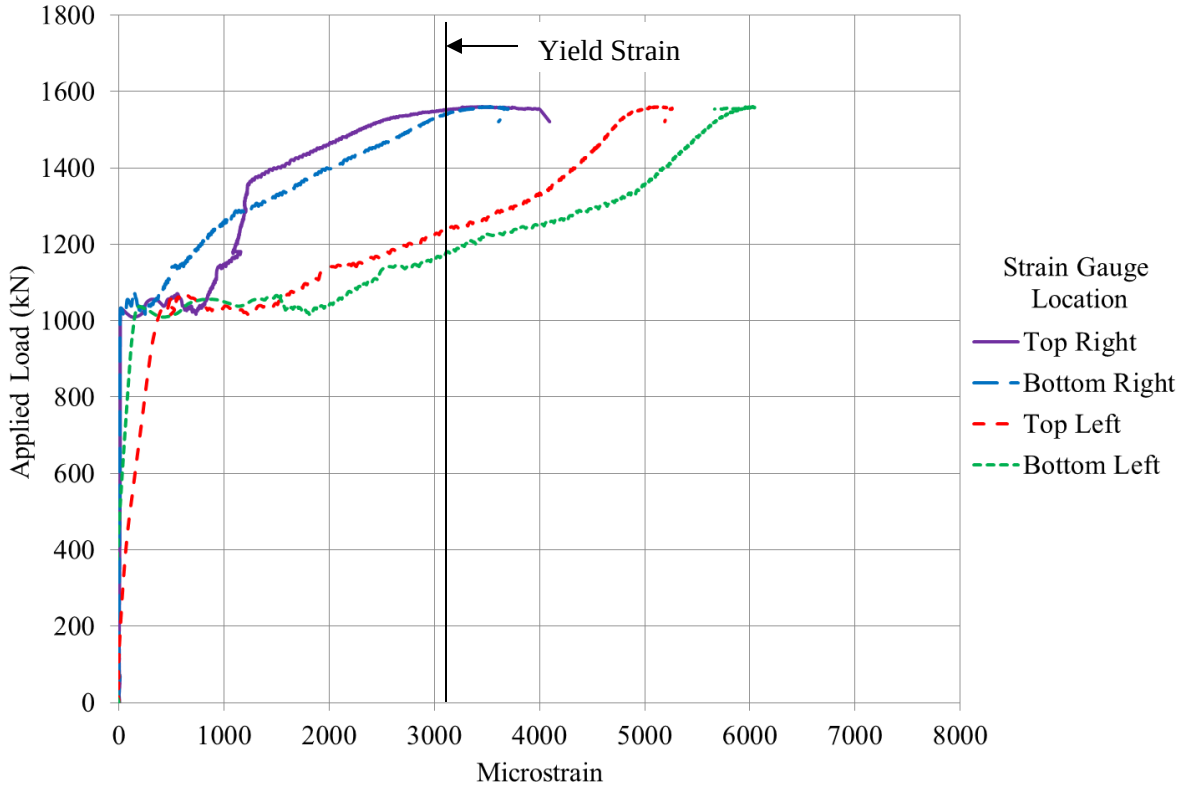

Figure 5-15: Load-Strain Curves for Specimen SL M-0

Figure 5-16 presents the load-slip curves for specimen SL S-53. As shown on the Figure, two sets of similar load-slip curves were obtained: one from the transducers on the right side of the specimen and the other obtained from the transducers on the left side. The right side of the specimen started to slip and behave nonlinearly at a load of 1200 kN. The left side of the specimen began to slip and behave nonlinearly at the load of 1335 kN. Both sides of the connection overcame local maximum peak loads before they displayed a large amount of deformation and slip in the nonlinear range. The four load-slip curves exhibited identical stiffness in the nonlinear range. It should be noted that the connection on the right side of the specimen exhibited more ductility than the connection on the left. The

specimen failed at an ultimate load of 1530 kN and the average maximum slip of the specimen before failure was 15 mm.

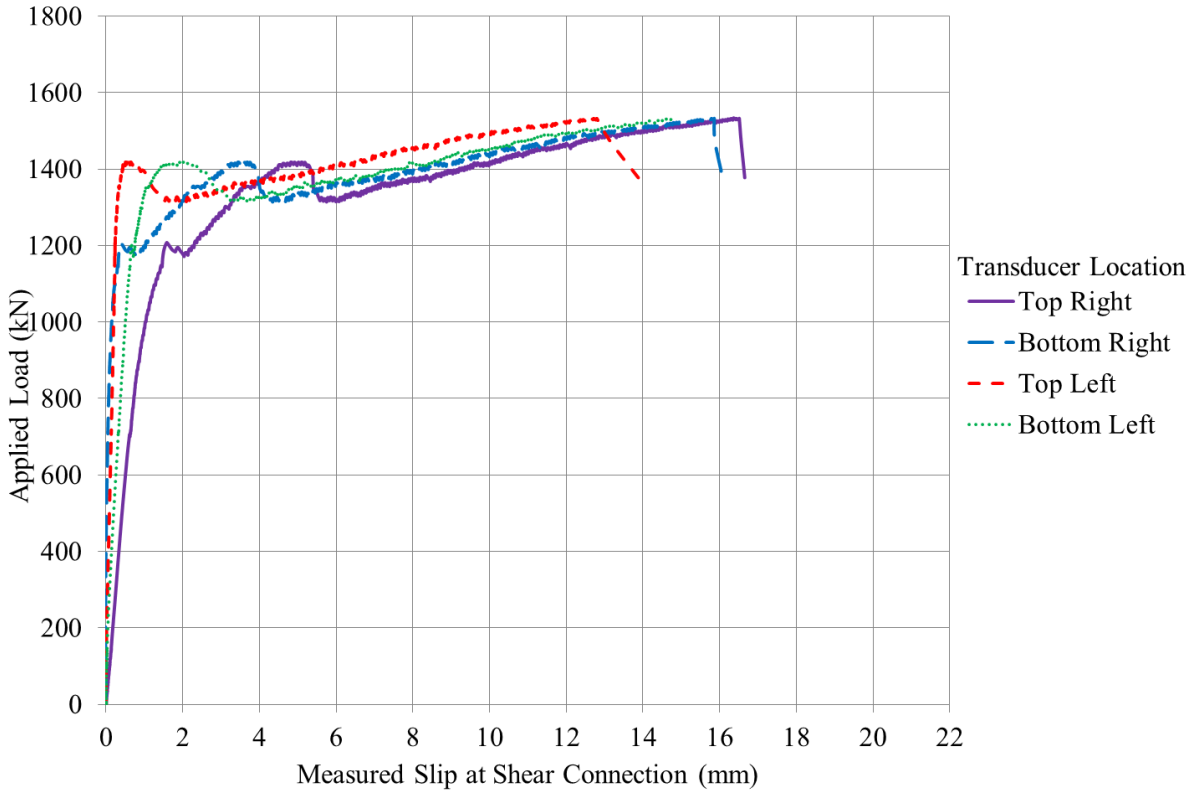

Figure 5-16: Load-Slip Curves for Specimen SL S-53

Figure 5-17 shows the load-strain curves for specimen SL S-53. No strain reading was recorded from the top right strain gauge because the gauge appeared to be damaged from the start of the test. All three load-strain curves are offset in this figure to an initial strain of 2087 microstrain because the bolts were pretensioned to 70% of their specified minimum tensile strength. The shape of the load-strain curve for the bottom right bolt is similar to the shape of the load-slip curves on the right side of the specimen, in the sense that the drop in load and onset of nonlinear behaviour appear to coincide. In the same way, the shapes of the load-strain curves for the bolts on the left side of the specimen are similar to the shapes of the load-slip curves representing the slip behaviour on the left side.

As mentioned before, the nominal yield strain of the ASTM A325 ½ inch (12.70 mm) diameter bolts was 3170 microstrain. According to the load-strain curves, all three bolts with strain gauge reading had yielded before specimen failure occurred.

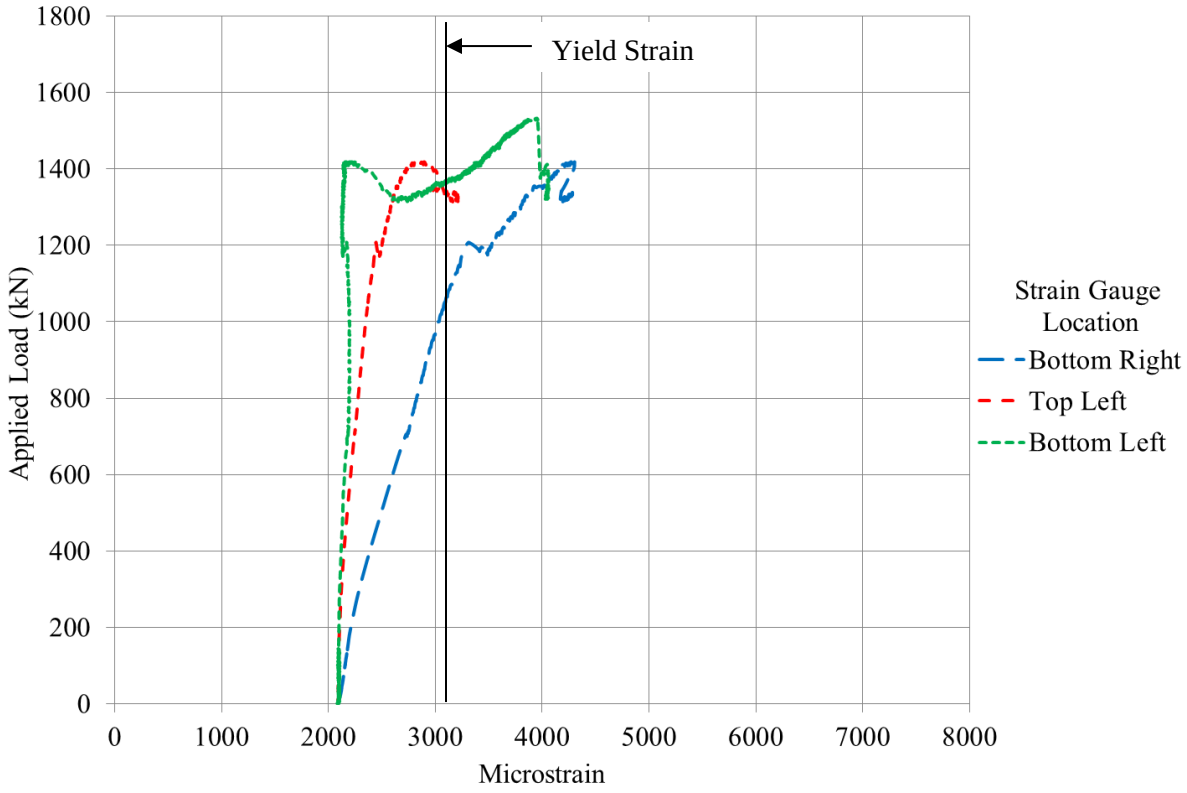

Figure 5-17: Load-Strain Curves for Specimen SL S-53

5.5 Test Results of Bolted Friction Enhanced Type I Connection

All friction enhanced type I specimens failed by fracturing of the bolts. Bolts fracturing happened progressively, not simultaneously. When each specimen reached its ultimate load capacity, several of the bolts fractured and then the applied loads from the test frame decreased to a lower load level. More bolts eventually fractured as each specimen was loaded at the lower load level. All bolt fractures occurred at the end of the threaded part of the bolts. The friction enhanced connection proved to have good structural redundancy because bolts failures from the connection happened progressively. After testing, no major damage was observed on the concrete slab panels except local concrete crushing underneath the bolts (Figure 5-18). Minor concrete flaking was observed on the panels at the steel-concrete interfaces (Figure 5-18). The flaked off concrete was also observed on the friction enhanced steel flanges (Figure 5-19).

Figure 5-18: Concrete Crushing under the Bolt Holes on Specimen FE1 L-53

Figure 5-19: Friction Enhanced Steel Flange Surface after Testing – Specimen FE1 L-53

Figure 5-20 shows the load-slip curves for specimen FE1 S-53. This specimen started to slip and behave nonlinearly at a load of 40 kN. As shown on the figure, two sets of similar nonlinear load-slip curves were obtained: one from the transducers on the right side of the specimen and the other from the transducers on the left side. The behaviour on the left side of the specimen appeared to be more

ductile. The average maximum slip of the specimen at failure was 11.1 mm. The specimen failed at an ultimate load of 430 kN.

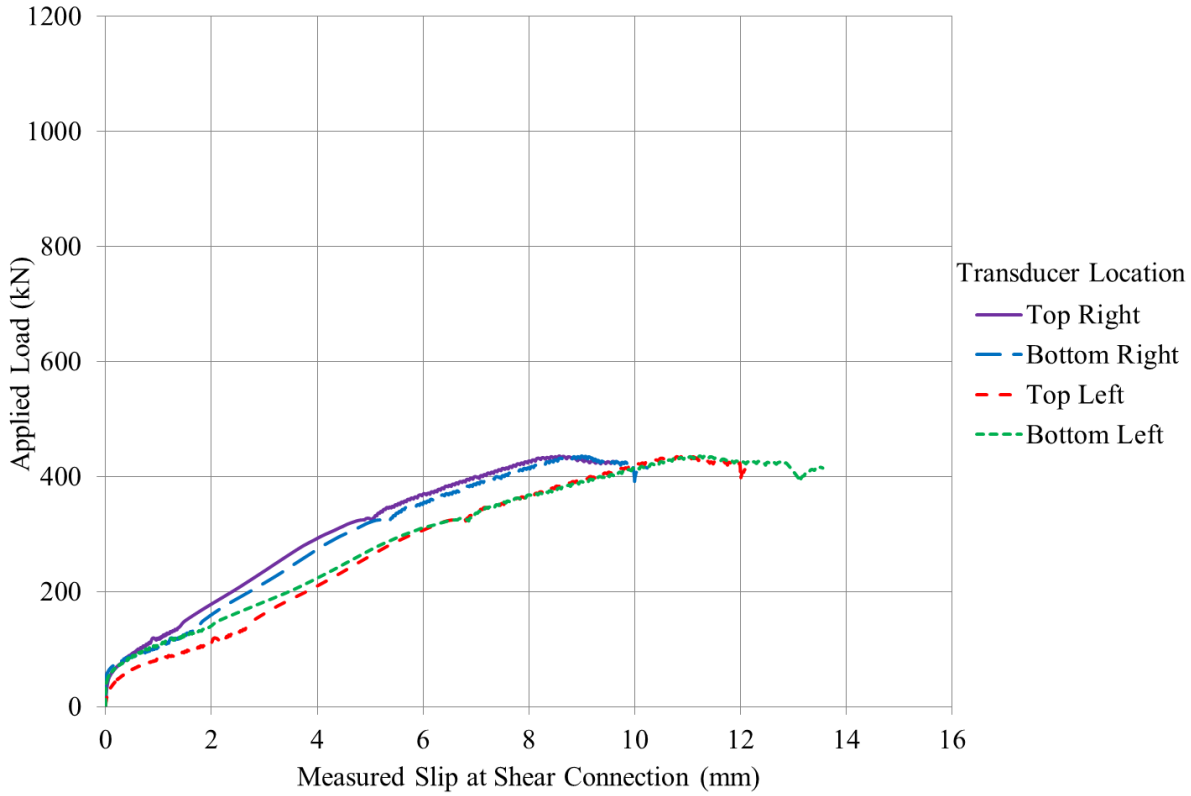

Figure 5-20: Load-Slip Curves for Specimen FE1 S-53

Figure 5-21 shows the load-slip curves for specimen FE1 M-85. This specimen started to slip and behave nonlinearly at a load of 55 kN. The load-slip curve obtained from the bottom left transducer exhibited significantly more deformation and slip than the other three curves. It also exhibited lower connection stiffness comparing to the other three load-slip curves. The other three curves appeared to be in good agreement with each other in terms of ductility and stiffness. They had similar slope values in their nonlinear range of the curves. They also shared similar slip values when the specimen reached an ultimate load of 660 kN. The average maximum slip of all four curves before specimen failure was 11.7 mm.

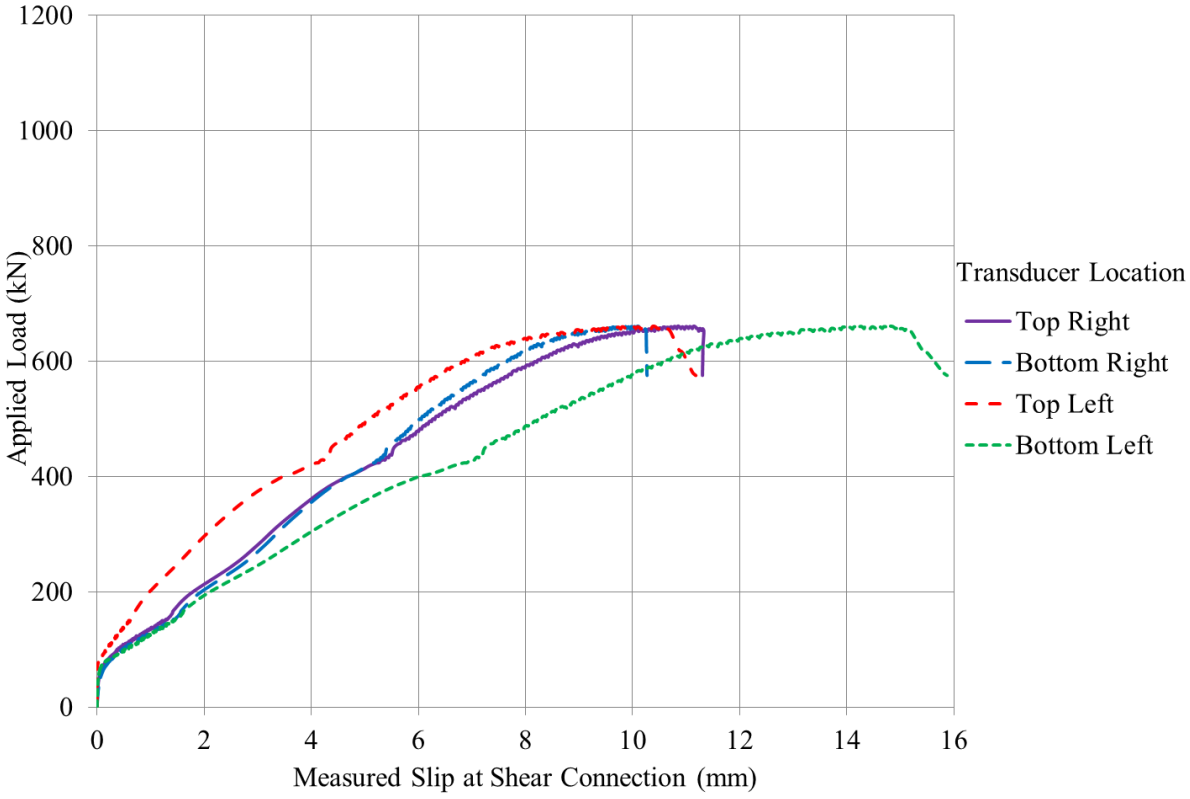

Figure 5-21: Load-Slip Curves for Specimen FE1 M-85

Figure 5-22 presents the load-slip curves for specimen FE1 L-125. The left side of the specimen started to slip and behave nonlinearly at a load of 115 kN. At the load of 225 kN, the right side of the specimen began to slip and behave nonlinearly. The four load-slip curves showed good agreement with each other in terms of their slopes in the nonlinear range. In other words, the stiffness of the connection on each side of the specimen was approximately the same. As shown on Figure 5-22, three of the four curves exhibited similar nonlinear load-slip behaviour. The other curve, representing data from the top left transducer, also showed similar behaviour but it had slightly greater slip values recorded. The average maximum slip of the specimen at failure was 11.1 mm. The specimen failed at an ultimate load of 1025 kN.

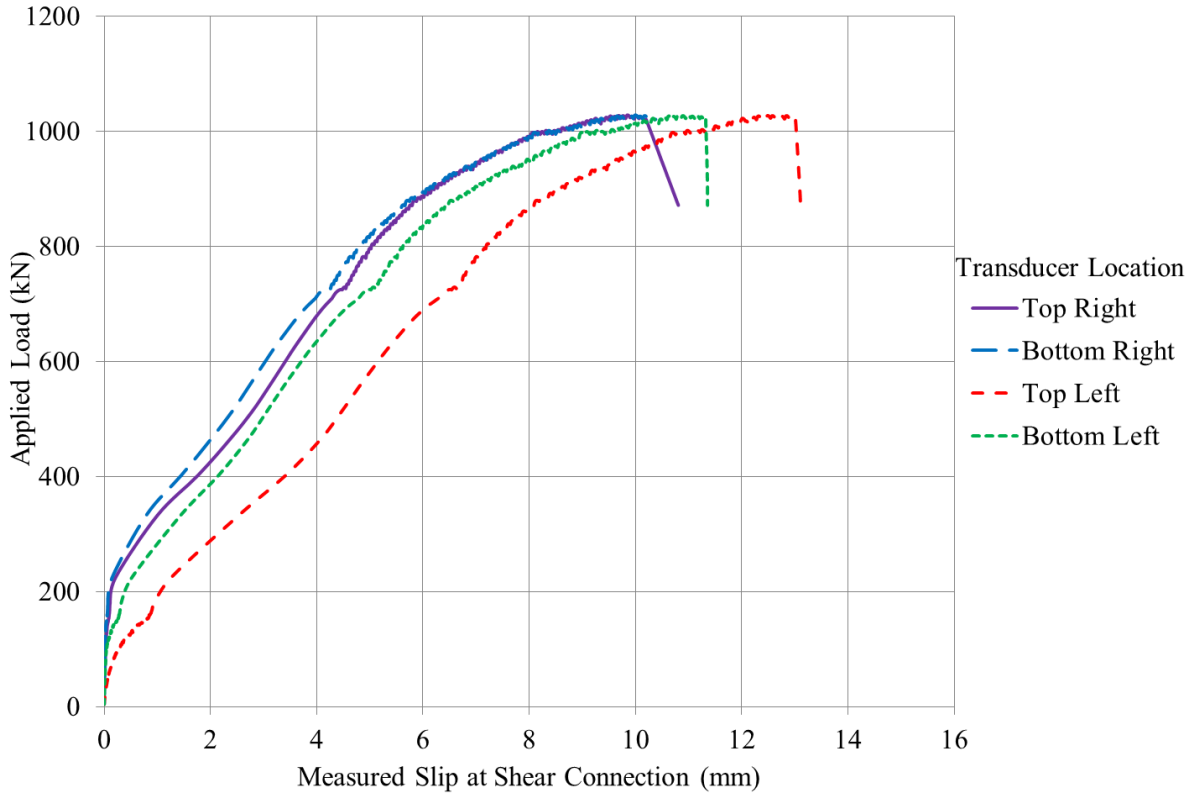

Figure 5-22: Load-Slip Curves for Specimen FE1 L-125

Figure 5-23 presents the load-slip curves for specimen FE1 M-53. As shown on the figure, two distinct sets of nonlinear load-slip curves were obtained: one from the transducers on the right side of the specimen and the other from the transducers on the left side. The right side of the specimen started to slip and behave nonlinearly at a load of 50 kN. The left side of the specimen also began to slip and behave nonlinearly at the load of 90 kN. Greater ductility was observed on the right side of the specimen. The connection on the right side of the specimen also had lower stiffness than the connection on the left. The specimen failed at an ultimate load of 640 kN. The average maximum slip of the specimen at failure was 11.2 mm.

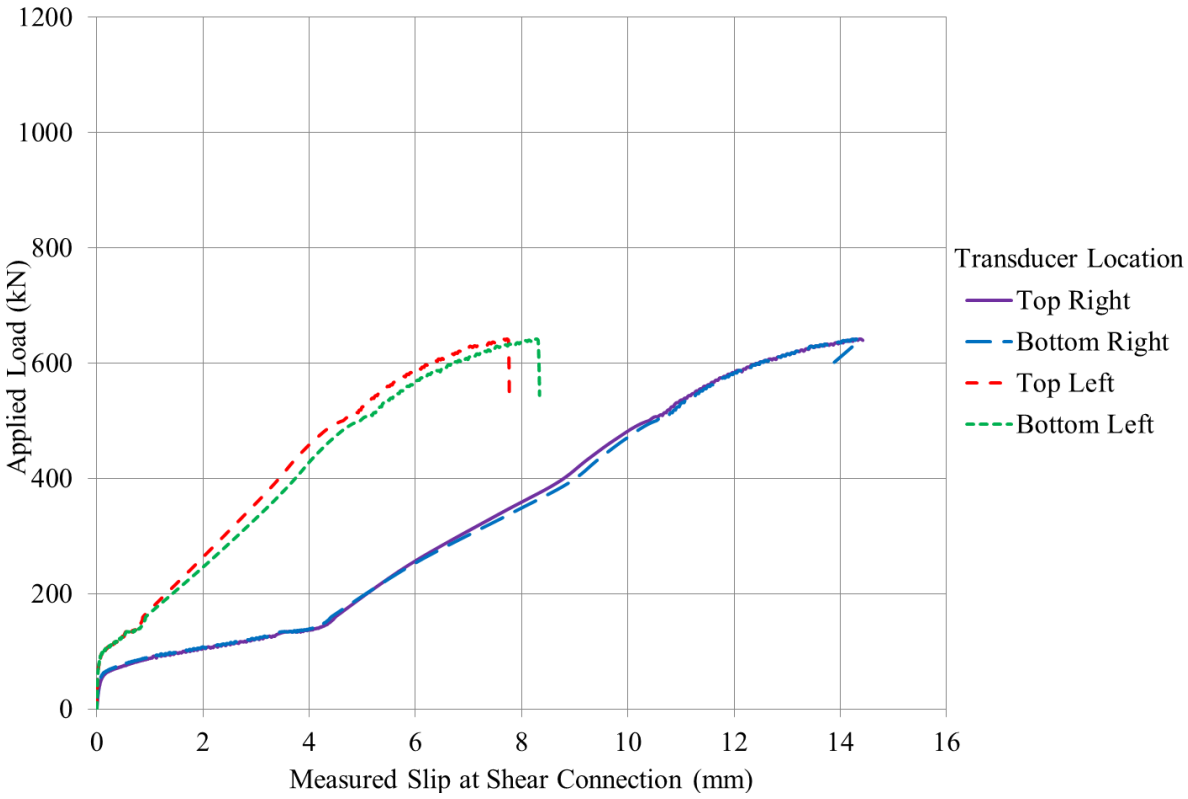

Figure 5-23: Load-Slip Curves for Specimen FE1 M-53

Figure 5-24 shows the load-strain curves for specimen FE1 M-53. All the load-strain curves were offset to have an initial strain of 1338 microstrain because the bolts were pretensioned to 70% of the specified minimum tensile strength of the ½ inch (12.70 mm) bolt. When the specimen started to slip, the strains in the bolts at the bottom right and top left of the specimen actually decreased. One possible explanation for this observation is that the strain gauge placements for these bolts might have been slightly skewed, resulting in compressive strains due to bending also being recorded in addition to the tensile axial strains. The shape of the load-strain curve for the bolt on the top right of the specimen was similar to the shape of the load-slip curves for the connection on the right side of the specimen, except that this load-strain curve stopped showing any strain increase after the load reached 400 kN. The shape of the load-strain curves for the bolt on the bottom left of the specimen, was also similar to the shape of the load-slip curves for the slip behaviour on the left. As the applied load increased, the slip increased and the associated bolt strain increased.

As mentioned in this section, the nominal yield strain of the ASTM A325 5/8 inch (15.88 mm) diameter bolts was 3170 microstrain. According to the load-strain curves, two out of the four bolts with strain gauge reading had yielded before specimen failure occurred.

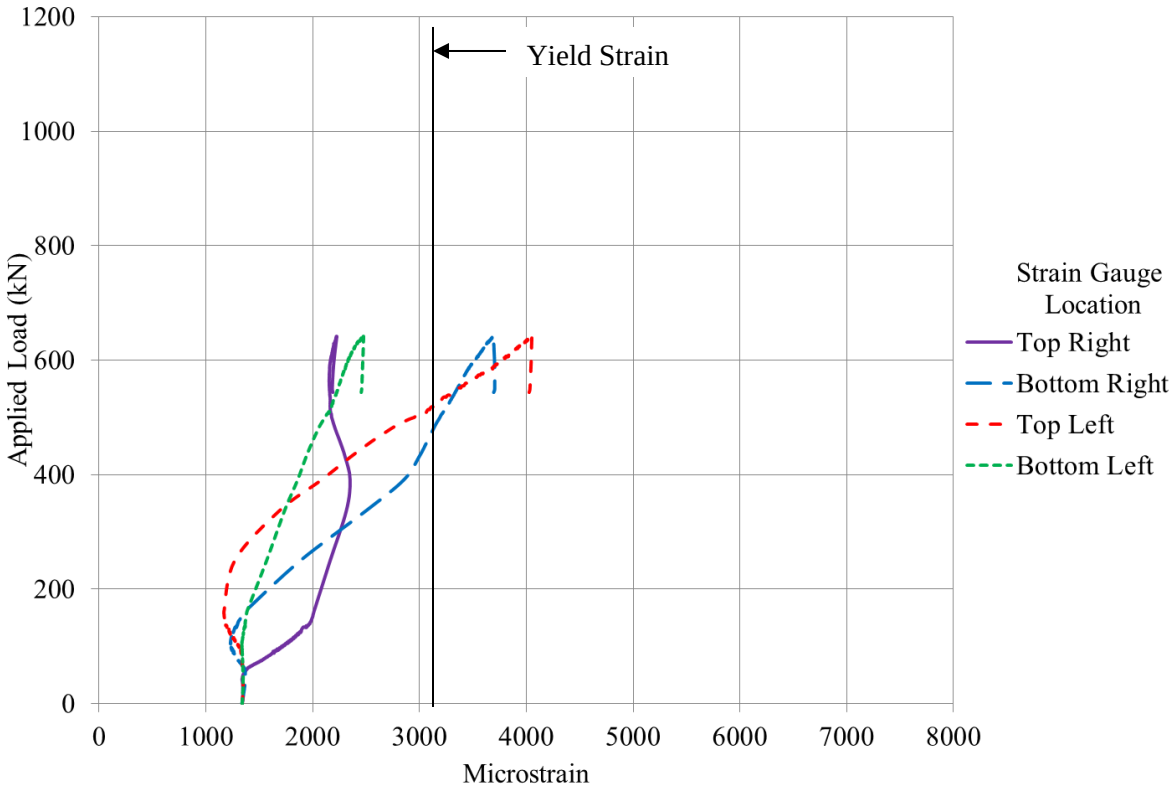

Figure 5-24: Load-Strain Curves for Specimen FE1 M-53

Figure 5-25 presents the load-slip curves for specimen FE1 L-53. This specimen started to slip and behave nonlinearly at a load of 50 kN. As shown on the Figure, the transducer at the bottom left location was lost when the load reached approximately 500 kN. This loss of transducer was due to the unbonding of the glue on the inner side of the steel flange. The load-slip curves obtained from the three other transducers were completely plotted to the ultimate load of the specimen. Their plots exhibited similar shape although their slip values and slope values differed at various load points. The average maximum slip of the specimen before failure was 11.4 mm. The specimen failed at an ultimate load of 850 kN.

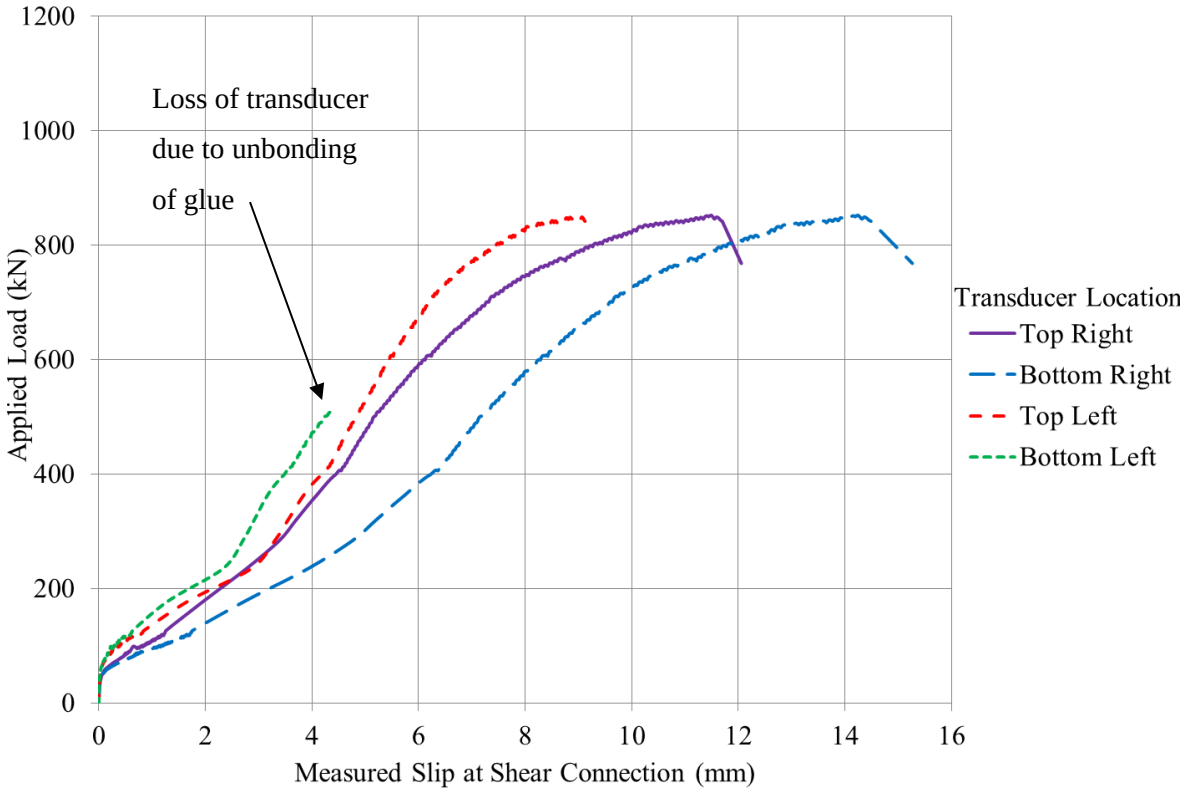

Figure 5-25: Load-Slip Curves for Specimen FE1 L-53

5.6 Test Results of Bolted Friction Enhanced Type II Connection

The failure condition and failure mode of the friction enhanced type II specimens were essentially the same as the ones exhibited by the friction enhanced type I specimens.

Figure 5-26 shows the load-slip curves for specimen FE2 S-53. As shown on the figure, two sets of similar nonlinear load-slip curves were obtained: one from the transducers on the right side of the specimen and the other from the transducers on the left side. The left side of the specimen slipped first and started to behave nonlinearly at a load of 60 kN. The right side of the specimen also began to slip and behave nonlinearly when the load reached 100 kN. The behaviour on the left side of the specimen appeared to be slightly more ductile as greater slip was recorded on the left side. Both sides of the specimen exhibited similar connection stiffness after the load reached 150 kN. The specimen failed at an ultimate load of 495 kN and the average maximum slip of the specimen at failure was 10.4 mm.

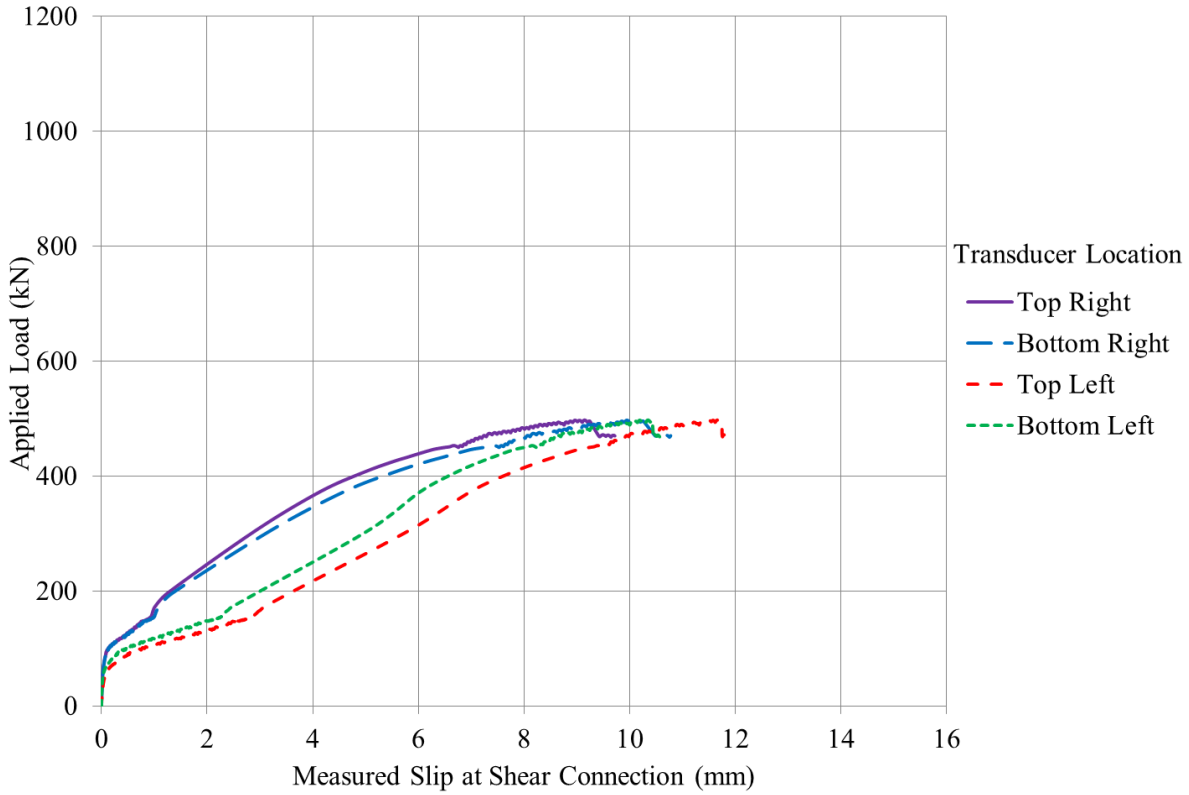

Figure 5-26: Load-Slip Curves for Specimen FE2 S-53

Figure 5-27 shows the load-slip curves for specimen FE2 M-85. This specimen started to slip and behave nonlinearly at a load of 105 kN. The load-slip curve obtained from the top right transducer exhibited less deformation and slip than the other three curves. It also exhibited higher stiffness in the nonlinear range of the curve comparing to the other three load-slip curves. The other three curves showed good agreement with each other in terms of stiffness and shape. They had similar slope values in their nonlinear range of the curves. The average maximum slip of all four curves before specimen failure was 9.6 mm. The specimen failed at an ultimate load of 700 kN.

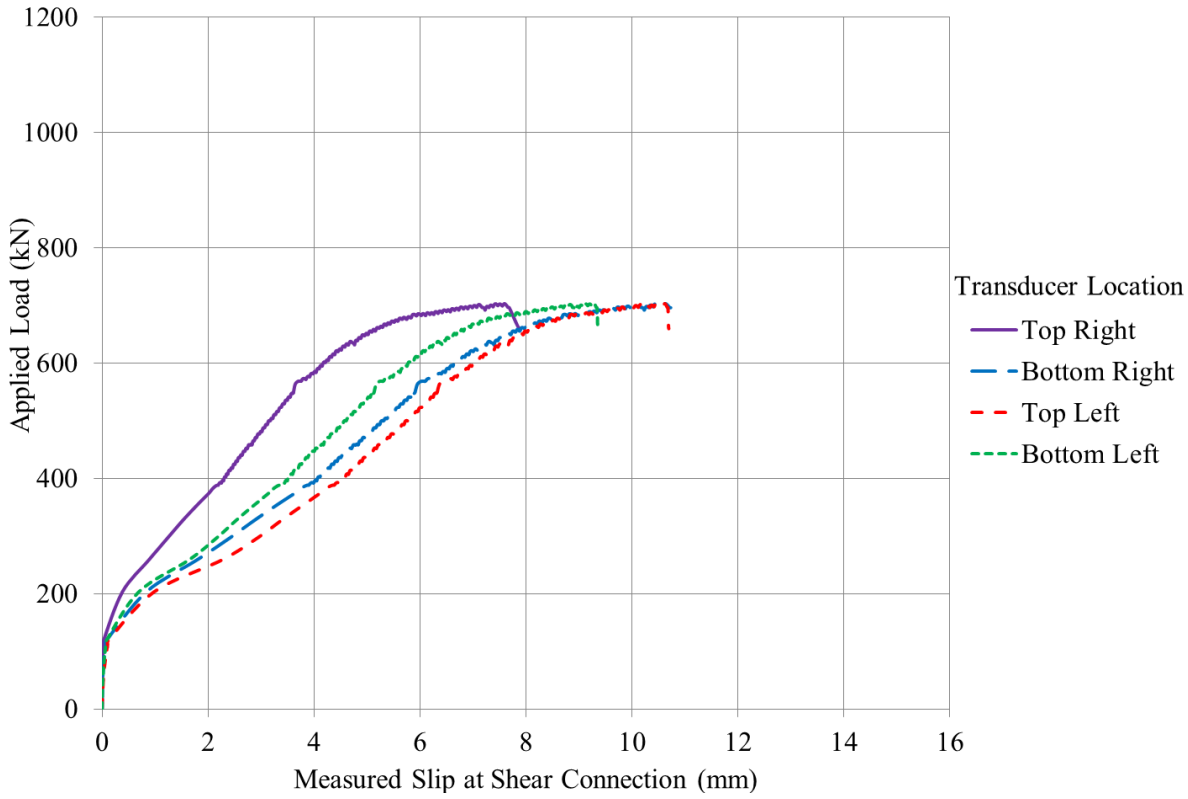

Figure 5-27: Load-Slip Curves for Specimen FE2 M-85

Figure 5-28 presented the load-slip curves for specimen FE2 L-125. This specimen started to slip and behave nonlinearly at a load of 125 kN. As shown on the figure, two sets of similar nonlinear load-slip curves were obtained: one from the transducers on the right side of the specimen and the other from the transducers on the left side. The behaviour on the right side of the specimen appeared to be more ductile in the nonlinear range as greater slip was recorded on the right side. Both sides of the specimen had the same initial stiffness. The specimen failed at an ultimate load of 1020 kN and the average maximum slip of the specimen at failure was 12.4 mm.

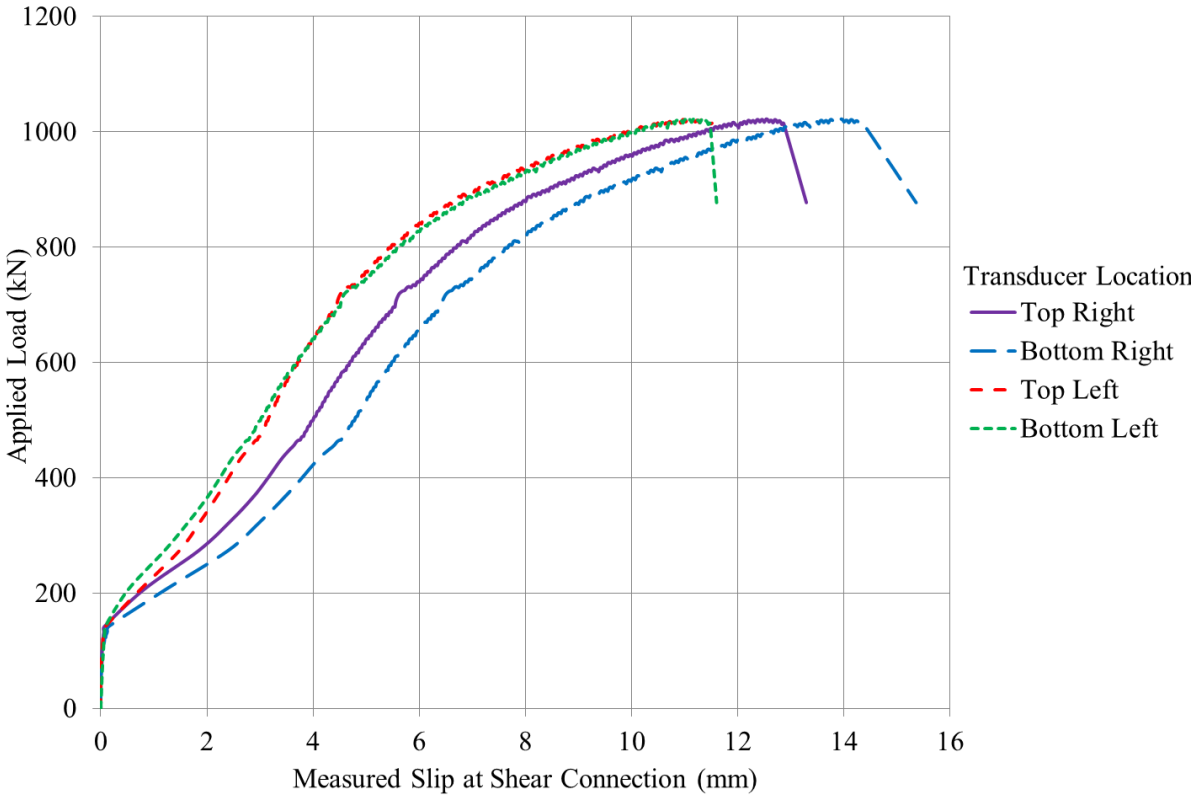

Figure 5-28: Load-Slip Curves for Specimen FE2 L-125

5.7 Concrete Compression Test Results

Table 5-3 shows the concrete compression test results. All of the actual concrete strengths, based on the concrete compression tests, were greater than the specified concrete strength of 35 MPa. The 7-days early strength of the concrete was 37.22 MPa. The 28 days strength of the concrete was 49.65MPa. As shown in the table, the concrete strength on the day of testing for the 13 push test specimens were in the range of 47.39 MPa to 56.50 MPa.

Table 5-3: Concrete Compression Test Results

	f'_c of each Cylinder (MPa)			Average f'_c (MPa)
7 Days Early Strength	38.07	36.92	36.67	37.22
28 Days Strength	48.93	48.85	51.17	49.65
Specimen NS-0	54.47		53.92	54.19
Specimen P M-85	48.03		48.17	48.10
Specimen SL S-0	51.32		50.75	51.04
Specimen SL M-0	N/A		N/A	N/A
Specimen SL S-53	54.41		56.52	55.46
Specimen FE1 S-53	N/A		N/A	N/A
Specimen FE1 M-85	47.54		55.70	51.62
Specimen FE1 L-125	53.69		59.32	56.50
Specimen FE1 M-53	48.99		54.23	51.61
Specimen FE1 L-53	49.48		47.99	48.74
Specimen FE2 S-53	47.89		49.32	48.61
Specimen FE2 M-85	50.08		47.59	48.84
Specimen FE2 L-125	48.23		46.55	47.39

Chapter 6
Analysis of Bolted Connection Behaviour

In this chapter, the experimental results of the 13 push tests are examined and analyzed. First, the effects of the varied test parameters are presented and discussed in Section 6.1. These parameters include friction enhancing surfaces, bolt diameter and bolt pretension. In Section 6.2, the factors that affect the slip load of the specimens are outlined and analyzed. This section also explains what parameters are contributing to the increase in shear capacity after the specimens have slipped. It concludes by proposing analytical models that are capable of predicting the ultimate shear capacity of the bolted connections without shear lugs.

6.1 Effects of Varied Test Parameters

Table 6-1 summarizes the experimental results of the 13 push tests. This table documents the load that corresponds to the slip initiation of each specimen and the peak load attained by each specimen. Finally, the average maximum slip of each specimen before specimen failure occurred is calculated and its value is presented in Table 6-1.

Table 6-1: Experimental Results of Push Test Specimens

Specimen	Slip Load (kN)	Peak Load (kN)	Max Slip, δ_{slip} (mm)
NS – 0	1300	1575	8.4
P M-85	150	890	9.0
SL S-0	990	1435	19.4
SL M-0	1030	1560	13.7
SL S-53	1200	1530	15
FE1 S-53	40	430	11.1
FE1 M-85	55	660	11.7
FE1 L-125	115	1025	11.1
FE1 M-53	50	640	11.2
FE1 L-53	50	850	11.4
FE2 S-53	60	495	10.4
FE2 M-85	105	700	9.6
FE2 L-125	125	1020	12.4

Recall that four load-slip curves were plotted for each specimen based on the data collected from the four displacement transducers. A single load versus average slip curve was obtained for each specimen after each set of four displacement values was averaged. The load versus average slip curves of each specimen were used to examine the effects of the varied test parameters.

Figure 6-1 presents the load versus average slip curves for specimens P M-85, FE1 M-85 and FE2 M-85. These three bolted specimens utilized medium size (15.88 mm diameter) bolts, where the bolts were pretensioned to 70% of their specified minimum tensile strength. The only difference between these three specimens was their steel-concrete interface conditions. Specimen P M-85 had a plain steel-concrete interface condition and it had a slip load and peak load of 150 kN and 890 kN, respectively. When the plain interface condition was replaced with a type I friction enhanced surface, the specimen's slip load and peak load decreased to 55 kN and 660 kN, respectively. When a type II friction enhanced surface was used, the specimen had a slip load and peak load of 105 kN and 700 kN, respectively. Based on the above results, it was concluded that the use of a type I or type II friction enhanced surface did not provide any benefits to the bolted connection as the capacity of the bolted connection to resist shear force actually decreased. It should be noted that the type II friction enhanced surface allowed the bolted connection to carry a higher shear force than the type I friction enhanced surface (Figure 6-1). The maximum slips of specimens P M-85 and FE2 M-85 were 9 mm and 9.6 mm, respectively. These maximum slip values were very similar. In contrast, the maximum slip of specimen FE1 M-85 was 11.7 mm, which is greater than that of the other two specimens.

Based on the small scale friction tests that were conducted (Section 5.1), a plain steel-concrete interface had a friction coefficient of 0.83. Furthermore, the friction enhanced type I and type II surfaces had a friction coefficient of 1.11 and 1.28, respectively. As outlined in Section 5.1, the friction test results indicated that the friction coefficient increased whenever friction enhanced surface was used. In contrast, the push test results suggest that the friction coefficient decreased when the friction enhanced surfaces were used since the ability of the push test specimens to resist shear load decreased (Figure 6-1). The disagreement between the friction test results and the push test results was likely due to the difference in the applied normal stress on the steel-concrete interface. When the small scale friction tests were conducted, the applied normal stress on the interface was 0.004 MPa. When the push tests were conducted, the minimum applied normal stress on the interface was 1.48 MPa. The significant difference in the applied normal stress between these two test setups may have caused disagreement between the two sets of test results. When the applied normal stress on the

interface was higher, the microaggregates along the interface surface were more likely to shear each other off, as oppose to go over each other, as the surface slip. Shearing of the microaggregates would smoothen the interface surface and decrease the recorded values of friction coefficients. Based on the above reason, it is believed that the friction test results do not represent the actual behaviour of the bolted connection surfaces. Therefore, the friction coefficients obtained from the small scale friction tests should not be used to represent the bolted connections behaviour.

The push test results suggest that the friction coefficient decreased when the friction enhanced surfaces were used. The friction coefficient may have decreased because the friction enhanced surfaces were made unevenly rough as concrete sand was adhered onto the steel flange surfaces. When the friction enhanced surfaces were not uniformly created, the direct bearing area between the steel flanges and the deck panels decreased and the friction coefficient of the interface decreased.

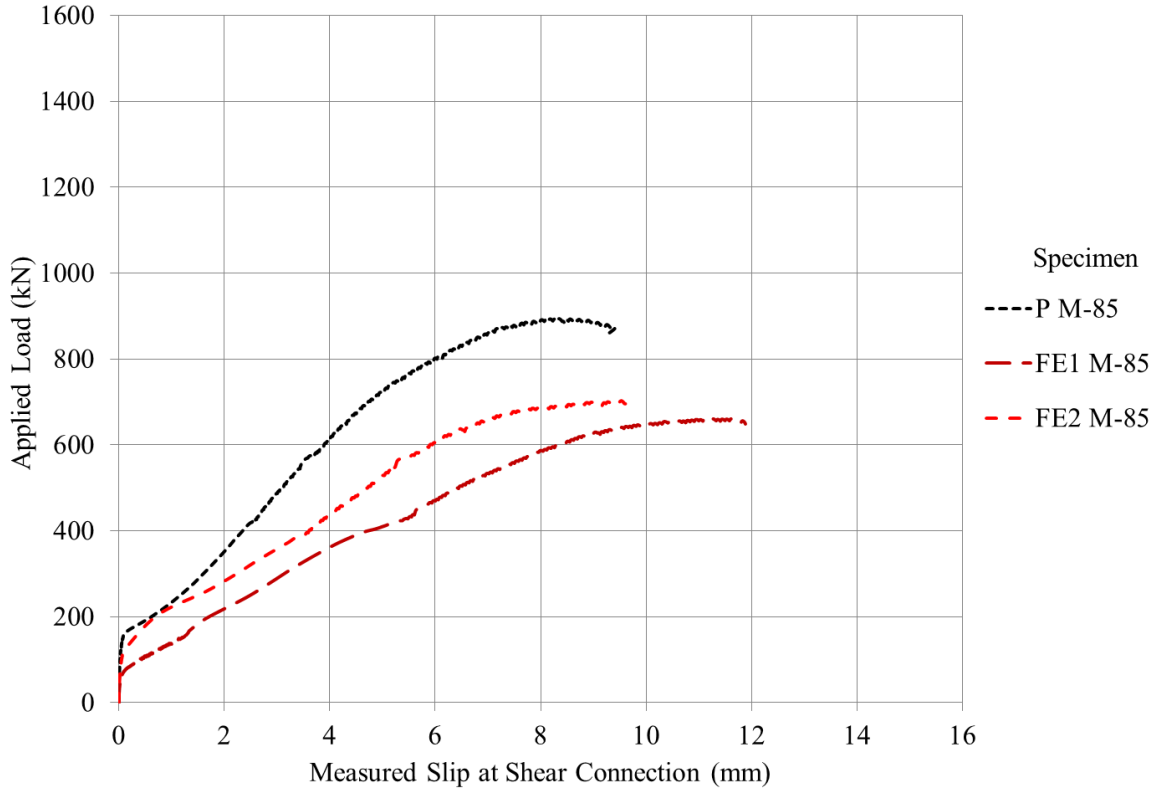

Figure 6-1: Load-Slip Curves for Specimen P M-85, FE1 M-85 and FE2 M-85

Figure 6-2 presents the load versus average slip curves for specimen SL S-53, FE1 S-53 and FE2 S-53. These three bolted specimens utilized small size (12.70 mm diameter) bolts, where the bolts were pretensioned to 70% of their specified minimum tensile strength. The only difference between these

three specimens was their steel-concrete interface conditions. Specimen SL S-53 had a shear lug welded onto each outside flange of the steel beam. It had a slip load and peak load of 1200 kN and 1530 kN, respectively. When the shear lugs were replaced with type I friction enhanced surface, the specimen's slip load and peak load decreased to 40 kN and 430 kN, respectively. When type II friction enhanced surface was used, the specimen had a slip load and peak load of 60 kN and 495 kN, respectively. Based on the above results, it was concluded that that the use of the shear lugs significantly enhanced the shear transfer between the steel I-beam and the precast concrete deck panels. The slip load and the peak load of specimen SL S-53 were much higher than those from specimen FE1 S-53 and FE2 S-53 because the shear lugs provided bearing capacity against the concrete. The above results also confirmed the finding which type II friction enhanced surface was able to transfer more shear force than type I friction enhanced surface. The specimen with shear lugs had an ultimate slip value that was greater than those of the friction enhanced specimens. The maximum slip of specimen SL S-53 was 15 mm. In contrast, the maximum slip of specimen FE1 S-53 and FE2 S-53 were 11.1 mm and 10.4 mm, respectively. Since more slip and displacement was recorded for the shear lug specimen, the use of shear lugs slightly increased the specimen's ductility.

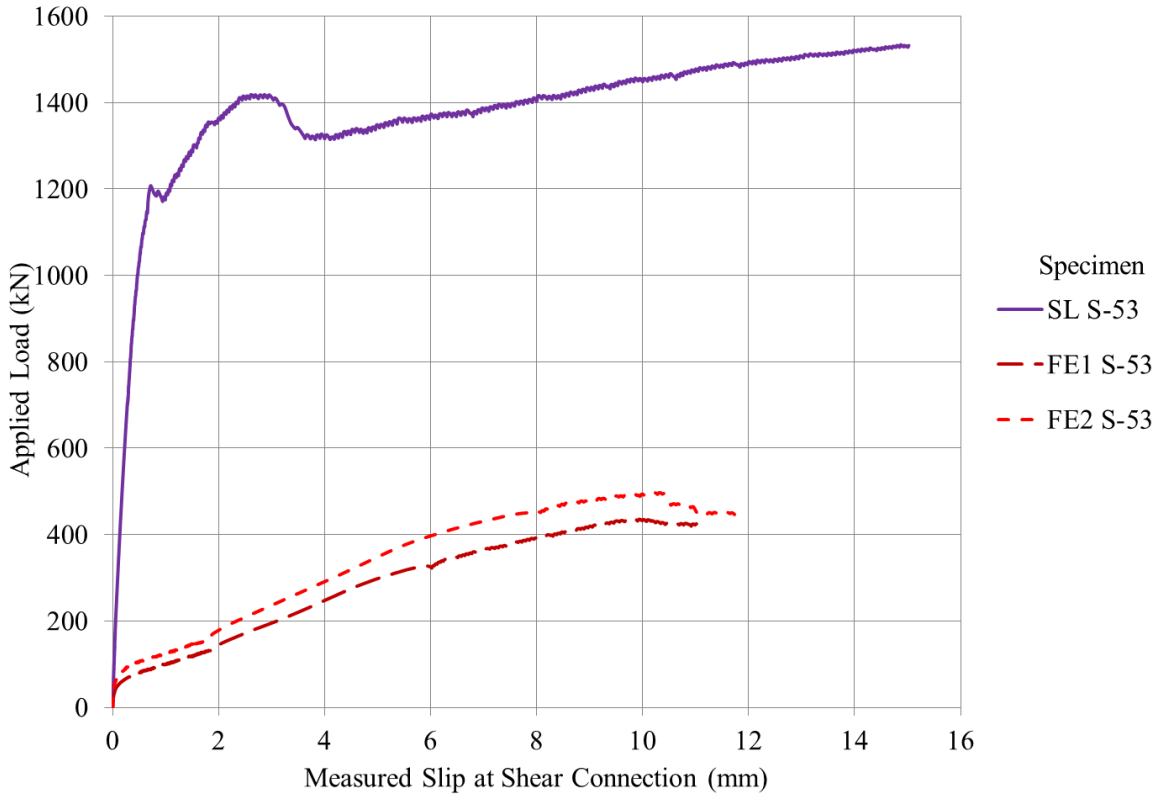

Figure 6-2: Load-Slip Curves for Specimen SL S-53, FE1 S-53 and FE2 S-53

Figure 6-3 presents the load versus average slip curves for specimen SL S-0 and SL M-0. All of the bolts from these two shear lug specimens were not pretensioned. The only difference between these two specimens was that specimen SL S-0 utilized 12.70 mm diameter bolts while specimen SL M-0 utilized 15.88 mm diameter bolts. Specimen SL S-0 had a slip load and peak load of 990 kN and 1435 kN, respectively. When the bolt diameter of the specimen was increased to 15.88 mm, the slip load and peak load increased to 1030 kN and 1560 kN, respectively. The use of larger bolt size increased the slip load and peak load of the specimen because larger bolts had greater shear capacity. Specimen SL S-0 and SL M-0 had a maximum slip value of 19.4 mm and 13.7 mm, respectively. In other words, the maximum slip value decreased when the bolt size was increased in the shear lug specimen. This phenomenon may be due to the fact that larger bolts would be able to resist more shear and bending deformation. Specimen SL M-0 was less ductile than specimen SL S-0 because smaller slip values were recorded for specimen SL M-0. In the nonlinear range of the load versus average slip curves, specimen SL M-0 had greater stiffness than specimen SL S-0. In other words, specimen SL M-0 picked up loads faster as the specimen slip value increased. The connections stiffness in the

plastic range increased when the bolt size increased because larger bolts had greater ultimate shear capacity.

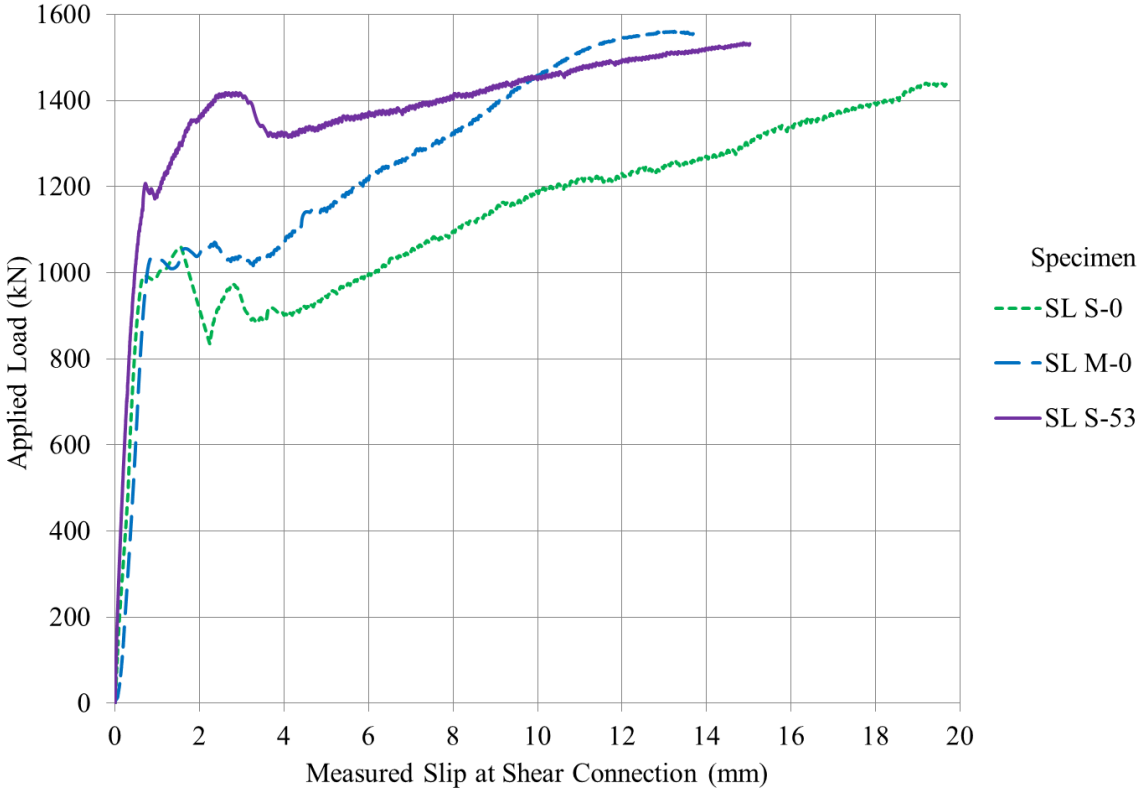

Figure 6-3: Load-Slip Curves for Specimen SL S-0, SL M-0 and SL S-53

Figure 6-3 also presents the load versus average slip curves for specimen SL S-0 and SL S-53. Both of these two shear lug specimens utilized small size (12.70 mm diameter) bolts. The only difference between these two specimens was the applied bolt tensioning force: the bolts of specimen SL S-0 were not pretensioned while the bolts of specimen SL S-53 were pretensioned to 70% of their specified minimum tensile strength. Specimen SL S-0 had a slip load and peak load of 990 kN and 1435 kN, respectively. When the bolts of the specimen were pretensioned, the slip load and peak load increased to 1200 kN and 1530 kN, respectively. The presence of bolt tension force created clamping force that fastened the steel beam and the precast concrete deck panels together. The clamping force made the specimen harder to slip because it increased the frictional force at the steel-concrete interface. Pretensioning the bolts increased the specimen's slip load because the pretensioned specimen needed to overcome the increased in frictional force to slip. Specimen SL S-0 and SL S-53 had a maximum slip value of 19.4 mm and 15 mm, respectively. In other words, the maximum slip

value decreased when the bolts were pretensioned. Pretensioning the bolts created clamping forces, which increased the frictional force at the steel-concrete interface and made the specimen harder to slip under shear load. In the nonlinear range of the load versus average slip curves, specimen SL S-53 picked up load slower than specimen SL S-0 because it had to overcome the increased in frictional force due to bolt tensioning to slip.

Figure 6-4 presents the load versus average slip curves for specimen FE1 S-53, FE1 M-85 and FE1 L-125. These three friction enhanced type I specimens utilized bolts that were pretensioned to 70% of the bolts specified minimum tensile strength. The only difference between these three specimens was their bolt sizes. Specimen FE1 S-53 utilized small size (12.70 mm diameter) bolts and it had a slip load and peak load of 40 kN and 430 kN, respectively. When the bolt diameter was increased to 15.88 mm, the slip load and peak load of the specimen increased to 55 kN and 660 kN, respectively. When the bolt diameter was further increased to 19.05 mm, the slip load and peak load of the specimen increased to 115 kN and 1025 kN, respectively. The use of larger bolt size increased the slip load and peak load of the specimen. As shown from the above test results, the ultimate load of the specimen increased by 54% whenever the bolt diameter was increased by 3.18 mm (1/8 inches). The increase in ultimate load was proportional to the increase in bolt diameter as larger bolts had greater shear capacity. On the other hand, the increase in slip load was proportional to the increase in bolt pretensioned force. The slip load of the specimens increased as the bolt size increased because larger bolts had higher pretensioned force. Specimen FE1 S-53, FE1 M-85 and FE1 L-125 had a maximum slip value of 11.1 mm, 11.7 mm and 11.1 mm, respectively. The maximum slip values of these three friction enhanced specimens were very similar. In the plastic range of the load versus average slip curves, the stiffness of the connections increased when the bolt size increased. In other words, the slope of the nonlinear load-slip curves increased when the bolt size was increased. The connections stiffness in the plastic range increased when the bolt size increased because larger bolts had greater ultimate shear capacity.

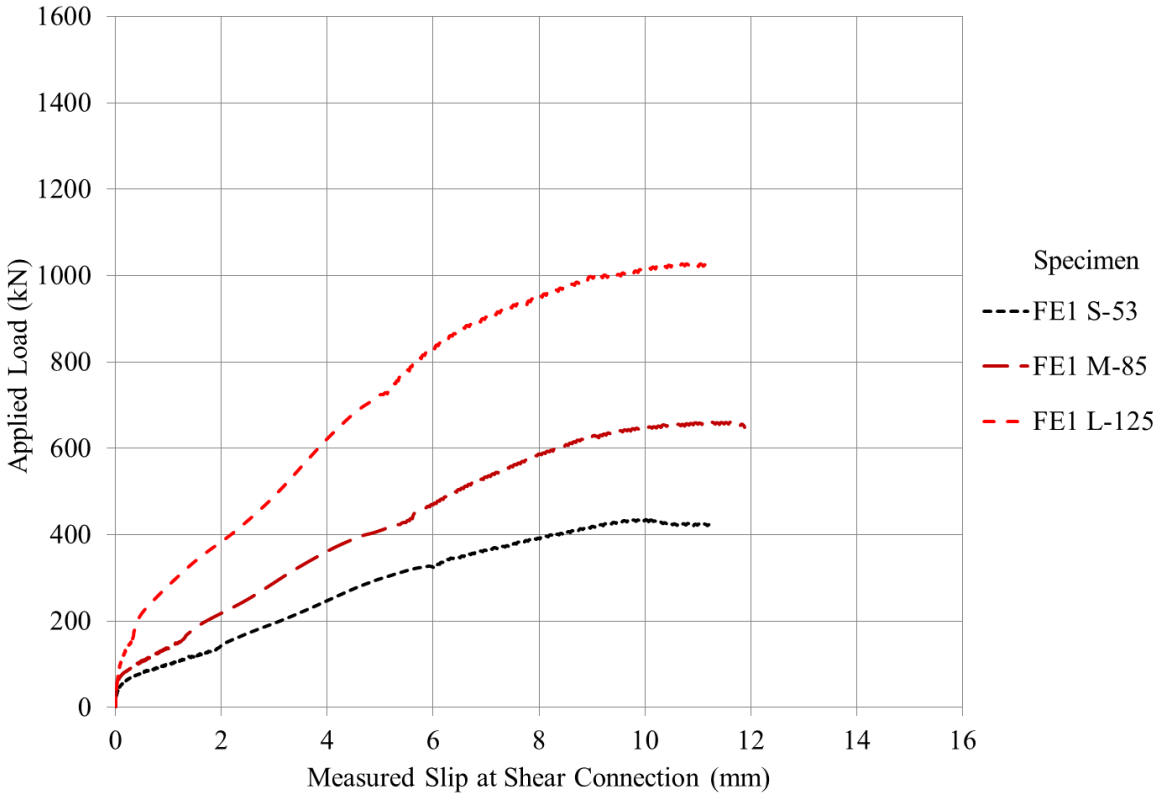

Figure 6-4: Load-Slip Curves for Specimen FE1 S-53, FE1 M-85 and FE1 L-125

Figure 6-5 presents the load versus average slip curves for specimen FE2 S-53, FE2 M-85 and FE2 L-125. These three friction enhanced type II specimens utilized bolts that were pretensioned to 70% of the bolts specified minimum tensile strength. The only difference between these three specimens was their bolt sizes. Specimen FE2 S-53 utilized small size (12.70 mm diameter) bolts and it had a slip load and peak load of 60 kN and 495 kN, respectively. When the bolt diameter was increased to 15.88 mm, the slip load and peak load of the specimen increased to 105 kN and 700 kN, respectively. When the bolt diameter was further increased to 19.05 mm, the slip load and peak load of the specimen increased to 125 kN and 1020 kN, respectively. As mentioned in the previous paragraph, the use of larger bolt size increased the slip load and peak load of the specimen. When the bolt diameter was increased from 12.70 mm to 15.88 mm, the ultimate capacity of the specimen increased 42%. When the bolt diameter was increased again by 3.18 mm (1/8 inches), the ultimate capacity of the specimen increased 45%. It could be concluded that the ultimate capacity of the specimen was approximately proportional to the size of the bolts. The slip load of the specimens increased as the bolt size increased because larger bolts had higher pretensioned force. As mentioned in the previous paragraph, the

increase in slip load was proportional to the increase in bolt pretensioned force. Specimen FE2 S-53, FE2 M-85 and FE2 L-125 had a maximum slip value of 10.4 mm, 9.6 mm and 12.4 mm, respectively. In the plastic range of the load versus average slip curves, the stiffness of the connections increased when the bolt size increased. In other words, the slope of the nonlinear load-slip curves increased when the bolt size was increased. The connections stiffness in the plastic range increased when the bolt size increased because larger bolts had greater ultimate shear capacity.

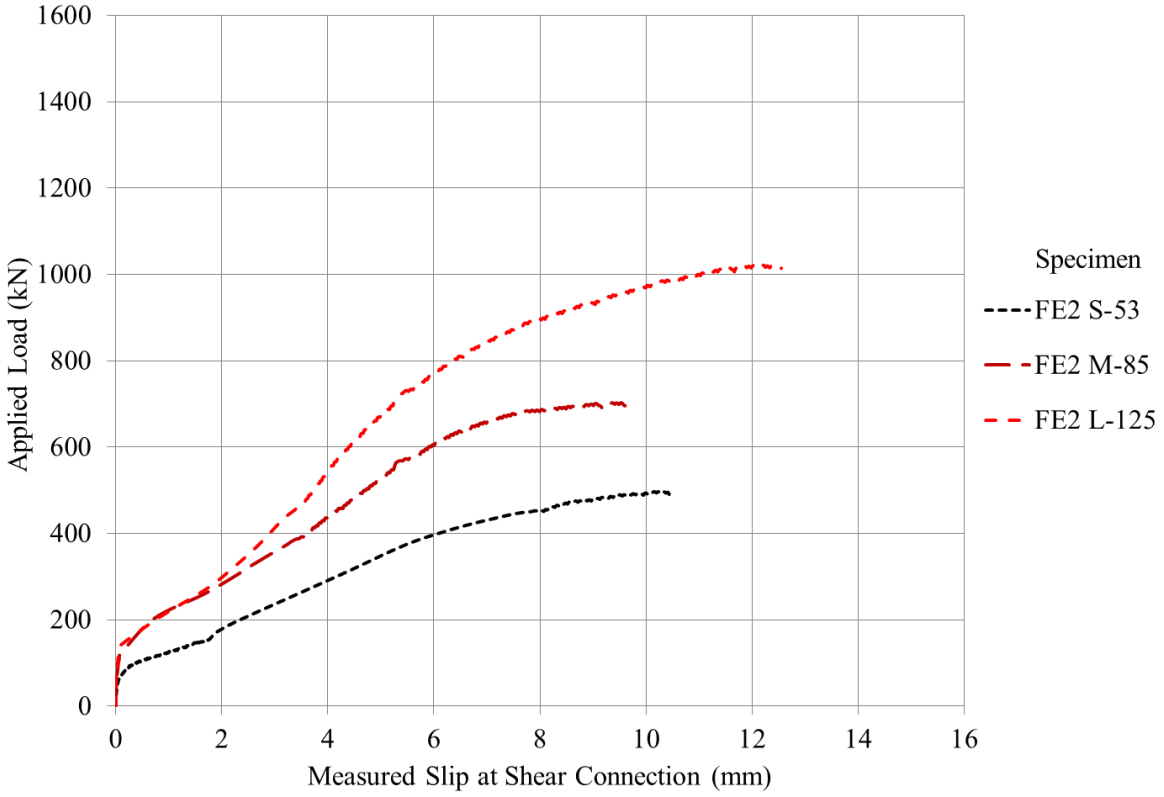

Figure 6-5: Load-Slip Curves for Specimen FE2 S-53, FE2 M-85 and FE2 L-125

Figure 6-6 presents the load versus average slip curves for specimen FE1 S-53, FE1 M-53 and FE1 L-53. These three friction enhanced type I specimens utilized bolts that were pretensioned to 53 kN. In other words, all the bolts were pretensioned to the same force, taken as 70% of the specified minimum tensile strength of the small size (12.70 mm diameter) bolts. The only difference between these three specimens was their bolt sizes. Specimen FE1 S-53 utilized small size (12.70 mm diameter) bolts and it had a slip load and peak load of 40 kN and 430 kN, respectively. When the bolt diameter was increased to 15.88 mm, the slip load and peak load of the specimen increased to 50 kN and 640 kN, respectively. When the bolt diameter was further increased to 19.05 mm, the slip load of

the specimen remained at 50 kN and the peak load of the specimen increased to 850 kN. As shown on Figure 6-6, the slip loads of the three specimens remained fairly constant even as the bolt size increased. All of the different size bolts were pretensioned to the same amount of force; therefore, every specimen was subjected to the same amount of clamping action and every specimen was experiencing the same amount of frictional force at the steel-concrete interface. The slip loads from the three specimens remained fairly constant because each specimen needed to overcome the same amount of interface friction to slip. As shown in Figure 6-6, the use of larger bolt size increased the ultimate load of the specimen because the larger bolts had greater ultimate shear capacity. When the bolt diameter was increased from 12.70 mm to 15.88 mm, the ultimate capacity of the specimen increased 49%. When the bolt diameter was increased again by 3.18 mm (1/8 inches), the ultimate capacity of the specimen increased 33%. Even though the incremental increase in bolt size was the same, the increase in ultimate capacity of the specimen was not the same. The second increase in ultimate capacity was smaller than the first because the medium bolts and the large bolts were pretensioned to 70% of the small bolts' specified minimum tensile strength. If every bolt was pretensioned to 70% of the bolt size's specified minimum tensile strength, then the increase in ultimate capacity would be proportional to the increase in bolt size. Figure 6-4 presents the test results that confirm the above statement.

Specimen FE1 S-53, FE1 M-53 and FE1 L-53 had a maximum slip value of 11.1 mm, 11.2 mm and 11.4 mm, respectively. The maximum slip values of these three friction enhanced specimens were very similar. In the plastic range of the load versus average slip curves, the stiffness of the connections increased when the bolt size increased. In other words, the slope of the nonlinear load-slip curves increased when the bolt size was increased. The connections stiffness in the plastic range increased when the bolt size increased because larger bolts had greater ultimate shear capacity.

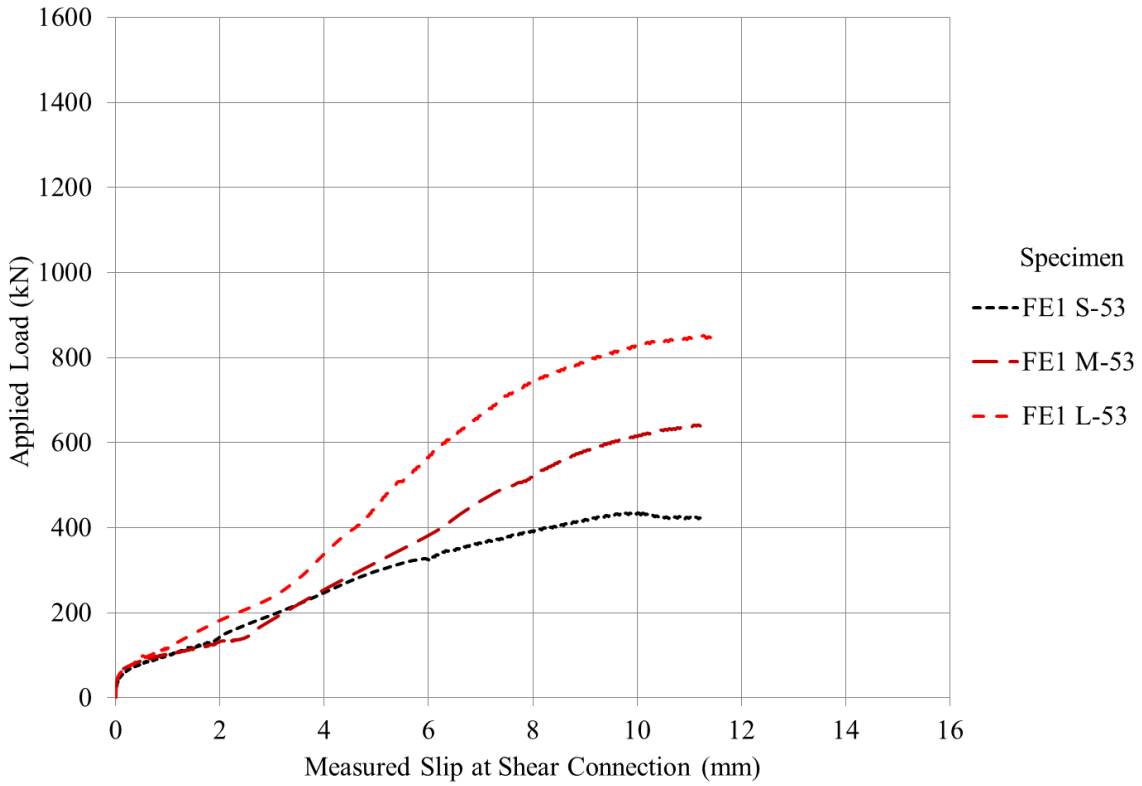

Figure 6-6: Load-Slip Curves for Specimen FE1 S-53, FE1 M-53 and FE1 L-53

6.2 Mechanistic Modelling of Bolted Connection Behaviour

As mentioned in Section 2.3.1, the slip load of a bolted joint can be modelled by using Equation 2.3. This equation is based on first principals of mechanics and it expresses the slip load in terms of the slip coefficient, k_s, and the bolt clamping force, T_i, for a given number of slip planes and bolts. The slip coefficient depends on the surface condition of the connected materials and it can only be determined from experiments [Kulak et al., 1987].

Equation 2.3 can be re-arranged and written as Equation 6.1 in order to find the slip coefficient, k_s, for each bolted specimen. By using Equation 6.1, the slip coefficient for each bolted specimen is found based on the recorded slip load and the applied pretension force of the specimen. Table 6.2 presents the slip coefficient of each specimen. It should be noted that each specimen consists of 8 bolts (i.e. n = 8) and each bolt intercepts 1 shear plane (i.e. m = 1).

$$k_s = \frac{V_{slip}}{m\, n\, T_i} \tag{6.1}$$

Table 6-2: Slip Coefficients of Push Test Specimens

Specimen	Bolt Pretension, T_i (kN)	Total Clamping Force, $8 \times T_i$ (kN)	Slip Load, V_{slip} (kN)	Slip Coefficient, k_s
P M-85	85	680	150	0.22
FE1 S-53	53	424	40	0.09
FE1 M-85	85	680	55	0.08
FE1 L-125	125	1000	115	0.12
FE1 M-53	53	424	50	0.12
FE1 L-53	53	424	50	0.12
FE2 S-53	53	424	60	0.14
FE2 M-85	85	680	105	0.15
FE2 L-125	125	1000	125	0.13

As shown on the above table, the slip coefficient of each surface condition is reasonably consistent. The plain steel-concrete surface condition has a slip coefficient of 0.22. Moreover, the type I friction enhanced surface has an average slip coefficient of 0.11. Finally, the type II friction enhanced surface has an average slip coefficient of 0.14. These three slip coefficient values can be used in conjunction with Equation 2.3 to estimate the slip load of bolted connections with a plain, FE1 or FE 2 surface condition.

It is important to point out the differences between slip coefficient, k_s, and friction coefficient, μ. These two coefficients represent different mechanism. The slip coefficient relates the initial slip load of the bolt connection to the bolt pretension force. It is a measure of when the slip-critical connection will slip into bearing. The applied normal load across the connection surface is not uniformly distributed since it is induced by the bolts. In contrast, friction coefficient relates the applied shear stress to the applied normal stress across a surface. It is a measure of surface roughness and such measurement does not involve the use of fasteners such as bolts. The applied normal stress across the surface is uniformly applied. The slip coefficient is used as part of the shear capacity models in this Chapter because it is more appropriate and its value is readily available from push tests.

After the slip load of a bolted joint is overcome by external loading, the connected parts slip until they bear against the bolts. The capacity of bolted connections to further transfer shear load after the connections have slipped depends on the following three factors: interface surface condition, bolt

clamping force and bolt dowel action. The interface surface condition affects the frictional resistance at the steel-concrete interface; therefore, it affects the shear transfer of bolted connections even after slip has been initiated. The interface that possesses a higher friction resistance is capable of transfer more shear force. As the bolt connections continue to slip after slip initiation, the bolts become elongated in tension. The elongation increases the tensile force in the bolts, thus increasing the clamping action on the bolted materials. The increase in clamping action causes the frictional resistance at the steel-concrete interface to increase, increasing the shear transfer capacity. The shear transfer capacity of bolted connections also depends on the dowel action of bolts. Once the bolt slip is initiated, the bolts will undergo shear and bending deformation when they are subjected to shear load. The shear and bending deformation of bolts is known as the dowel action and provides a further contribution to the shear transfer between the connected materials.

As implied in the previous paragraph, the total shear capacity of the bolted connections is the sum of the friction resistance and the additional resistance due to bolt dowel action. In other words, the total shear capacity of the bolted connections can be modelled by using Equation 6.2:

$$V_{total} = V_{friction} + V_{dowel} \tag{6.2}$$

where V_{total} is the total shear capacity of the bolted connection, $V_{friction}$ is the friction resistance from the connection interface and V_{dowel} is the resistance due to bolt dowel action.

The friction resistance from the bolted connection interface can be modelled using Equation 2.3, which expresses the slip resistance of the bolted connection. It represents the amount of shear force required to overcome the friction resistance at the connection interface.

The bolt dowel action can be modelled as a fraction of the shear strength of the bolt. Modelling the bolt dowel action as a fraction of the bolt shear strength seems appropriate because a significant part of the bolt shear strength is contributed by the bolt dowel action.

Equation 6.2 can be written as Equation 6.3 when the friction resistance of the connection interface is modelled by using Equation 2.3 and the bolt dowel action is modelled as a fraction of the bolt's shear strength. As mentioned in Section 2.3.2, the unfactored (i.e. $\phi_b = 1$) shear strength of the bolts is a product of $0.6\ m\ n\ A_b\ F_u$.

$$V_{total} = k_s\ m\ n\ T_i + \omega\ (0.6\ m\ n\ A_b\ F_u) \tag{6.3}$$

where V_{total} is the total shear capacity of the bolted connection, k_s is the slip coefficient, m is the number of shear planes crossing the bolts, n is the number of bolts in the connection, T_i is the bolt pretension, ω is the reduction factor that relates the bolt dowel action to the bolt shear strength, A_b is the nominal cross-section area of a bolt and F_u is the ultimate tensile strength of the bolt.

Equation 6.3 is denoted as Model 1 and it is used to predict the ultimate shear capacity of the bolted connections. Table 6-3 shows the predicted ultimate shear capacity of the bolted connections and the shear capacity of the specimens according to test results. A reduction factor, ω, of 0.75 is used in order to make the prediction. This reduction factor value is chosen to minimize the discrepancy between the predicted shear capacity and the experimental shear capacity of the bolted connections. In other words, the reduction factor is a coefficient chosen to fit the predicted values with the experimental data. As shown on Table 6-3, the majority of the predicted shear capacities match closely with the experimental results. Most of the ratios between experimental value and predicted value are close to 1.00. Figure 6-7 shows that the experimental shear capacity and the predicted shear capacity exhibit good correlation.

Table 6-3: Predicted Shear Capacity of Bolt Connections by Using Model 1

Specimen	Experimental V_{total} (kN)	Model 1 V_{total} (kN)	E / M Ratio
P M-85	890	738	1.21
FE1 S-53	430	417	1.03
FE1 M-85	660	643	1.03
FE1 L-125	1 025	961	1.07
FE1 M-53	640	638	1.00
FE1 L-53	850	896	0.95
FE2 S-53	495	437	1.13
FE2 M-85	700	693	1.01
FE2 L-125	1 020	971	1.05

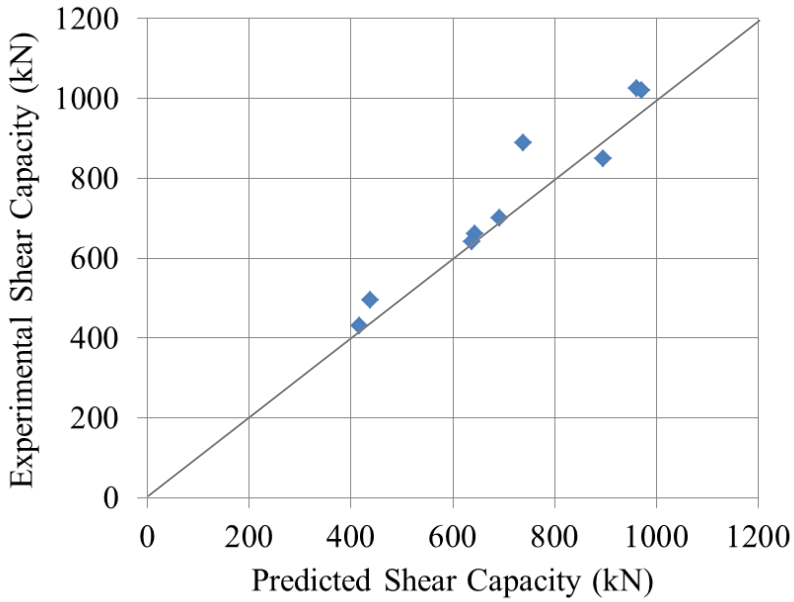

Figure 6-7: Correlation Between Experimental and Model 1 Predicted Shear Capacity

The prediction of the ultimate shear capacity of the bolted connections can be improved by considering the fact that the bolts become inclined to the shear plane after they slip. As a result, the axial force in the bolt has a force component in the direction of the shear loading, which contributes to the shear resistance of the connection. Equation 2.7 presents a model of shear transfer strength that accounts for the situation of having shear reinforcement inclined to the shear plane. The $\mu \sin\alpha + \cos\alpha$ term of the equation accounts for the change in frictional resistance due to the angle, α, between the reinforcement axis and the shear plane. By incorporating the $\mu \sin\alpha + \cos\alpha$ term into Equation 6.3, the total shear capacity of the bolted connection can be modelled using Equation 6.4:

$$V_{total} = (k_s \sin\alpha + \cos\alpha)\, m\, n\, T_i + \omega\, (0.6\, m\, n\, A_b\, F_u) \qquad (6.4)$$

where V_{total} is the total shear capacity of the bolted connection, k_s is the slip coefficient, α is the angle between the bolt axis and the shear plane, m is the number of shear planes crossing the bolts, n is the number of bolts in the connection, T_i is the bolt pretension, ω is the reduction factor that relates the bolt dowel action to the bolt shear strength, A_b is the nominal cross-section area of a bolt and F_u is the ultimate tensile strength of the bolt.

It should be noted that the applied load on a set of bolts is typically not shared equally between those bolts. This would explain why the bolt shear strength is not the same as the bolt dowel action.

To use Equation 6.4 to predict the ultimate shear capacity of bolt connections, the angle between the bolt axis and the shear plane must be determined. When the specimens were under ultimate load, the bolted connections had significantly slipped and the bolts were elongated in tension. In an idealized situation, plastic hinges would have formed near the top and bottom of the bolts (Figure 6-8). By using the specimen geometry and by considering the maximum slip of the bolted connections, the angle between the bolt axis and the shear plane can be found through trigonometry. Table 6-4 presents the calculated angle, α, between the bolt axis and the shear plane for each specimen. It should be noted that the concrete deck was 152 mm thick and this value was used to calculate α. The steel flange thickness was not used as part of the calculation because it was not considered as part of the bolt deformation length. The bolt holes were drilled, where the hole diameters were a maximum of 2 mm larger than the specified hole dimension. Under this tight hole tolerance, the bolts did not deform inside the steel flange.

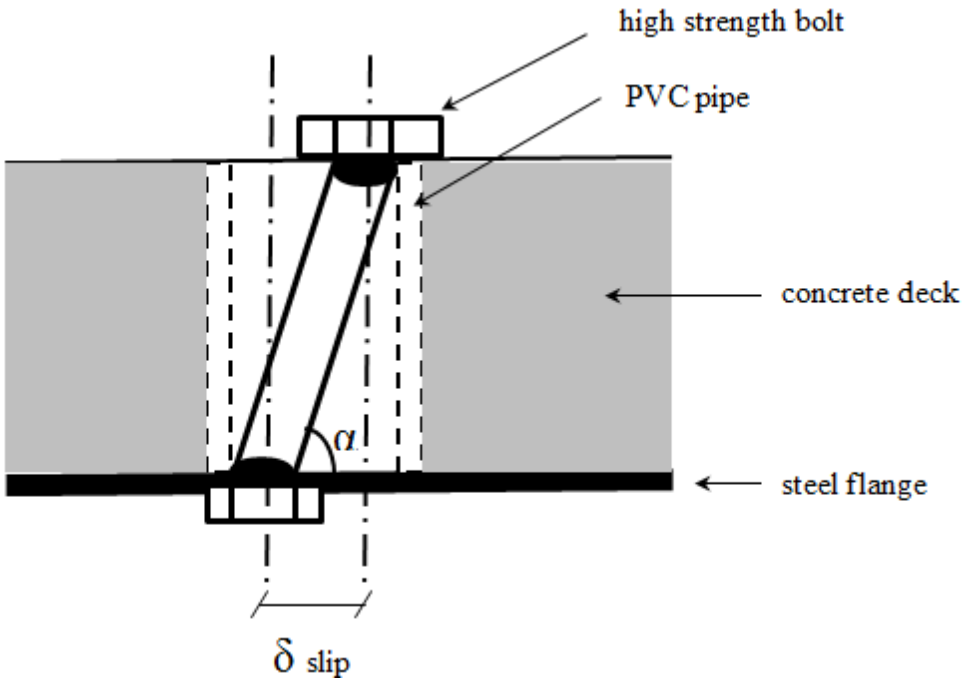

Figure 6-8: Idealized Bolt Tension Failure Mode

Equation 6.4 is denoted as Model 2 and it is used to predict the ultimate shear capacity of the bolted connections. Table 6-5 shows the predicted ultimate shear capacity and the shear capacity of the specimens according to test results. A reduction factor, ω, of 0.7 is used in order to make the prediction. This reduction factor value is chosen to minimize the discrepancy between the predicted

shear capacity and the experimental shear capacity of the bolted connections. As shown on Table 6-5, the majority of the predicted shear capacity of each specimen matches closely with the experimental results. Most of the ratios between experimental value and predicted value are close to 1.00. Figure 6-9 shows that the experimental shear capacity and the predicted shear capacity exhibit good correlation. This correlation is very similar to the one exhibited from Figure 6-7. In other words, the predicted shear capacity from Model 1 and Model 2 both shows good correlation with the experimental results.

Table 6-4: Angle (α) Between the Bolt Axis and the Shear Plane for Each Specimen

Specimen	Max Slip, δ_{slip} (mm)	α
P M-85	9.0	86.61°
FE1 S-53	11.1	85.82°
FE1 M-85	11.7	85.60°
FE1 L-125	11.1	85.82°
FE1 M-53	11.2	85.79°
FE1 L-53	11.4	85.71°
FE2 S-53	10.4	86.09°
FE2 M-85	9.6	86.39°
FE2 L-125	12.4	85.34°

Table 6-5: Predicted Shear Capacity of Bolt Connections by Using Model 2

Specimen	Experimental V_{total} (kN)	Model 2 V_{total} (kN)	E / M Ratio
P M-85	890	739	1.20
FE1 S-53	430	424	1.01
FE1 M-85	660	656	1.01
FE1 L-125	1 025	977	1.05
FE1 M-53	640	631	1.01
FE1 L-53	850	873	0.97
FE2 S-53	495	442	1.12
FE2 M-85	700	697	1.00
FE2 L-125	1 020	995	1.03

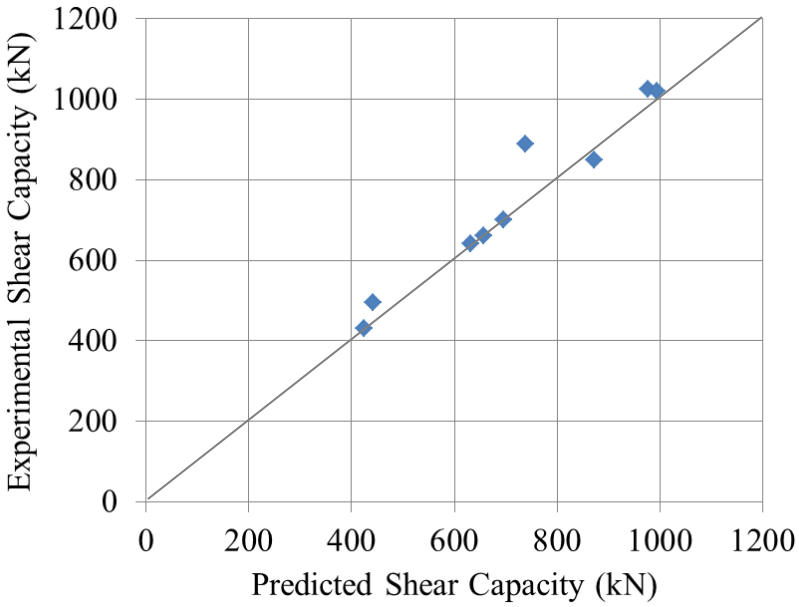

Figure 6-9: Correlation Between Experimental and Model 2 Predicted Shear Capacity

Equation 6.4 can be further improved by considering the bolt tension force increase due to the connection slip. As discussed previously, as the connection slips, the bolts become elongated in tension, increasing the bolt tension force from their initial pretension. Therefore, the total tensile force experienced by the bolts should be the sum of the bolt pretension and the bolt tension due to connection slip.

Equation 6.4 can also be improved by considering the combined shear and tension effect to determine the bolt dowel action. According to Clause 10.18.2.4.2 of the Canadian Highway Bridge Design Code [2006], bolts subjected to combined shear and tension at ultimate load must satisfy the requirement given in Equation 6.5, which is an interaction equation for shear and tension force that can be applied on the same bolt. It can be used to calculate the bolt resistance due to dowel action when the total tensile force experienced by the bolts is known. To calculate the bolt resistance due to dowel action, Equation 6.5 is written as Equation 6.6. The unfactored (i.e. ϕ_b = 1) shear and tensile resistance of the bolts from the Canadian Highway Bridge Design Code [2006] have been substitute into Equation 6.6. It should be noted that the tensile resistance used in Equation 6.6 is the nominal tensile resistance. In other words, the 0.75 factor that accounts for the reduction in cross-section area of the bolts due to the threads has been removed. This factor has been removed because the length of thread that was

included in the bolt model was relatively small in comparison to the length of the modelled non-treaded part of the bolt.

Equation 6.5 and Equation 6.6 are shown in the following. Equation 6.7 is also presented after Equation 6.6 is rearranged to solve for V_{dowel}.

$$[\frac{V_f}{V_r}]^2 + [\frac{T_f}{T_r}]^2 \leq 1 \tag{6.5}$$

where V_f is the applied shear force on the bolted connection, V_r is the shear resistance of the bolts, T_f is the applied tension force on the bolted connection and T_r is the tensile resistance of the bolts.

$$[\frac{V_{dowel}}{0.6\, n\, A_b\, F_u}]^2 + [\frac{n\, T_{total}}{n\, A_b F_u}]^2 \leq 1 \tag{6.6}$$

$$V_{dowel} = 0.6\, n\, A_b F_u \sqrt{1 - [\frac{n\, T_{total}}{n A_b F_u}]^2} \tag{6.7}$$

where V_{dowel} is the shear force acting on the bolt due to dowel action, T_{total} is the sum of the bolt pretension and the bolt tension due to connection slip, n is the number of bolts in the connection, A_b is the nominal cross-section area of a bolt and F_u is the ultimate tensile strength of the bolt.

Equation 6.8 is proposed to predict the ultimate shear capacity of the bolted connections. This equation considers the effects of bolt tension force increase due to the connection slip and the shear strength of bolts subjected to combined shear and tension.

$$V_{total} = (k_s\, sin\alpha\ + cos\alpha)\, m\, n\, T_{total} + V_{dowel} \tag{6.8}$$

where V_{total} is the total shear capacity of the bolted connection, k_s is the slip coefficient, α is the angle between the bolt axis and the shear plane, m is the number of shear planes crossing the bolts, n is the number of bolts in the connection, T_{total} is the sum of the bolt pretension and the bolt tension due to connection slip and V_{dowel} is the shear force acting on the bolt due to dowel action calculated by using Equation 6.7.

The total tensile force experienced by the bolts is calculated by using the specimen geometry (Figure 6-8) and the basic mechanics of materials. First, the pretension bolt strain, $\varepsilon_{initial}$, is calculated based on the linear-elastic stress-strain relationship of the steel. Secondly, the bolt strain due to the connection slip, $\Delta\varepsilon$, is calculated according to the deformed shape of the bolts (Figure 6-8). The total strain of the bolts ($\varepsilon_{total} = \varepsilon_{initial} + \Delta\varepsilon$) is then used to calculate the total stress in the bolts, σ_{total}. A

bilinear stress-strain relationship of the bolts is assumed for the calculation (Figure 6-10). As shown on Figure 6-10, the bolts have a nominal yield and ultimate tensile stress of 634 MPa and 825 MPa, respectively. They have a yield and ultimate strain of 3.17×10^{-3} and 0.08, respectively. The ultimate strain of 0.08 is assumed after examining the ASTM A325 bolt coupon tests conducted by Kulak et al. [1987]. If the total bolt strain is less than the bolt yield strain, then the total bolt stress is a product of the steel modulus of elasticity and the total bolt strain. If the total bolt strain exceeds the bolt yield strain, then strain hardening of the bolt is taken into account to calculate the total bolt stress (Figure 6-10). Table 6-6 shows the calculated values of the pretensioned bolt strain, the bolt strain due to connection slip, the total bolt strain, the total bolt stress and the total bolt tension. It should be noted that all calculated values are based on one bolt of a particular specimen. As shown on Table 6-6, the calculated values of the total bolt stress are very similar and slightly above the nominal yield stress.

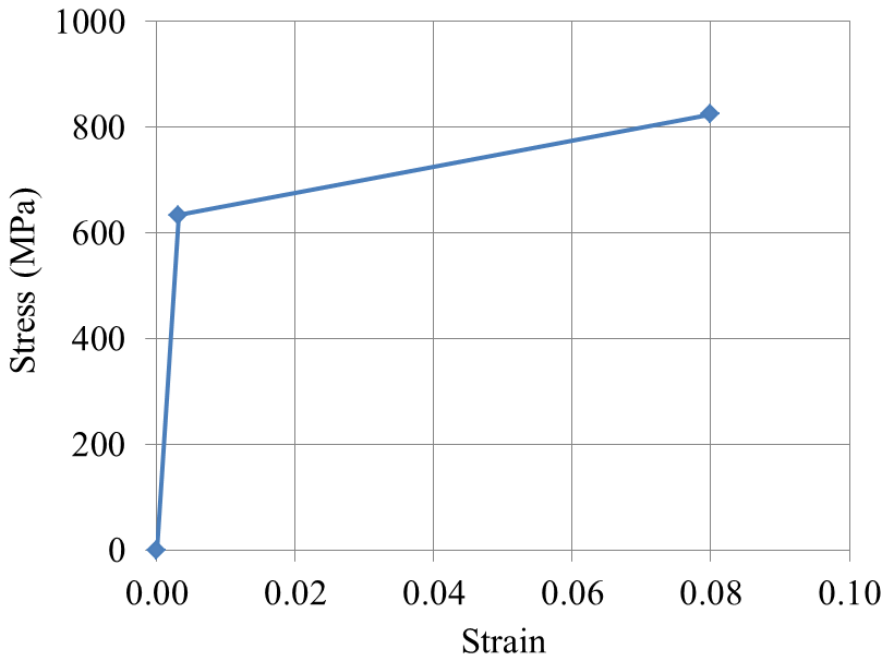

Figure 6-10: Idealized Stress-Strain Curve for ASTM A325 Bolts

The shear force acting on the bolt due to dowel action, V_{dowel}, can be determined by using Equation 6.7 after the total bolt tension, T_{total}, is calculated. This equation accounts for the combined shear and tension interaction of the bolts. In other words, it can determine the remaining shear and bending capacity of the bolts after the bolts have been placed under a tension force of T_{total}.

Table 6-6: Total Bolt Strain, Bolt Stress and Bolt Tension Force (one bolt)

Specimen	$\varepsilon_{initial}$ (10^{-3})	$\Delta\varepsilon$ (10^{-3})	ε_{total} (10^{-3})	σ_{total} (MPa)	T_{total} (kN)
P M-85	2.17	1.75	3.92	637	126
FE1 S-53	2.17	2.66	4.83	639	81
FE1 M-85	2.17	2.96	5.12	640	127
FE1 L-125	2.17	2.66	4.83	639	182
FE1 M-53	1.39	2.71	4.10	637	126
FE1 L-53	0.97	2.81	3.77	636	181
FE2 S-53	2.17	2.34	4.50	638	81
FE2 M-85	2.17	1.99	4.16	637	126
FE2 L-125	2.17	3.32	5.49	641	183

Equation 6.7 and Equation 6.8 are denoted as Model 3 and used to predict the ultimate shear capacity of the bolted connections. Table 6.7 shows the predicted ultimate shear capacity and the shear capacity of the specimens according to test results. The majority of the predicted shear capacity of each specimen matches closely with the experimental results. Most of the ratios between experimental value and predicted value are close to 1.00. Figure 6-11 shows that the experimental shear capacity and the predicted shear capacity exhibit good correlation. This correlation is very similar to the one exhibited from Figure 6-7 and Figure 6-9. In other words, the predicted shear capacity from each model shows good correlation with the experimental results.

Table 6-7: Predicted Shear Capacity of Bolt Connections by Using Model 3

Specimen	Experimental V_{total} (kN)	Model 3 V_{total} (kN)	E / M Ratio
P M-85	890	778	1.14
FE1 S-53	430	432	1.00
FE1 M-85	660	677	0.97
FE1 L-125	1 025	969	1.06
FE1 M-53	640	676	0.95
FE1 L-53	850	976	0.87
FE2 S-53	495	453	1.09
FE2 M-85	700	701	1.00
FE2 L-125	1 020	1 032	0.99

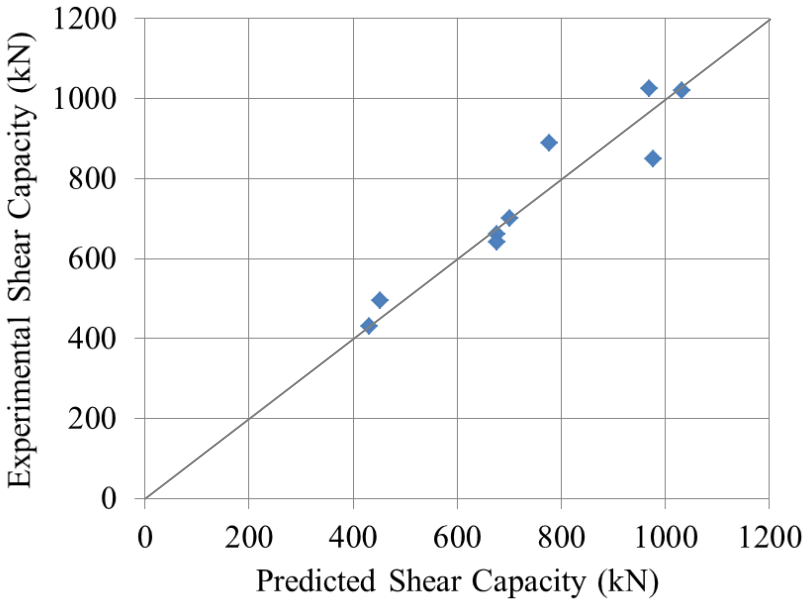

Figure 6-11: Correlation Between Experimental and Model 3 Predicted Shear Capacity

Model 3 is the best analytical model that represents the bolted connections behaviour. Both Model 1 and Model 2 do not include the increase in bolt tension force after the connection slip has been initiated. Both of these models rely on an experimentally calibrated reduction factor, ω, which relates the bolt dowel action to the bolt shear strength. In contrast, Model 3 includes the increase in bolt tension force due to the connection slip. Moreover, it utilizes an established combined shear and

tension interaction equation to determine the bolt dowel action. Since Model 3 considers more of the mechanisms taking place in the real tests and does not depend on a calibrated factor, it is expected that this model will perform better when used to extrapolate to other test conditions. Model 3 is therefore recommended to be used to predict the ultimate shear capacity of the bolted connections.

Model 3 can be used to design bolts that connect the steel members to the precast concrete members. The designers need to know the slip coefficient, k_s, and the connection slip, δ_{slip}, in order to use this model to calculate the predicted ultimate shear capacity of the bolted connection. The slip coefficient of a certain steel-concrete interface condition has to be determined experimentally. This thesis presents the slip coefficient values for plain, FE1 and FE2 surface. Designers are advised to conduct experiments or review literature if they need to determine the slip coefficients, k_s, of other types of steel-concrete interface conditions. Experiments should also be conducted to determine the bolted connection slip values, δ_{slip}. Table 6-4 shows the measured maximum bolted connection slip values for nine of the test specimens. After the designers know the slip coefficient, k_s, and the measured connection slip, δ_{slip}, they can follow the steps as mentioned in this Section to calculate the unfactored ultimate shear capacity of the bolted connection.

As shown on Figure 6-2, the behaviour of the shear lug specimens is significantly different than that of the other bolted specimens. Modelling the behaviour of the shear lug connections is not considered to be part of the scope of this research project.

Chapter 7
Conclusions and Recommendations

This chapter presents the conclusions and recommendations of this research project. In Section 7.1, the significant findings of this research project are presented. Section 7.2 identifies additional work areas that are recommended for future study.

7.1 Conclusions

The conclusions of this research project are separated into two parts. The first part consists of significant findings drawn from the finite element analysis of panel end connections. The second part consists of significant findings drawn from the experimental study of bolted connections.

7.1.1 Finite Element Analysis of Composite Girders with Panel End Connections

Based on the finite element analysis of composite girders with panel end connections, the following conclusions are drawn:

- The panel end connected girder with actual (calculated) stiffness had a similar moment-displacement response to the shear stud girder. It had an ultimate moment capacity that was only 1% less than that of the shear stud girder. At ultimate load, the deflection of the panel end connected girder was 4% larger than that of the shear stud girder.
- When the stiffness of the panel end connections was reduced ten times, the ultimate moment capacity decreased by less than 1% and the deflection value increased by 13%.
- At service and ultimate load, strong composite action was observed at the maximum moment location for the shear stud and panel end connected girders. This observation was true even for the panel end connected girder with reduced connection stiffness.
- The level of composite action of the girders decreased when the shear stud connections were replaced with panel end connections. It decreased further when the panel end connection stiffness was decreased. The level of composite action of the girders was determined by examining the strain profiles through the composite girder depth. As the strain discontinuity at the steel-concrete interface increased, the level of composite action achieved was assumed to decrease.

- The plastic neutral axes of the shear stud and panel end connected girders were near the top flange of the steel girders. These finite element analysis results were in good agreement with the theoretical hand calculation results. Using the Canadian Highway Bridge Design Code [2006], the plastic neutral axis of the composite girder was found to be 4.7 mm below the top flange of the steel plate girder.
- When the shear stud connections were replaced with panel end connections, the shear flow at the steel-concrete interface decreased. In other words, the amount of shear force transferred at the interface decreased when the shear stud connections were replaced with panel end connections. When the stiffness of the panel end connections was decreased ten times, the shear flow at the steel-concrete interface was further decreased.

7.1.2 Experimental Study of Bolted Connections

The following conclusions are drawn based on the experimental push tests of bolted connections and the analysis of bolted connection behaviour:

- All 12 bolted specimens failed by fracture of the bolts. Bolt fractures occurred at the end of the threaded part of the bolts. The bolted connections exhibited good structural redundancy because the bolt fractures did not happen simultaneously at failure. Due to the shear and bending deformation of the bolts, every specimen had local concrete crushing underneath the bolts (at the edge of the bolt hole) at failure.
- Prior to the bolt fracture failure, all shear lug specimens experienced shearing of the concrete wedges underneath the shear lugs. These specimens developed significant cracks on the exterior panel surfaces. The crack development prior to bolt fracture meant that the shear lug connections would exhibit warning before the failure would occur. These connections also exhibited good ductility before failure.
- The behaviour of the bolted connections was linear-elastic up to the slip load. The connections began to slip and behave nonlinearly above the slip load.
- The friction test results indicated that the friction coefficient increased whenever friction enhanced surface was used. In contrast, the push test results suggest that the friction coefficient decreased when the friction enhanced surfaces were used. According to the push test results, the capacity of the bolted connections to resist shear force decreased when type I

or type II friction enhanced surface was used as part the connection surface. The significant difference in the applied normal stress at the steel-concrete interface between these two test setups may have caused the disagreement between these two sets of test results.

- The use of the shear lugs significantly enhanced the shear transfer between the steel I-beam and the precast concrete deck panels. The slip load and the peak load of the shear lug specimens were much higher than those from the other bolted specimens because the shear lugs provided bearing capacity against the concrete. The shear lug specimens also had an ultimate slip value that was notably greater than those of the other bolted specimens.
- The use of a larger bolt size increased the peak load of the bolted connections because the larger bolts had greater ultimate shear capacity. The increase in the ultimate shear capacity of the bolted connections was proportional to the increase in bolt diameter. The use of a larger bolt size also increased the bolted connection stiffness in the plastic range.
- When the bolts of the specimen were pretensioned, the slip load of the specimens increased. The presence of bolt tension force created clamping force that fastened the steel beam and the precast concrete deck panels together. The clamping force increased the slip load because it increased the frictional force at the steel-concrete interface.
- The slip load of the bolted connections was directly proportional to the slip coefficient and the applied pretension force of the bolts. It was independent of the size of the bolts.
- The total shear capacity of the bolted connections is the sum of the friction resistance of the connections and the bolt dowel action resistance. The friction resistance of the connections depends on the interface surface condition and the bolt clamping force.
- An analytical model that can predict the ultimate shear capacity of bolted connections has been developed and recommended. This model accounts for the fact that the bolts are inclined to the shear plane after they slip. It calculates the bolt clamping force as the sum of the bolt pretension and the bolt tension due to connection slip. Moreover, it utilizes an established combined shear and tension interaction equation to determine the bolt dowel action. The proposed model is shown to give a reliable prediction of the experimental results.

7.2 Recommendations for Future Work

The following recommendations are made to further advance the research of shear connections for steel-precast composite bridges:

- Experimental testing of composite bridge girders with panel end connections could be conducted. The recorded experimental data could be used to verify the finite element analysis results from this research project.
- Friction tests or push tests could be conducted to evaluate the friction characteristic of other types of friction enhanced surfaces.
- The existing finite element models could be modified to study the load-displacement behaviour of composite girders with bolted connections.
- Experimental testing of composite bridge girders with bolted connections could be conducted. Instrumentation should be used to record the load-displacement behaviour of the girders and the strain profiles through the girder depth.
- Bolted push test specimens and shear lug push test specimens should be tested under fatigue load to investigate the effects of fatigue on bolted connections and shear lug connections.
- Small-scale test setups could be developed to determine the slip coefficients of various steel-concrete interface conditions.

Bibliography

American Association of State Highway and Transportation Officials. (2008). Bridging the Gap – Restoring and Building the Nation's Bridges. Retrieved March 14, 2013, from http://www.transportation1.org/bridgereport/docs/BridgingtheGap.pdf

American Concrete Institute. (2008). *Building Code Requirements for Structural Concrete and Commentary* (Publication No. ACI 318M-08).

Ardani, A. A., Lindsey, R., & Mallela, J. (2012). Rapid Removal and Replacement of 4500 South Bridge in Salt Lake City, Utah. *Transportation Research Record: Journal of the Transportation Research Board,* No. 2200, 12-16.

Au, A., Lam, C., & Tharmabala, B. (2010). Development of Bolted Deck Slab System to Expedite Bridge Construction. *The 8th International Conference on Short and Medium Span Bridges,* 091, 1-11.

Baskar, K., Shanmugam, N. E., & Thevendran, V. (2002). Finite-Element Analysis of Steel-Concrete Composite Plate Girder. *Journal of Structural Engineering*, September, 1158-1168.

Bowser, M. G. (2010). Development of a Shear Connection for a Portable Composite Bridge. *Master's Dissertation,* University of Waterloo.

Canadian Standards Association. (2006). *Canadian Highway Bridge Design Code* (Publication No. CAN/CSA-S6-06).

Carreira, D. J., & Chu, K., H. (1985). Stress-Strain Relationship for Plain Concrete in Compression. *ACI Journal*, Proceeding 82(11), 797-804.

Fisher, J. M., & Kloiber, L. A. (2006). *Base Plate and Anchor Rod Design* (2th Edition). American Institute of Steel Construction.

Forgues, S. (2007). Extending the Fatigue Life of Bridges Using Stressonic Needle Peening. Retrieved March 10, 2013, from www.profile-ind.com/index.php/download_file/-/view/10

Hanswille, G., Porsch, M., & Ustundag, C. (2006). Resistance of Headed Studs Subjected to Fatigue Loading - Part II: Analytical Study. *Journal of Constructional Steel Research,* 63, 485-493.

Huh, B., Lam, C., & Tharmabala, B. (2010). Effect of Shear Stud Clusters in Composite Girder Design. *The 8th International Conference on Short and Medium Span Bridges,* 055, 1-11.

Hungerford, B. E. (2004). Methods to Develop Composite Action in Non-Composite Bridge Floor Systems: Part II. *Master's Dissertation,* University of Texas at Austin.

Issa, M. A., Yousif, A. A., Issa, M. A., Kaspar, I. I., & Khayyat, S. Y. (1995). Field Performance of Full Depth Precast Concrete Panels in Bridge Deck Reconstruction. *PCI Journal,* May-June, 82-94.

Kayir, H. (2006). Methods to Develop Composite Action in Non-Composite Bridge Floor Systems: Fatigue Behavior of Post-Installed Shear Connectors. *Master's Dissertation,* University of Texas at Austin.

Kosmatka, S. H., Kerkhoff, B., Panarese, W. C., MacLeod, N. F., & McGrath, R. J. (2003). *Design and Control of Concrete Mixtures* (7th Edition). Cement Association of Canada.

Kulak, G. L. (2005). *High Strength Bolting for Canadian Engineers* (1st Edition). Canadian Institute of Steel Construction.

Kulak, G. L., Fisher, J. W., & Struik, J. H. (1987). *Guide to Design Criteria for Bolted and Riveted Joints* (2nd Edition). John Wiley & Sons, Inc.

Kulak, G. L., & Grondin, G. Y. (2006). *Limit States Design in Structural Steel* (8th Edition). Canadian Institute of Steel Construction.

Kwon, G., Engelhardt, M. D., & Klingner, R. E. (2010). Behaviour of Post-Installed Shear Connectors under Static and Fatigue Loading. *Journal of Constructional Steel Research,* 66, 532-541.

Lam, C., & Tharmabala, B. (2011). Implementation of Prefabricated Bridge Technology in Ontario. *The Canadian Civil Engineer,* Spring, 10-14.

Newman, L., & Sennah, K. (2011). Accelerated Bridge Construction. *The Canadian Civil Engineer,* Spring, 1-7.

Ollgaard, J. G., Slutter, R. G., & Fisher, J. W. (1971). Shear Strength of Stud Connectors in Lightweight and Normal-Weight Concrete. *AISC Engineering Journal,* Vol. 8, No. 2, 55-64.

Ontario Provincial Standard Specification. (2011). *Material Specification for Aggregates - Concrete* (Publication No. OPSS 1002).

Ontario Provincial Standard Specification. (2010). *Construction Specification for Concrete Structures* (Publication No. OPSS.PROV 904).

Papastergiou, D. T., & Lebet, J. (2010). New Steel-Concrete Connection for Composite Bridges. *The 8th International Conference on Short and Medium Span Bridges*, 330, 1-11.

Portland Bolt and Manufacturing Company. (2012). Bolt Torque Chart – Suggested Starting Torque Values. Retrieved September 24, 2012, from http://www.portlandbolt.com/technicalinformation/bolt-torque-chart.html

Precast / Prestressed Concrete Institute. (2003). *Precast Prestressed Concrete Bridge Design Manual* (Publication No. MNL-133-97).

Salmon, C. G., & Johnson, J. E. (1990). *Steel Structures: Design and Behaviour* (3rd Edition). Harper Collins Publishers Inc.

Schaap, B. A. (2004). Methods to Develop Composite Action in Non-Composite Bridge Floor Systems: Part I. *Master's Dissertation,* University of Texas at Austin.

Sika Canada. (2012). Sikadur 330 Impregnation Resin for Fabric Reinforcement. Retrieved May 28, 2012, from http://can.sika.com/en/solutions_products/02/02a013/02a013sa06.html

U.S. Department of Transportation – Federal Highway Administration. (2011). *Accelerated Bridge Construction Final Manual* (Publication No. HIF-12-013).

Vachon, M., & Islam, Q. (2011). Bridge Rapid Replacement with Self-propelled Modular Transporters. *The Canadian Civil Engineer*, Spring, 14-31.